4-19-2010

Purification and Structural Characterization of a Novel Class of Protein- Based Magnetic Resonance Imaging Contrast Agents

Kendra Lynette Hubbard
Georgia State University, khubbard1@student.gsu.edu

PURIFICATION AND STRUCTURAL CHARACTERIZATION OF A NOVEL CLASS OF PROTEIN-BASED MAGNETIC RESONANCE IMAGING CONTRAST AGENTS

by

KENDRA LYNETTE HUBBARD

Under the Direction of Dr. Jenny J. Yang

ABSTRACT

More than one-third of all Magnetic Resonance Imaging (MRI) scans employ image-enhancing contrast agents to increase the differential signal intensity between diseased and normal tissue. Because current clinical contrast agents exhibit low relaxivity (mM^{-1} s^{-1}), low dose efficiency, and rapid secretion, we have designed a group of protein-based MRI contrast agents with multiple gadolinium binding sites. In this study, the developed purification method for Class ProCA-3 agents allows for a quick and cost-effective way to abstract up to 109 mg of pure, soluble protein from a 1L *E. Coli* cell pellet devoid of DNA or RNA "contamination" for extensive animal studies. Circular dichroism far-UV spectra ensure the metal stability of the agents, revealing maintenance of their native α-helical structure in the presence and absence of metal ions. Furthermore, substantial evidence supports the high dose efficiency of these agents, exhibiting up to five folds higher relaxivity than their analogous commercial competitors.

INDEX WORDS: Magnetic resonance imaging, Contrast agents, Gadolinium, Circular dichroism, Fluorescence resonance energy transfer, Relaxivity

PURIFICATION AND STRUCTURAL CHARACTERIZATION OF A NOVEL CLASS OF PROTEIN-BASED MAGNETIC RESONANCE IMAGING CONTRAST AGENTS

by

KENDRA LYNETTE HUBBARD

A Thesis Submitted in Partial Fulfillment of the Requirements for the Degree of

Master of Science

in the College of Arts and Sciences

Georgia State University

2010

PURIFICATION AND STRUCTURAL CHARACTERIZATION OF A NOVEL CLASS OF PROTEIN-BASED MAGNETIC RESONANCE IMAGING CONTRAST AGENTS

by

KENDRA LYNETTE HUBBARD

Committee Chair: Dr. Jenny J. Yang

Committee: Dr. Aimin Liu
Dr. Zhi-Ren Liu
Dr. Jenny J. Yang

Electronic Version Approved:

Office of Graduate Studies
College of Arts and Sciences
Georgia State University
May 2010

DEDICATION

Firstly and above all, I would like to dedicate this work and my future to my Lord and Saviour Jesus Christ. The provisions you have made for me during this research program and in every aspect of my life are too many to count! I could never repay you for the insight and wisdom you have imparted to me thus far in my journey. Thank you for divinely guiding me here and teaching me many valuable lessons along the way. It is only by your grace and unfailing love that I have the opportunity to serve you and allow you to shine through me. Lord bless this work and may it continue to prosper and bring glory to your Holy name.

I would also like to dedicate this work to my family and close friends, both new and old. To my mother, Irene Hubbard, also known as "boss," for being my #1 supporter and always encouraging me to live out my dreams. To my dad, Kenneth Hubbard, for all of your refreshing ideas on how I can apply the skills I have acquired to maximize my career potential. To my brother and sister, Alista and K.J., for being my absentee roommates this past year lol! You have lovingly created a home for us all to share. To my brother from another mother, Xiaojun "Maximillo" Xu, for pure, unrestricted friendship and the countless encouraging speeches that we have had. You truly are the big brother God has blessed me with. Last, but not least, I would like to thank all of my true friends. I prayed to the Lord for true friends from whom we could both enrich each other's lives by bringing glory to His name and one by one, the Lord lovingly sent you to me. Each of you has encouraged me and believed in the vision that the Lord has for me, even when I failed to do so. I'm so glad you all have joined me on this journey and I look forward to the many great experiences we will share. I love you all!

Kendra L. Hubbard (May 2010)

ACKNOWLEDGEMENTS

I must express great gratitude to Dr. Jenny Yang and Georgia State University for giving me the opportunity to expand my foundational knowledge on biochemical principles and for challenging me to grow into an outstanding scientist. My relationship with Dr. Yang began as my principle investigator and has now evolved into becoming both one of my mentors and a supportive friend. Her passion for her research continues to inspire me to chase after and reach for my dreams. I would also like to thank senior graduate student Shenghui "David" Xue for ushering me into this project and teaching me the necessary skills to critically analyze the observed results. A special thanks is due to Dr. Jin Zhou for his aid in helping me to design and interpret the data of many relaxivity experiments. I'd also like to thank Jie "Jasmine" Jiang for her willingness to answer countless questions and offer advice regarding many elements of my project. Last, but not least, I would like to thank the rest of Dr. Yang's lab for their noteworthy suggestions during our group discussions and for their overall support in the lab.

This work was supported in part by a supplemental grant received from the Department of Health and Human Services of the National Institutes of Health, which aids in promoting diversity and providing financial support in scientific research.

TABLE OF CONTENTS

LIST OF TABLES

LIST OF FIGURES

1. INTRODUCTION

1.1. Modern Methods for Medical Imaging

1.1.1. Background

Medical imaging is a clinical discipline referring to the techniques and processes used to create *in vivo* images of the human body for clinical applications or medicinal science [1]. In its broadest sense, the incorporation of radiology, medical photography, nuclear medicine, investigative radiological sciences, endoscopy, thermography and microscopy allows this division of the medical field to improve diagnoses and medical care for patients [1-2]. When applied effectively, medical imaging enables less-invasive prognosis and diagnosis, detects disease at its earliest and most curable stage, and allows for decreased post-treatment disability, leading to greater patient comfort and improved treatment selection. Thus, this standard of modern medical care not only "continues to empower doctors and medical professionals to view the human body and its organ systems with ever increasing clarity and accuracy" but as a result, has the potential to drastically reduce the cost of healthcare by shortening hospital stays due to faster recovery times. This is evidenced by fewer pre- and post-operative complications [2]. Therefore, the clinical and medicinal scientific communities are actively developing a number of different imaging techniques, striving to improve their role in disease prognosis, diagnosis, and treatment (Figure 1.1).

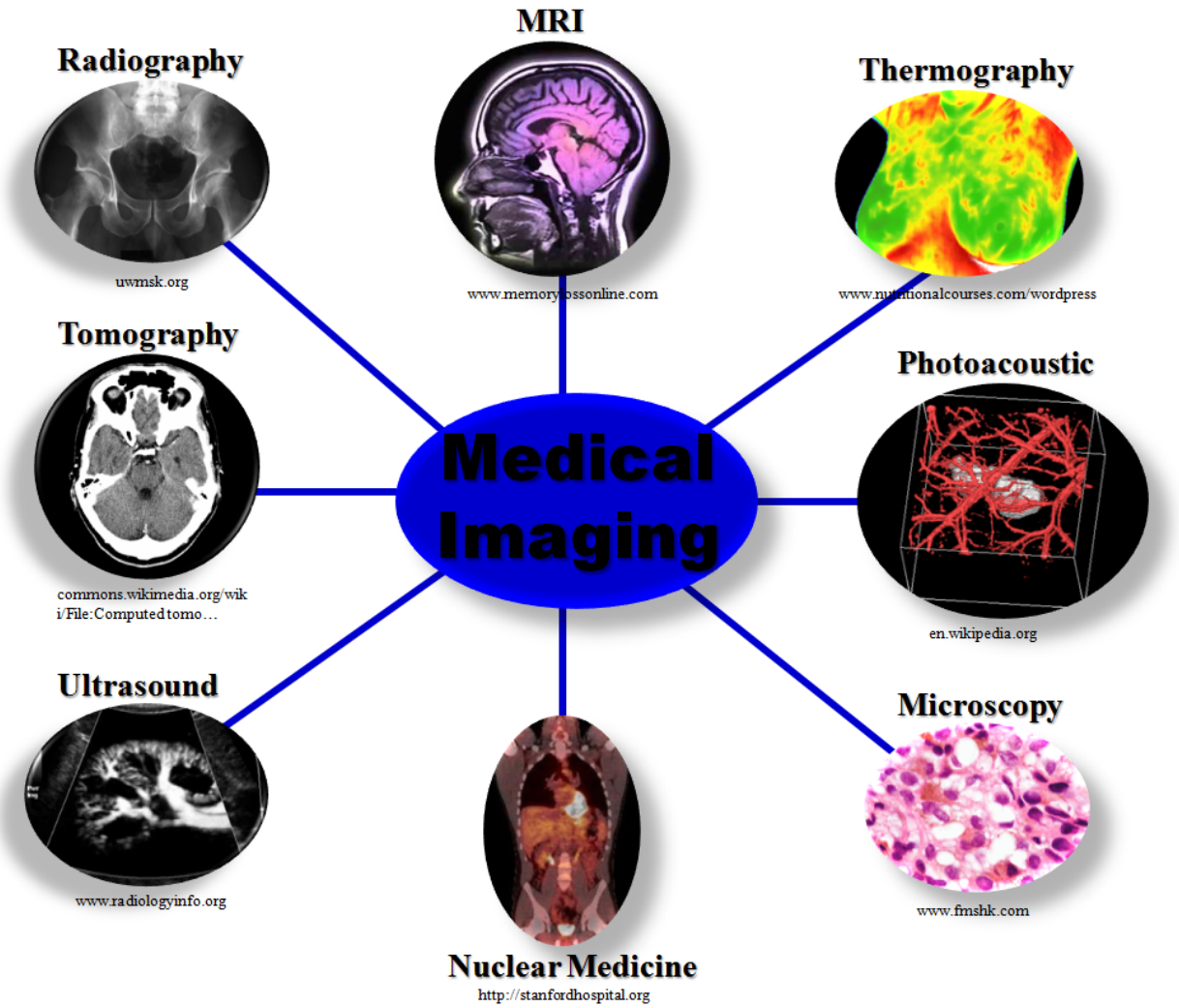

Figure 1.1. Summary of current clinically applied imaging techniques for disease diagnosis.

The availability of a wide variety of imaging techniques allows the physician and relevant medical staff to optimize patient treatment outcomes. In most cases, one or more of the techniques are combined with another to effectively diagnose and treat a patient [2].

Although medical imaging technologies provide a wide range of clinical and patient benefits, many of the techniques use X-ray radiation (X-rays and CT scans), posing dose-dependent risks to patients. The "approach taken by the FDA is that the slight risk from radiation is outweighed by the medical benefit of medically necessary CT scans and X-rays [2]." Still,

there are alternative imaging techniques that function without the use of radiation and allow for excellent resolution between diseased and normal tissue. For example, like Computed Tomography (CT), MRI also has the ability to create a two- and three-dimensional image of a thin slice of the body. However, unlike CT, MRI does not involve the use of ionizing radiation and is therefore not associated with the same health hazards such as the possibility of inducing cancer due to absorbed X-rays. Additionally, in contrast to X-ray and CT methodologies, there are no limitations to the number of MRI scans a patient can receive [1]. Although MRI can provide high-resolution images via optimized instrumental parameters and pulse sequences, it has a low sensitivity and achieves better images with supplementation of a contrast agent that increases the signal to noise ratio detected by changes in water relaxivity. Thus, the development of MRI contrast enhancing agents proves as an excellent technique to further improve medical imaging and thus medical diagnoses and treatment [3].

1.1.2. Principles of MRI and the Use of Contrast Agents

MRI is a non-invasive nuclear magnetic resonance (NMR) imaging technique that exploits the magnetic properties of hydrogen and its interaction with both a large external magnetic field and radiowaves to produce high resolution three-dimensional images of the body for disease diagnosis [4]. Although biological tissues are predominantly ^{12}C, ^{16}O, ^{1}H, and ^{14}N, hydrogen is the most abundant [5]. The majority of hydrogen protons observed in clinical imaging are of water molecules because they "have a significant magnetic moment and are nearly 70% abundant in the human body" [4-5]. As will be later explained, the varying molecular structures and the amount of hydrogen in various tissues affect how the protons behave in an external magnetic field and thus allow for potential delineation between different tissues.

The principles detailing the mechanism behind MRI signals are complex. From a simplified "classical" view, the nucleus of an atom is composed of subatomic particles protons and neutrons that spin about their axis [4]. More relevant to MRI signals, each nuclei of the hydrogen atoms in solution contain a single proton spinning about its axis, producing an angular momentum (J) and a magnetic moment (μ) (Figure 1.2) [4].

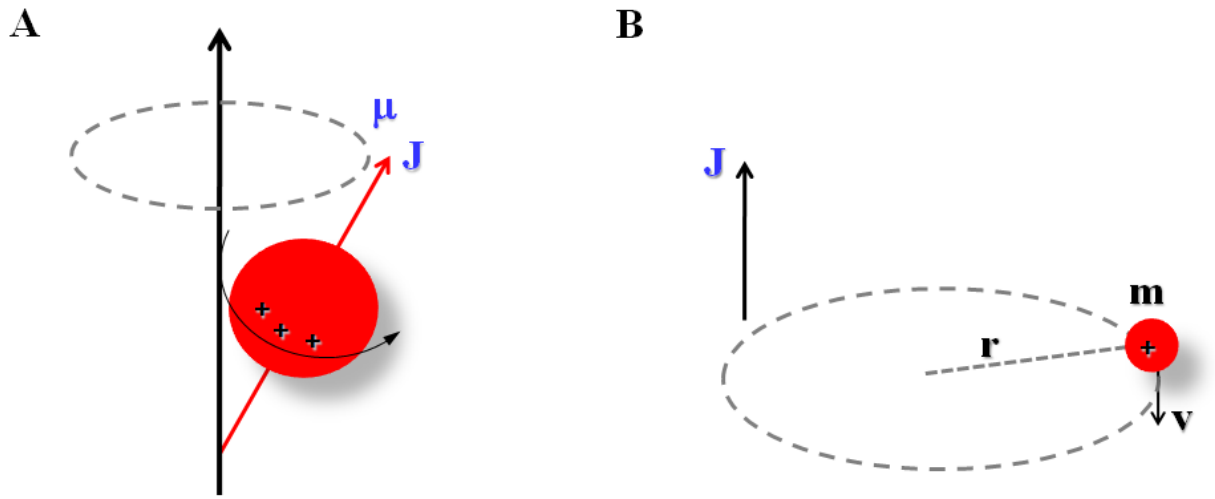

Figure 1.2. Simplified schematic illustration of the intrinsic properties of the hydrogen proton in its original state. (A) Hydrogen proton spinning about its axis. (B) Generated angular momentum from the proton spin.

The following equations are descriptive of the angular momentum and the magnetic moment:

$$J = m\omega = mvr \qquad \text{(Equation 1.1)}$$

where m is the mass of the proton, v is the velocity of the proton, and r is the radius or distance of the proton from the fulcrum [5], and

$$\mu = \tau_{max} / B \qquad \text{(Equation 1.2)}$$

where τ_{max} is the maximum torque generated and B is the magnetic field generated by the movement of the proton [5].

The angular momentum and magnetic property of the nuclei mentioned above stems from the mass and positive charge of the proton. Nuclei containing an even number of protons and

neutrons possess a net angular momentum of zero while those with an odd mass or odd atomic number (protons) possess a certain angular momentum and have net spins of one of two possible orientations characterized by *magnetic quantum number* of ± 1/2. For the purposes of MRI and NMR, atoms with paired spins tend to cancel so atoms containing an odd number of protons (like hydrogen) or neutrons are ideal for observing changes in the local magnetic field [5]. These net spins generate small magnetic fields due to their vibrational and rotational motions, giving rise to the magnetic moment. The ratio between the angular momentum and magnetic moment of the nuclei gives rise the gyromagnetic ratio (γ), a constant specific to each magnetically active nuclei (Equation 1.3) [5]. The gyromagnetic ratio of hydrogen is 42.6 MHz/Tesla [6].

$$\mu = \gamma J \qquad \text{(Equation 1.3)}$$

In the absence of an external magnetic field, these charged nuclei are in a lower energy level and have randomly oriented spins of equal energy. When an external magnetic field (B_0) is applied, the axis of rotation of the nuclei will precess around that of the applied magnetic field. The frequency of precession is termed Larmor frequency, a parameter that must be optimized for efficient relaxation of a contrast agent [7]. Subsequently, in this excited state, the spins of the nuclei will align parallel or antiparallel (with or opposed) to the magnetic field. Combined with the magnetic and electromagnetic fields, MRI uses non-ionizing radiation radiowaves in the form of a radiofrequency pulse (RF) to manipulate the magnetization of protons and perturb their alignment to the external magnetic field. As the radiofrequency pulse is removed, the spins of the nuclei decay from the higher energy state to their lower energy state through a process termed relaxation. It's important to note that there are radiofrequency pulse sequences designed to highlight T1 and T2 changes, two distinct relaxation processes [8]. The change in "distribution of the magnetic moments of the protons from random to directed and their return to normal" via

relaxation constitutes the MRI signal [8]. The basic principles of MRI are summarized in Figure 1.3.

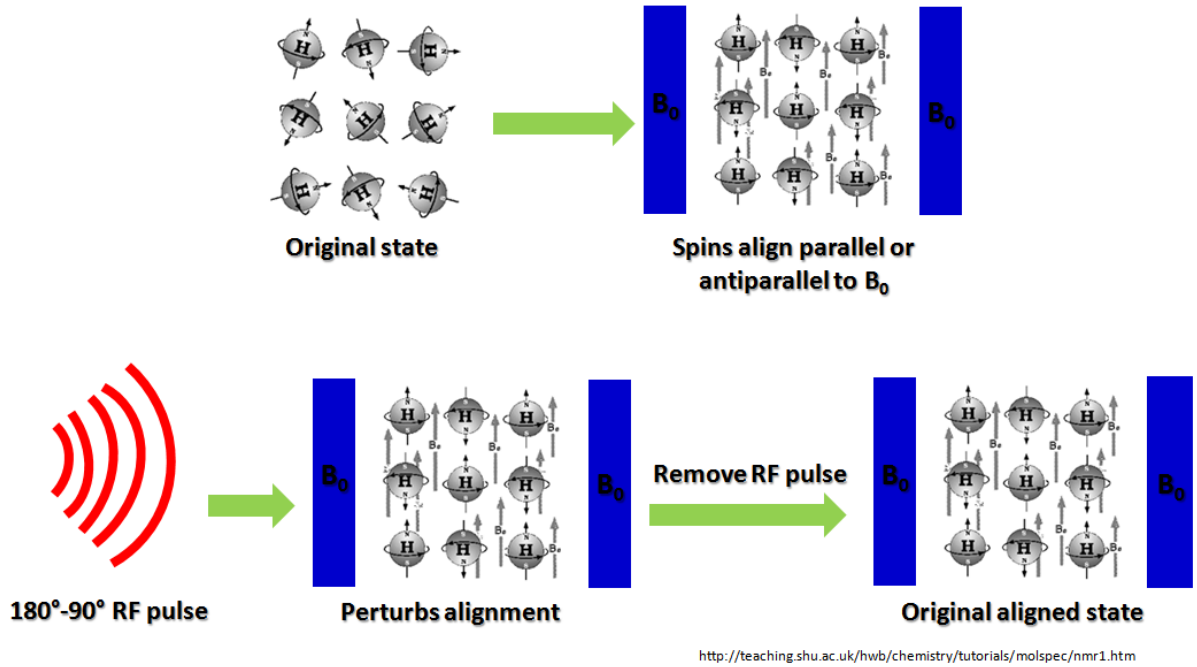

Figure 1.3. Simplification of the basic principles underlying MRI.

There are two dominant relaxation processes: spin-lattice (longitudinal) relaxation and spin-spin (transverse) relaxation [9]. The nuclei spins aligned parallel or perpendicular to the external magnetic field are generally dominated by spin-lattice relaxation time T1. The *lattice* is descriptive of the sample in which the nuclei are held. The *lattice field* results from the magnetic field caused by the vibrational and rotational frequencies of the nuclei [9]. Components of the lattice field can interact with high energy state nuclei and cause them to lose energy, relaxing them back to their lower energy state. The average time -it takes for the higher energy state nuclei to relax to a lower energy state with respect to the lattice field is termed longitudinal relaxation time T1 and is dependent on the gyromagnetic ratio of the nucleus and the mobility of the lattice [9]. Not only are the spins of nuclei in the presence of an external magnetic field influenced by components of the lattice field, but also by neighboring nuclei with identical

precessional frequencies but differing magnetic quantum states. Though there is no net change in Boltzmann distribution of the nuclei, a nucleus in the lower energy level will be excited while an excited nucleus relaxes to the lower energy state. The average time it takes for the higher energy state nuclei to relax to a lower energy state with respect to neighboring nuclei is termed transverse relaxation time T2 [9].

Because the detection sensitivity of MRI is low, it often requires a contrast agent to enhance the signal intensity related to the relaxation rate of water protons [8]. The term relaxivity describes how effective a contrast agent is at enhancing the signal intensity by shortening proton relaxation times. Contrast agents influencing the relaxation times of water protons must be paramagnetic, those found amongst the transition metals and lanthanides, meaning they possess a number of unpaired electrons. Here, proton relaxivity is directly proportional to the efficiency of the paramagnetic ion to enhance the relaxation rate of water protons [8]. Gadolinium, bearing seven unpaired electrons, has been found to exhibit the strongest effect of all elements on T1. This is due to the dipole-dipole interactions between proton nuclear spins and the fluctuating local magnetic field caused by the unpaired electron spins of gadolinium [8]. Because free ions of heavy metals are toxic, lanthanides are typically complexed with a suitable metal chelator/ligand. When the metal is bound to the chelator, it gives rise to a contrast agent capable of influencing water relaxation.

1.1.3. Factors Contributing to MRI Relaxivity

There are a number of molecular parameters of contrast agents that govern relaxivity: rotational diffusion, inner- and outer/second-sphere hydration (q), water exchange rates (k_{ex}), ion-proton distances, and the electronic properties (T_{ie}) of the paramagnetic ion [8]. The strength of the applied magnetic field (B_0) and solution viscosity also play a role in relaxation processes.

Proton exchange rate, rotational correlation time, electronic relaxation times, Gd-proton distance, and hydration number directly influence the inner sphere proton relaxivity [8]. If the proton exchange is very slow relative to the relaxation rate of the coordinated protons to gadolinium, then it will become a limiting factor, hampering optimal relaxation. If the proton exchange is fast relative to the coordinated protons, proton relaxivity will be largely determined by the relaxation rate of the coordinate protons [8].

Maximum relaxivity is attained when the correlation time (τ_{ci}) equals the inverse proton Larmour frequency (ω_i) [8]. The correlation times characteristic of the relaxation processes are as follows:

$$1/\tau_{ci} = 1/\tau_R + 1/T_{ie} + 1/\tau_m = \omega_i, \text{ where } i = 1, 2 \quad [8]. \qquad \text{(Equation 1.4)}$$

More importantly, the rotational correlation time (τ_R), proton exchange ($k_{ex} = 1/\tau_m$), and electronic relaxation rates ($T_{1,2e}$) must be optimized simultaneously to achieve maximum relaxivities. Equation 1.5 addresses the effects of inner sphere relaxivity and how manipulation of its terms can increase the overall relaxivity of a contrast agent.

$$r_1^{IS} = (q/[H_2O])/ (T_{1m} + \tau_M) \quad [8, 10] \qquad \text{(Equation 1.5)}$$

where r_1^{IS} is the relaxivity due to the inner sphere of water surrounding a paramagnetic metal ion, q is the hydration number, $[H_2O]$ is the water concentration in mM, T_{1m} is the T1 of the water hydrogen in the inner sphere, and τ_M is the water residency time ($\tau_M = 1/k_{exchange}$ of water in the inner sphere). This equation reveals that an increase in hydration (q) or decrease in T_{1m} or τ_M can increase the overall relaxivity of a contrast agent [10]. However, the FDA approved gadolinium-based contrast agents have not effectively optimized these parameters.

1.2. Commercial MRI Contrast Agents and Development

Currently, it has been estimated that 40-50% of all MR images are supplemented with a contrast agent [11]. Gadolinium-based contrast agents are implicated to achieve a number of these images. The six FDA approved commercial gadolinium-based MRI contrast agents are T1-weighted agents, meaning they yield brightened images when introduced into a system (Figure 1.4).

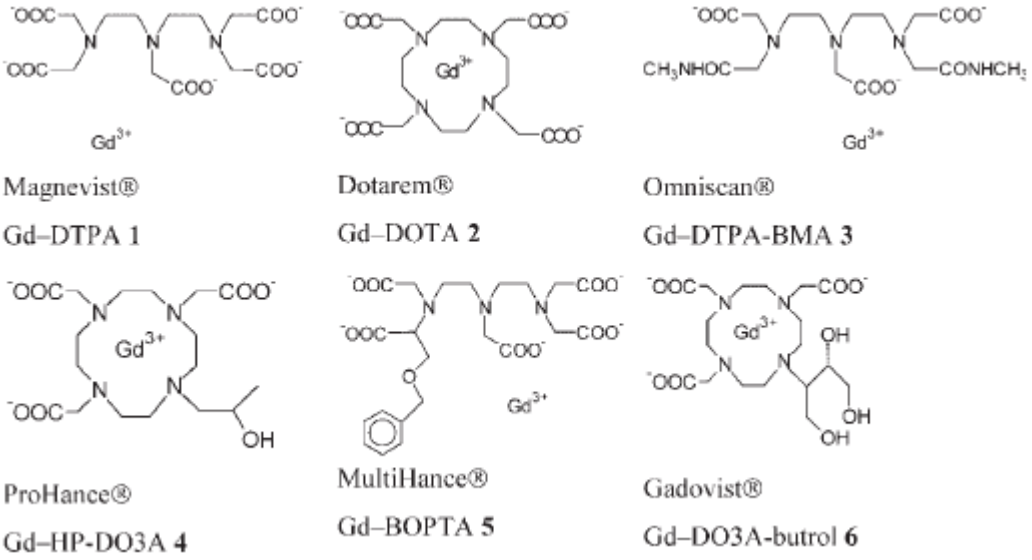

Figure 1.4. FDA Approved Commercial Contrast Agents [12].

The basic chelate design ranges from linear to acyclic structures. Because of their enhanced thermodynamic stability and kinetic inertness, Gd^{3+}-based MRI contrast agents derived from DOTA-like macrocyclic ligands have advantages over their linear counterparts (DTPA) [13]. Overall, these small molecular Gd-chelates maintain relaxivities of 4-6 mM^{-1} s^{-1} [14]. However, these agents have theoretically attainable relaxivity values of over 100 mM^{-1} s^{-1} (Figure 1.5A). It has been proposed that they fail to reach their maximum relaxivity due to their fast rotation time (100 ps) and slow water exchange in the inner sphere (Figure 1.5B) [3, 8].

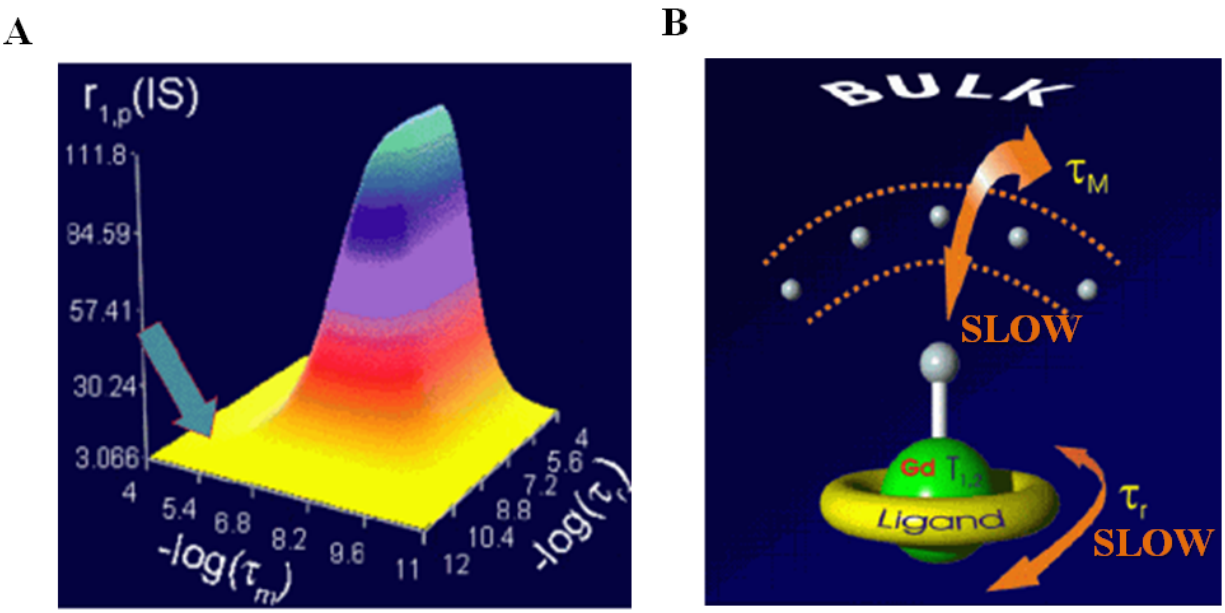

Figure 1.5. The need for improved MRI gadolinium-based contrast agents. (A) Low relaxivity of commercial contrast agents compared to theoretical values. (B) Explanations for low observed relaxivity for commercial agents [7-8, 15].

Furthermore, the aforementioned contrast agents are only effective at high concentrations (>0.1 mM) [10]. Currently, the average clinical injection dosage of commercial contrast agents is approximately 500 mM/kg at an injection rate of 2-3 mL/s to achieve high sensitivity to the changes in water relaxation [14]. Even higher doses are required for imaging of blood vessels in Magnetic Resonance Angiograpy (MRA) [14]. Because of their small size, the systemic retention time of these agents is relatively short, maintaining a half-life of 1.5-2 hours in healthy adults and thus requiring a large dose to achieve an enhanced image [14]. However, in patients with kidney disease, the renal clearance is significantly decreased. Studies have shown that kidney-impaired patient exposure to gadolinium-based contrast agents has been linked to local necrosis at the injection site and nephrogenic systemic fibrosis (NSF) or nephrogenic systemic dermopathy (NSD) due to their weak binding affinity to gadolinium leading to the release of free gadolinium in the body and the accumulation of the contrast agent in the kidney (lack of proper excretion) [14].


Figure 1.6. Visible symptoms or signs of NSF/NSD [16-17].

NSF/NSD is a life-threatening disorder that may develop over a short period of days to several weeks (full development) [18]. As shown in Figure 1.6, it is characterized by swelling and tightening of the skin, usually limited to the extremities, and severely affected patients may be unable to walk, or fully extend the joints of their arms, hands, legs, and feet [18]. More specifically, the release of free gadolinium correlated with NSF has been known to cause many toxic systemic effects such as inhibiting calcium-flux-dependent physiological processes, blocking many voltage-gated calcium channels at nano- to micro-molar concentrations, and depressing the reticuloendothelial system [14, 19]. For this reason, in May 2007, the FDA issued a black box label warning to be placed on five of the six approved gadolinium-based contrast agents (with the exception of Dotarem®) in the United States, warning health professionals and patients of the association between the use of gadolinium-based contrast agents and NSF [20]. Because of their low dose efficiency due to low relaxivity and to low retention time and health hazards, there has been considerable effort to effectively improve contrast agent design and enhance the sensitivity of MRI devoid of such toxic effects. Agents with higher relaxivities and

optimal retention times can be detected at lower doses, providing greater signal contrast images at equivalent doses to commercial compounds with lower relaxivity [10].

The demand for the development of improved MRI contrast agents has become increasingly widespread. The two primary approaches taken by the scientific community to increase molecular relaxivity are optimization of the aforementioned molecular parameters that govern relaxivity and linking multiple gadolinium tetraazacyclododecanetetraacetic acid (DOTA) or diethylenetriaminopentaacetic acid (DTPA) complexes together (Figure 1.7) [10].

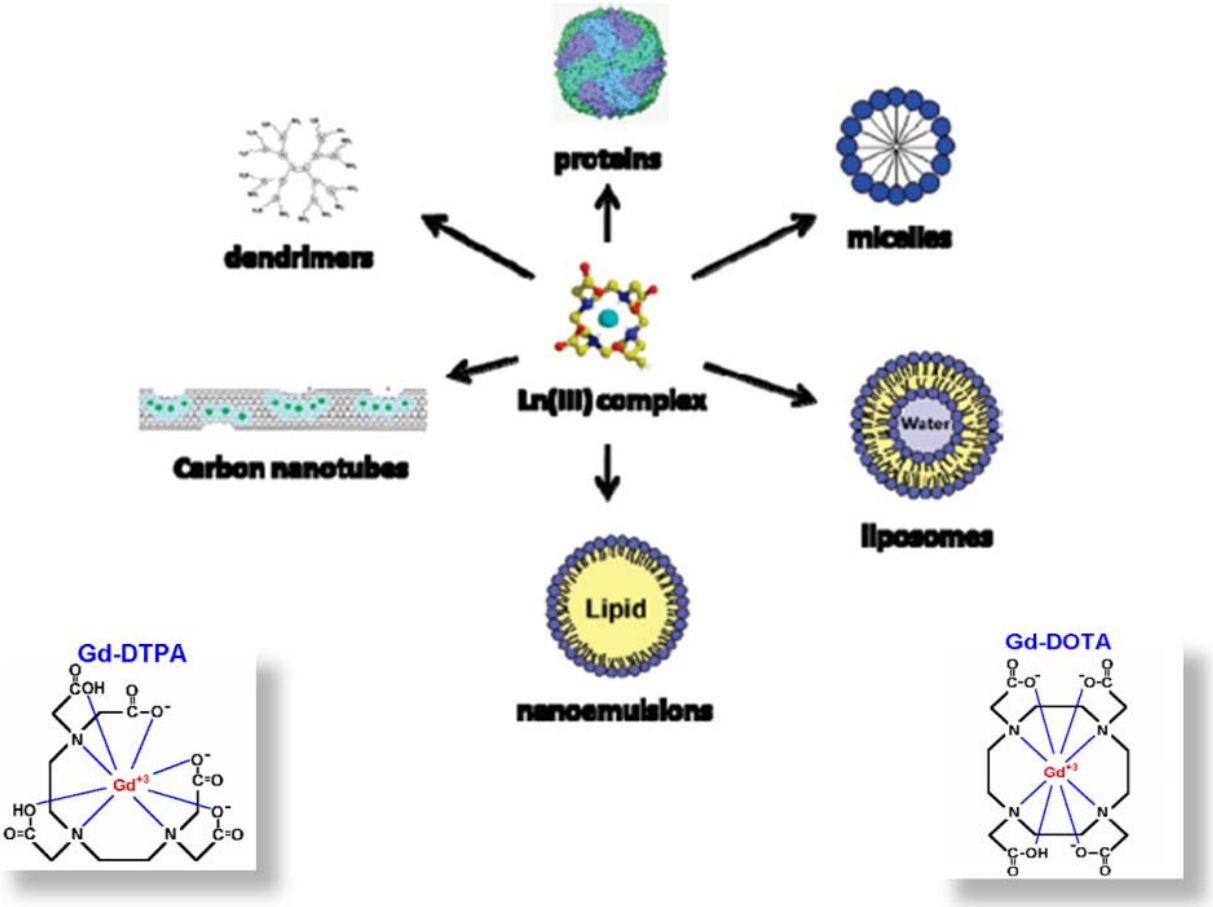

Figure 1.7. Current MRI contrast agent development.

These newly developed classes of contrast agents predominantly address the rapid rotational time of commercial agents by covalently linking chains of Gd-DTPA or Gd-DOTA to larger

biomolecules such as dendrimers, carbon nanotubes, nanoemulsions, liposomes, micelles, or proteins [21]. However, while these agents address the overall rotational time associated with molecular tumbling in solution, they do not achieve significantly higher relaxivities than the commercial analogues due to their intrinsic internal mobility and restricted water exchange rate [3]. Furthermore, their large particle size (10-100 nm) prevents them from being properly excreted from the body, raising greater toxicity concerns of gadolinium-based agents. As a result, a novel class of protein-based MRI contrast agents has been designed with high dose efficiency due to higher relaxivity, strong metal stability, and optimized pharmokinetics.

1.3. Criteria for Contrast Agent Design

Because contrast agents have the potential to be invaluable clinical probes for enhancing magnetic resonance images, it is of crucial importance to design an agent with a high relaxivity, strong binding affinity to gadolinium versus other physiological metal ions, and high metallo-structural stability. The achieved higher relaxivity agent will not only improve the sensitivity of MR imaging, but also greatly reduce the amount of agent necessary to achieve significant contrast. Thus, the dose efficiency of the contrast agent is increased, providing higher contrast capability due to the incorporation of multiple designed gadolinium-binding sites into a scaffold structure and to obtaining an optimal τ_R in the nanosecond range. The strong binding affinity of the designed contrast agent to gadolinium will confer high metal selectivity to avoid potential adverse competition from other systemic metals and alleviate many of the toxic concerns associated with the release of free gadolinium into the system. Furthermore, heightened structural tolerance of mutations, high blood serum stability, and high solubility will reduce the potential instability of the scaffold contrast agent design. To add to the previously mentioned determining factors in design, the developed class of contrast agents must have no reported

interactions with other biomolecules, possess an optimal systemic retention time to successfully acquire an MR image, and be properly excreted via the kidneys or liver metabolism.

1.4. Theory Preceding the Development of Protein-Based Contrast Agents

Dr. Jenny Yang's lab of Georgia State University has developed a novel approach to designing improved contrast agents via protein engineering. Protein-based MRI contrast agents offer a number of advantages compared to the aforementioned commercial analogs. To improve relaxivity, proteins can be modified to achieve an optimal metal-site rotational time of 10ns, optimal hydration of inner and second-sphere hydration, and optimal water exchange rates of 1-30ns [3, 8]. The obtained higher relaxivity will improve the dose efficiency associated with gadolinium-based MRI contrast agents. Therefore, a lower concentration and volume of agent will be required to significantly improve the contrast to noise ratio of MR images, reducing the potential for the toxic effects associated with NSF/NSD. Their modifiable, compact molecular size (12 kDa) is suitable for sufficient intravascular distribution and easy renal excretion. Additionally, choosing a stable host protein tolerant of various mutations, affords the opportunity to design gadolinium-binding sites into its structure and confer metal selectivity via tuned metal binding affinity [3]. Improved solubility and reduced immunogenicity can be achieved by covalently attaching polyethylene glycol (PEG) chains to lysine or cysteine residues of the protein [22]. Using this approach to develop improved agents, Dr. Yang's lab previously designed and conducted significant studies on Class ProCAi-CD2 agents (i = 1, 2, 3….9). These agents were developed through the introduction of single high-coordination gadolinium binding sites into stable CD2 protein using amino acid residues and water molecules as metal coordinating ligands [3]. The designed proteins showed strong selectivity for gadolinium over physiological metal ions such as calcium, zinc, and magnesium, exhibited a 20-fold increase in

T1 and T2 relaxation rate values over the conventional small-molecule contrast agents, e.g., Gd-DTPA, and possessed stronger contrast enhancement and longer blood retention time than Gd-DTPA in mice models [3]. With a new generation of contrast agents on the horizon, we hope to address the following question: Can we design multiple gadolinium-binding site agents to further increase contrast agent dose efficiency, increase stability, and reduce toxicity?

1.5. Designed Multi-Binding Site Contrast Agents by Protein Engineering

Dr. Jenny J. Yang's lab specializes in two approaches to studies of calcium-binding proteins, the design and grafting approaches. The design approach involves site-directed mutagenesis to tune metal-binding affinities of calcium-binding proteins, conserving the number of amino acids in their primary sequence and maintaining their structural integrity. This approach was created in order to "develop a general methodology to design metal binding sites with high coordination numbers such as calcium and lanthanides, understand the mechanism of calcium-regulated biological process such as ligand-induced conformational changes in cell adhesion, and monitor calcium signaling in vivo" [23]. The grafting approach engineers an EF-hand calcium-binding loop into a protein to understand "site-specific metal binding affinity and selectivity of individual calcium binding motifs and to estimate the contribution of conformational change and cooperativity between paired EF-hand motifs" [23].

Using the design approach, two gadolinium-binding sites were engineered into a stable host protein, which in its native state, has little to no reported interactions with other biomolecules. It is with great hopes that the increased number of binding sites will enhance the measured relaxivity compared to commercial agents, and thus improve the dose efficiency. Provided the binding affinity of gadolinium to the protein is significantly strong, the toxic effects associated with the release of free gadolinium into the system are greatly reduced.

1.6. Parvalbumin as an Excellent Scaffold for Engineering Multiple Gadolinium Binding Sites

Parvalbumin is a small, 12 kDa acidic protein ubiquitously distributed throughout the vertebrate phylum [24-25]. The mammalian form is found in fast twitch muscle fibers, neuronal cells, and several endocrine glands [25]. Furthermore, parvalbumin has two isoforms: α and β. Though both forms have a conserved helix-turn-helix motif, the α-form maintains 109 amino acids and is believed to serve mainly as a cytosolic calcium-buffering protein with no known interacting partners [26-27]. This six α-helical protein, helices termed A through F, contains three EF-hand motifs, only two of which functionally bind calcium (CD and EF sites) (Figure 1.8). The β-form, or better termed oncomodulin, maintains 108 amino acids, functioning more so as a calmodulin-like enzyme —— often active during cellular proliferation [24, 27]. This form of parvalbumin possesses two different metal binding domains, one calcium specific and one calcium/magnesium mixed site [27]. For the purposes of this project, we will mainly focus on studies of the rat derived α-form.

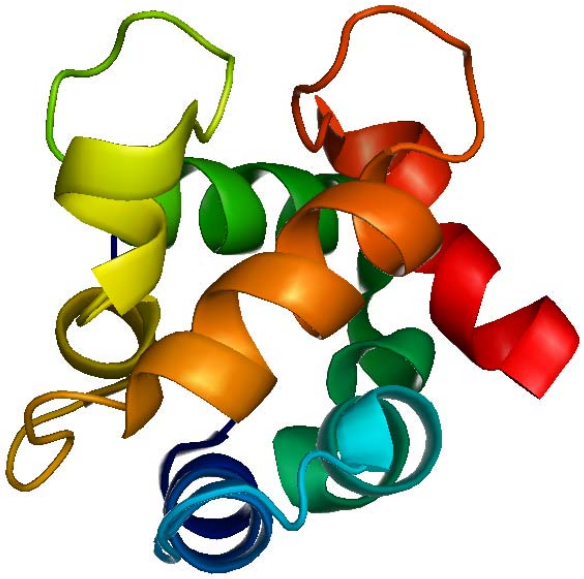

Figure 1.8. Pymol structure of rat-derived α-parvalbumin.

The CD site EF-hand motif of parvalbumin is modified through single mutations within a calcium-binding site. Maintaining pentagonal bipyramidal geometry (Figure 1.9), its residues 1, 3, 5, 7, 9, and 12 are the conserved residues subject to mutagenesis [28]. Because calcium and gadolinium have comparable ionic radii and gadolinium, it is with great hopes that the increased charge of gadolinium will allow mutants to bind this metal with a much larger affinity than calcium. To enhance gadolinium-binding affinity and allow for experimental analysis, various mutations were introduced into the binding domains of parvalbumin (Figure 1.9).

- Cytosolic Ca^{2+} binding protein believed to serve mainly as Ca^{2+} buffers; no reported interactions with other proteins
- 12 kDa, 109 amino acids (**α-type**)
- Contains three EF-hand motifs; only two of which are functional (termed CD and EF sites)
- K_d(M) for Ca^{2+} and Mg^{2+} on the orders of 10^{-9} and 10^{-6} respectively

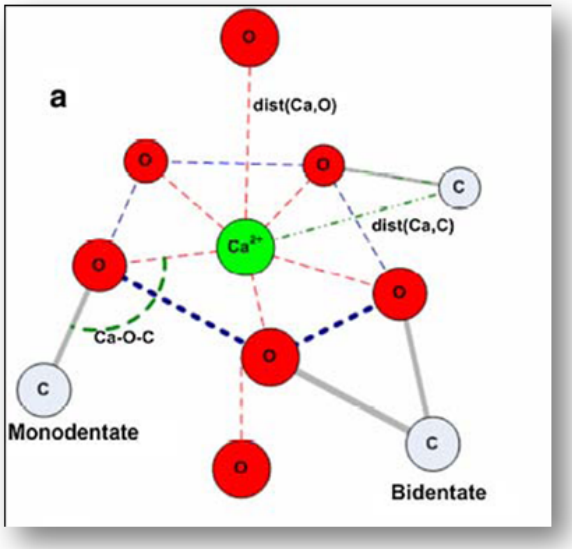

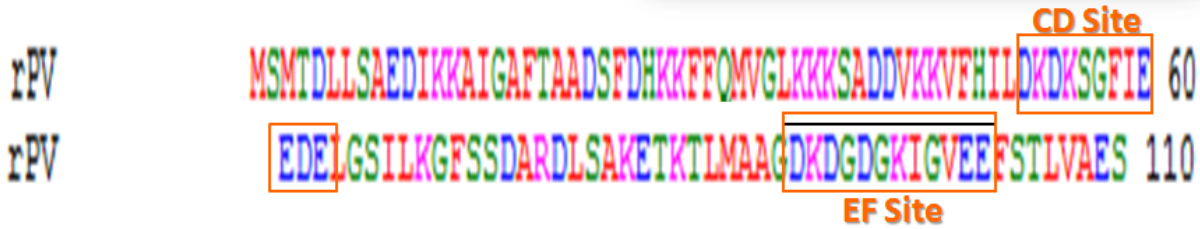

Figure 1.9. Summarizing the CD and EF binding domains of α-parvalbumin and their pentagonal bipyramidal geometries.

Residue 103, located outside the EF binding domain, was mutated from phenylalanine (F) to tryptophan (W) in order to complete terbium fluorescence experiments. Residue 56, located in position five of the CD EF-hand binding site, was mutated from serine (S) to aspartic acid (D) to

increase the proteins gadolinium-binding affinity. Residue 60, also located in the CD binding site but in position nine, was mutated from glutamic acid (E) to aspartic acid (D) to increase gadolinium-binding affinity and allow for the incorporation of a water molecule into the binding site. This incorporation should theoretically enhance the water exchange rate associated with the gadolinium-binding site and increase the relaxivity. The same can also be said for residue 99, located in the EF binding site, mutation from glycine (G) to aspartic acid (D). It is proposed that these mutations will not perturb the conformational fold and can effectively bind gadolinium with little negative competition from calcium or other biological metal ions at their respective physiological concentration. However, this must be further investigated in future experiments. Single and double mutations were introduced into the metal binding sites to observe the intrinsic metal selectivity properties of mutant forms of parvalbumin.

In this thesis, only single mutant forms of parvalbumin were studied. The significance of each mutation was previously discussed. Here, ProCA-30 represents wildtype parvalbumin. ProCA-31 is often referred as pseudo-wildtype parvalbumin because it bears a F103W mutation. ProCA-32 bears a S56D and F103W mutation. ProCA-33 encompasses an E60D and a F103W mutation. Collectively, these mutant proteins, or rather contrast agents, comprise four of many members of Class ProCA-3 agents (Table 1.1).

1.7. Overview of Objectives

In order to understand the key determinants for calcium-binding affinity and metal selectivity, the initial objective is to characterize the folding and metal-binding properties of parvalbumin. Based on the differentiation between 54 amino acid sequences, the human and rat α-forms maintain conserved residues within their EF-hand binding sites. Thus, characteristic *in vitro* studies of the rat derived form can allow one to draw conclusions about the functional

properties of the human form. The short-term goals of this project are to 1) isolate pure, functional rat parvalbumin (rPV) and its mutagenic components, 2) perform structural studies of rPV and its mutants by circular dichroism, and 3) complete calcium titration and metal binding competition experiments using fluorescence. The long-term goal is to control protein function by tuning metal binding affinities and eventually develop rPV and/or its mutants as site specific diagnostic and therapeutic MRI contrast agents.

As part of this new class of MRI contrast agents, the engineered mutagenic form of parvalbumin will have improved relaxivity through the binding of gadolinium and exhibit strong stability against pH changes. Moreover, it should be structurally tolerant of mutations, have a selective binding affinity for gadolinium, and maintain a molecular size suitable for intravascular distribution and easy renal excretion [3]. Coupled with low toxicity and high solubility, the ability to mass produce pure quantities of this protein at reduced costs will prove advantageous. This thesis will focus primarily on the expression and purification, metal-dependent structural changes, and relaxivity of four members of Class ProCA-3.

In chapter 2, the methods implemented for studies of Class ProCA-3 agents will be discussed. In chapter 3, the *E. Coli* expression and optimized purification of the designed contrast agents will be heavily expounded upon. In chapter 4, structural analysis of the purified agents in the presence of magnesium, calcium, gadolinium, and terbium and the effect that salt ions play on the structure will also be discussed. Chapter 5 will detail the measured *in vitro* relaxivities of Class ProCA-3 agents and their binding mode with gadolinium. Chapter 6 discusses the significance of this thesis and the future application of Class ProCA-3 agents. The discussed members of this class are summarized in Table 1.

Table 1.1. Summary of the discussed members of Class ProCA-3 agents.

Designed Contrast Agent	Mutation	Location	Molecular Weight
Pro CA-30	N/A	N/A	~ 11.925 kDa
ProCA-31	F103W	Just outside EF site	~ 11.964 kDa
ProCA-32	S56D, F103W	CD site (pos. 5)	~ 11.992 kDa
ProCA-33	E60D, F103W	CD site (pos. 9)	~11.950 kDa

2. MATERIALS AND METHODS

2.1. Cloning and Transformation

The DNA sequences for expression of the aforementioned contrast agents were cloned into pET-22b(+) by senior PhD student David Xue. The experimental details outlined in this thesis began at the level of transformation. Transformation is a commonly used technique to introduce genetic alterations into a host cell through the uptake of foreign DNA [29]. More specifically, the gene encoding for parvalbumin and its mutants were inserted into the pET-22b(+) vector between the Nde I and Xho I restriction enzyme sites and collectively transfected into *E.Coli* BL-21 pLys cells. (Figure 2.1).

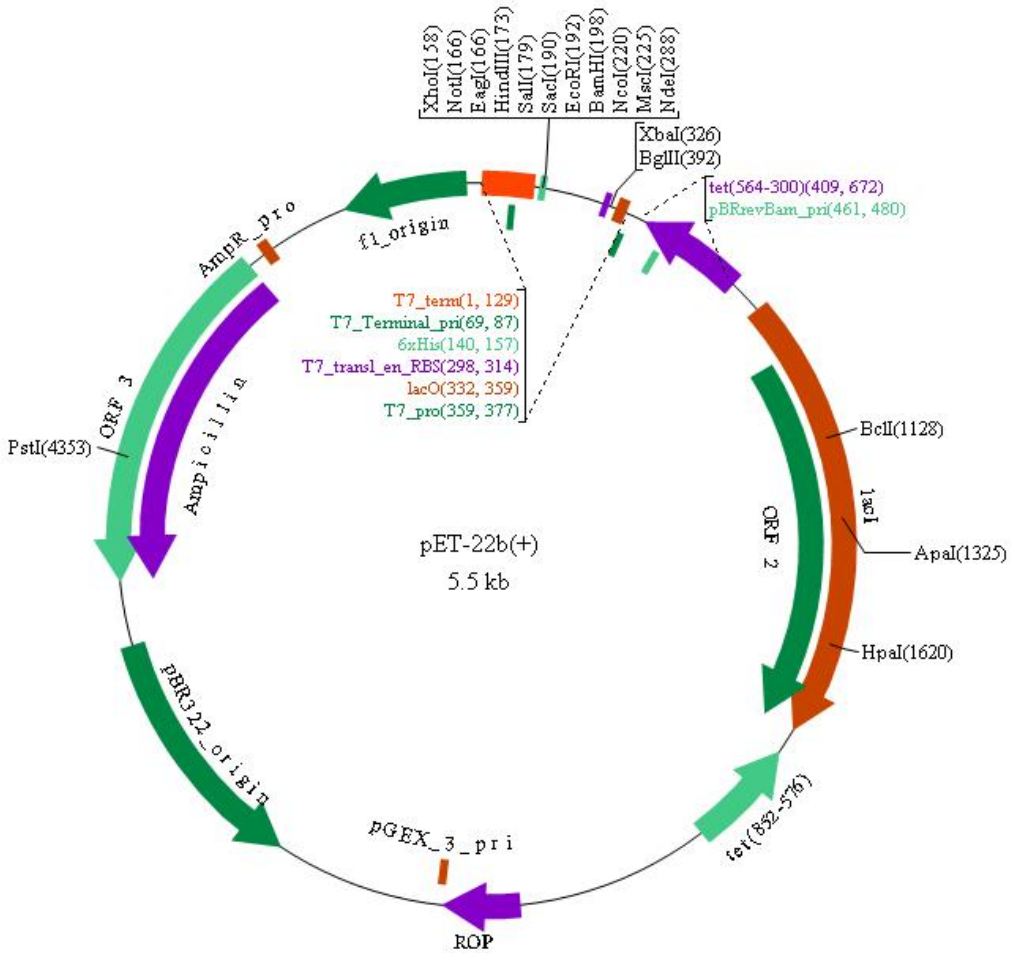

Figure 2.1. pET-22b(+) vector for Class ProCA-3 overexpression [30].

This particular bacterial system is ideal for overexpression of the designed proteins because it has the ability to produce large amounts of RNA, amplifying the translation of wildtype or genetically engineered mutant genes [29]. A volume of 0.5 μL of desired mutant DNA was mixed with 50 μL of thawed *E. Coli* BL-21 pLys competent cells with a pipette using an "up and down" pipetting technique and placed on ice for thirty minutes. The samples, including the negative controls containing only competent cells, were placed in a 42 ºC water bath for 90 seconds and placed on ice for an additional 2 minutes. A volume of 50 μL of LB was added to the samples and placed in the incubator at 37 ºC for 30 minutes. The samples were then streaked out with sterile L-shaped spreaders onto LB ampiscillin plates and left in the 37 ºC incubator overnight. The following morning yielded evidence of a large number of isolated colonies containing the transfected parvalbumin plasmid. One colony of each variant would be later used for innoculation.

2.2. Protein Overexpression

2.2.1. Pilot Expression

A recurrent problem with the purification of soluble, tagless proteins, such as those of Class ProCA-3 agents, is the inability to eliminate DNA/RNA contamination. It is well known that insoluble proteins are effectively isolated from coexisting nucleic acids via inclusion body formation. Therefore, to improve the purification process and increase the yield of isolated protein, pilot expression procedures were implemented with hopes of extracting ProCA-30 and its mutants from the inclusion bodies, since DNA normally lies in the supernatant following centrifugation of cell lysate. It has been proposed that certain bacterial strains have a preference to form more inclusion bodies than others at a specific temperature. Therefore, choosing one of these strains to express the protein might allow us to extract it from the cell pellet. In an attempt

to isolate the protein from nucleic acids following cell lysis, the pilot expression protocol modified from Invitrogen's pRSET A, B, C protocol manual was used to transform and express ProCA-30 in three different strains using two different concentrations of isopropyl β-D-1-thiogalactopyranoside (IPTG) (0.5 and 1 mM). The cell pellet following expression was fractionated by incremental exposure to dry ice and analyzed by SDS-PAGE analysis to determine whether PV was present in the inclusion body for the reasons previously stated.

2.2.2. Innoculation

A predetermined volume of Luria Bertani (LB) medium was prepared and autoclaved at 15 psi for 1 hour at 121 °C. Traditionally, two 1L flasks and one 250 mL flask were subjected to this sterilization process and allowed to cool for the overexpression of each ProCA-3 agent. In order to effectively overexpress each variant, an initial overnight growth of its cellular expression system must be achieved. One freshly transfected colony was immersed in a 250 mL culture of sterilized Luria Bertani (LB) medium containing 100 μg/mL of ampiscillin. Great care was taken to minimize contamination by use of a sterilized inoculating loop and by performing the transfer of clone to LB flask near an open flame. The flask was then placed in an environmental shaker to incubate overnight at 37 °C at a speed of 220 to 230 rpm. The following morning yielded a cloudy solution marked by cell growth. These cells were later to be transferred to a freshly sterilized LB-ampiscillin medium for optimal cell growth and eventual overexpression of the desired mutant.

2.2.3. Overexpression

A 50 mL volume of overnight culture was added to each of two 1L flasks of fresh media containing 100 μg/mL of ampiscillin. The two 1L flasks were incubated in a 37 ºC shaker at a speed of 220 to 230 rpm, allowing cellular growth to continue. Following induction of the

system with IPTG to overexpress the desired protein, the cells were allowed to grow for approximately three to four hours before reducing the incubation temperature to 25 °C at the same speed for overnight expression. The following morning, the cultured media was subjected to centrifugation and the cell pellet was isolated and frozen until purification methods were implemented.

Using Shimadzu UV-Visible Spectrophotometer (UVP), the optical density of the rapidly growing cloned cells immediately before induction (0.6000 to 0.8000 more) with inducer IPTG and at various time points after induction was observed and recorded at 600 nm. The absorbance readings were recorded and plotted in the Kaleidagraph 3.5 program to chart cellular growth. Then the samples used for the UVP were saved and spun down in microcentrifuge tubes. The supernatant was poured off and the cell pellet containing the targeted mutant was resuspended in a sample buffer containing dithiothreitol (DTT) and beta-mercaptoethanol, which reduce the disulfide bridges stabilizing the protein's tertiary structure, and sodium dodecyl sulfate (SDS), and anionic detergent that binds strongly to and denatures the protein [25]. The samples were boiled for ten minutes and an SDS-PAGE gel analysis was conducted. The protein is fully denatured by this gel electrophoresis experiment and opens up in a rod-shaped form with a number of negatively charged SDS molecules along the polypeptide chain, one SDS molecule for every two amino acid residues of the mutant [25]. The gel was run using a marker of known molecular weight (68, 29, 14.3, and 6.5 kDa) to chart where the target contrast agent (~12 kDa) was located in the resolving portion of the gel following its migration through the stacking portion, which "concentrates the protein sample into a sharp band before it enters the main separating gel…allowing relatively large sample volumes of the mutant (10 μL) to be applied to the gel without any loss of resolution" [31]. Once the samples had completely migrated to the

bottom of the resolving portion of the gel, the entire gel was stained with a Coomassie blue reagent and destained with a buffer containing methanol, acetic acid, and deionized water. The protein bands are visible after destaining the gel. It is generally accepted that a "very faint protein band is equivalent to about 0.1 µg of protein" [31]. Figure 2.2 summarizes the expression procedures implemented.

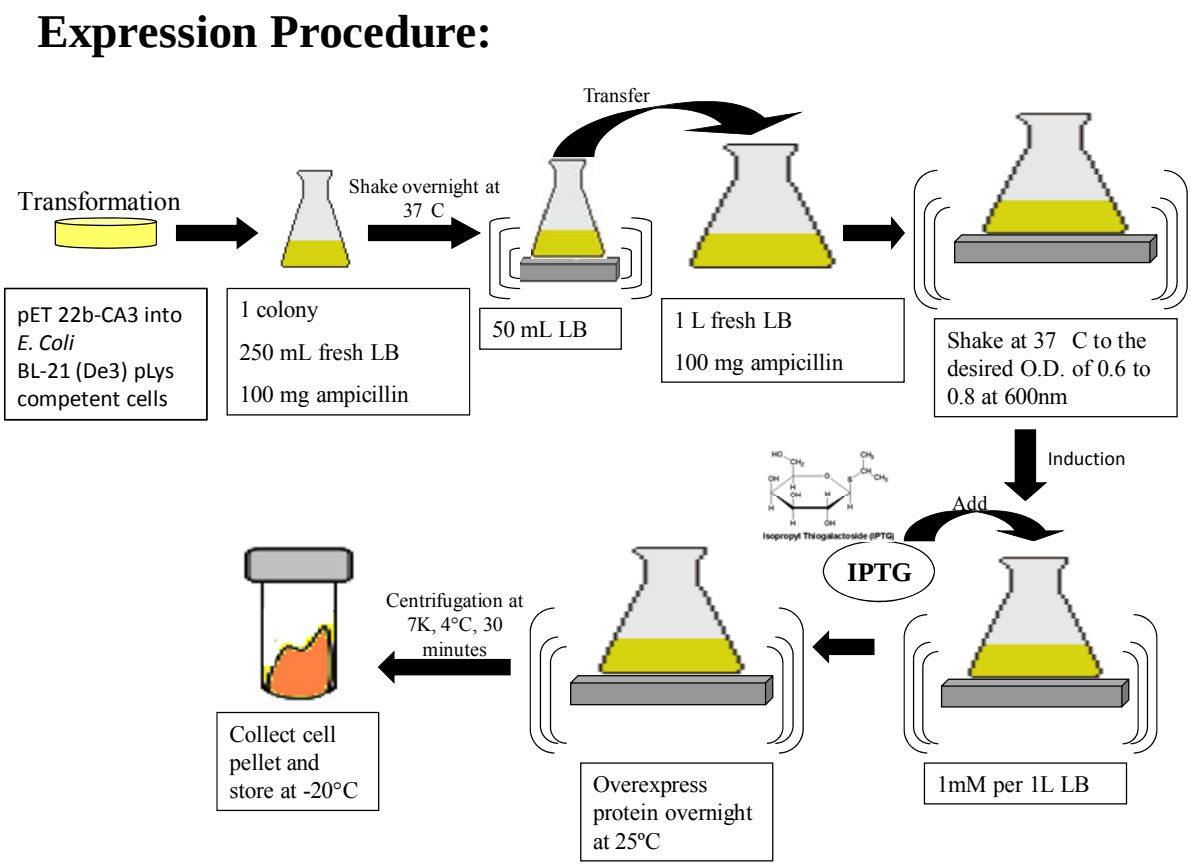

Figure 2.2. Summary of the Expression Procedures for ProCA3 Agents.

The most significant advantage of the overexpression of a recombinant protein is the ability to facilitate purification of high quantities of product. Following a collection of the cell pellet containing the desired protein from the cultured LB media, purification schemes using

sonication/French Press, nucleic acid precipitation, and ion exchange chromatography (IEC) were implemented to effectively extract the variant from the cells with a high degree of purity.

2.3. Tagless Purification

2.3.1. Sonication and French Press

In order to extract the contrast agent from the cultured *E. Coli* cells, their phospholipid bilayer must be fractionated. There are two commonly used techniques to achieve this effect: sonication and French press. Sonication is the act of applying high energy sound waves to disrupt cell membranes and release cellular contents (sonoporation) [32]. Due to its simplistic ease of operation, the sonicator is much easier to use when you have many samples. Additionally, it gives a sample in a water bath an even and consistent vibration, allowing one to achieve the same amount of cell breakage in each sample [32]. French pressure cell press, or French press, is an apparatus used in biological experimentation to disrupt the plasma membrane of cells by passing them through a narrow valve under high pressure [33]. Once past the valve, the pressure drops to atmospheric pressure and generates shear stress that disrupts the cells. French Press is more efficient and doesn't generate heat when breaking cells, but it has a minimum volume requirement (500 μL) [33]. Depending on the volume of protein expressed, researchers may prefer one over the other. There has been no notable difference in efficiency between the two methods for the purposes of these experiments so both were used interchangeably to lyse the cells.

The cell pellet from the expression of a target protein was thawed in a cool water bath and resuspended in 30 mL of 10 mM Tris/HCl pH 7.4 buffer. The mixture was then vortexed with 100 mM phenylmethanesulphonylfluoride (PMSF), a serine protease inhibitor, and separated into two 15 mL volumes to prepare for sonication. Protease inhibitors are necessary if the protein

has increased susceptibility to cleavage by a variety of proteases in solution. They help preserve the yield and quality of purified protein. There are four groups of proteases: serine, cysteine, aspartic and metallo-proteases. Based on protein sequence and published data, one can determine which type of protease inhibitor is best for the purification of his or her protein. The best protease inhibitor to be used for parvalbumin purification methods was one of serine derivation. Following its addition, each sample of protein was sonicated six times for 30 seconds, with one minute cooling increments. The mixture was then centrifuged at 17K for 30 minutes. The supernatant containing the soluble variant protein was collected and the cell pellet was discarded. Samples of both the supernatant and cell pellet were taken for SDS Page gel analysis by the previously described method within the expression protocol.

2.3.2. Nucleic Acid Precipitation

In efforts to isolate the soluble variant via tagless purification methods, DNA and RNA contamination must be removed from the supernatant. A concentration of 1.3µM of benzonuclease- $MgCl_2$, an endonuclease and its cofactor that degrades all forms of DNA and RNA while having no proteolytic activity, was added to the supernatant overnight at 4 ºC. Endonucleases compose a class of restriction enzymes produced by bacteria that typically recognize specific 4- to 8-base pair palindromic sequences, called restriction sites, and then cleave both DNA strands at this site. Thus, the choice for endonuclease type was made based on the sequence of the pET-22b(+) vector.

Previous experiments conducted prior to the Summer 2009 semester were done to determine which concentration of streptomycin sulfate (1%, 3%, 5%, or 10%) was optimal for the removal of nucleic acids and other proteins not thermally stable at high temperatures. It was found that 5% streptomycin sulfate concentration is optimal for nucleic acid precipitation from the protein

supernatant following overnight cleavage of nucleic acids with benzonuclease. Thus, the process of precipitation began with adding 5% streptomycin sulfate, a nucleic acid precipitant, to the solution overnight at 4 ºC. The supernatant was centrifuged and the cell pellet was frozen while subsequent steps of the procedure were applied to the resulting supernatant containing the soluble contrast agent. Incubation in an 85 ºC water bath for 10 minutes and immersion in an ice bath allowed for a visible precipitation of fragmented nucleic acids and proteins lacking thermostability at such a high temperature. For thermostable proteins, the addition of nucleic acid precipitant aids in a higher yield from purification. The extent of protein precipitation is dependent upon the pH of solution and the ratio of precipitant to protein. Streptomycin sulfate is generally favorable over other commercially available precipitants such as, protamine sulfate and manganese chloride. One can also use varying concentrations of ammonium sulfate (concentration depends on properties of protein) to precipitate desired protein from a solution.

The mixture was spun down again at 17K for 30 minutes, allowing one to collect the supernatant and freeze the cell pellet. To lower the salt concentration introduced into the protein supernatant system by streptomycin sulfate, the protein was dialysed in 10mM Tris/HCl pH 7.4 overnight at 4ºC and for two 2 hour sessions under the same conditions the following day in freshly prepared buffer. Next, the supernatant was brought to a concentration of 5 mM EDTA to remove magnesium or calcium from the variant system over a period of one hour. Because the overall negative charge of the protein is reduced in the holo-form, the removal of metals from its binding site hopefully increases the protein's affinity for the chromatographic methods of separation to be discussed. It was then filtered via a syringe through a 0.2 µM membrane and injected onto anionic Q-column using a FPLC system. Samples of both the supernatant and cell

pellet following cell lysis, nucleic acid precipitation, and dialysis were taken for SDS Page gel analysis by the previously described methods.

2.3.3. Ion Exchange Chromatography

The method of chromatographic column separation using FPLC is dependent upon the physical and chemical properties of a protein. If the protein carries a negative charge at the pH of buffer used, as in the case with parvalbumin and its variants, the Q sepharose column, an anionic binding column separating based on charge, is a great method for separation. Using an Amersham Biosciences FPLC system, a 10mL volume of diluted protein supernatant (ranged from a 1:10 to a 1:5 dilution of protein to Buffer A) was injected onto the Q column. Using Buffer A: 10mM Tris/HCl 5mM EDTA pH 8.5 and Buffer B: 10mM Tris/HCl 5mM EDTA 1M NaCl pH 8.5 combination, a modified FPLC separation program was implemented to elute the desired protein at 25% concentration of Buffer B.

Initially, the contrast agent binds to the column with the introduction of Buffer A. Theoretically, any positively charged proteins at pH 8.5 with little affinity for the column will not bind to the column, maintaining a lower retention time than that of parvalbumin or nucleic acids. Thus, these proteins along with smaller fragments of nucleic acids will elute from the column in the first peak monitored by ultraviolet light at 260nm for mutants lacking a tryptophan and at 280nm for those containing a tryptophan. As the Buffer B concentration increases to 25%, the contrast agent will elute from the column in the second peak. The final peak eluted at 100% of Buffer B corresponds to nucleic acids that were initially present in the sample. Previous FPLC experimental conditions allowed for a second FPLC run during which Buffers A and B contained 3mM Ca instead of EDTA. However, this step was eliminated to reduce the number of steps required to isolate the apo-form of the proteins for metal analysis via circular dichroism,

relaxivity, and fluorescence. It is well known that parvalbumin binds calcium with a high affinity and calcium. Additionally, with each successive step of the purification process, there are subsequent consequential losses of protein. Thus, the elimination of this step may also allow for isolation of a higher quantity of protein.

The appropriate peak observed was collected from each injection. The desired protein fractions were concentrated down to a final resuspension in a 4 to 6 mL volume of fresh 10mM Tris/HCl chelexed at pH 7.4. The protein was then dialysed against 10mM Tris/HCl chelex overnight and then for two 2 hour increments the following day at 4˚C. Figure 2.3 and Figure 2.4 summarize the purification procedures.

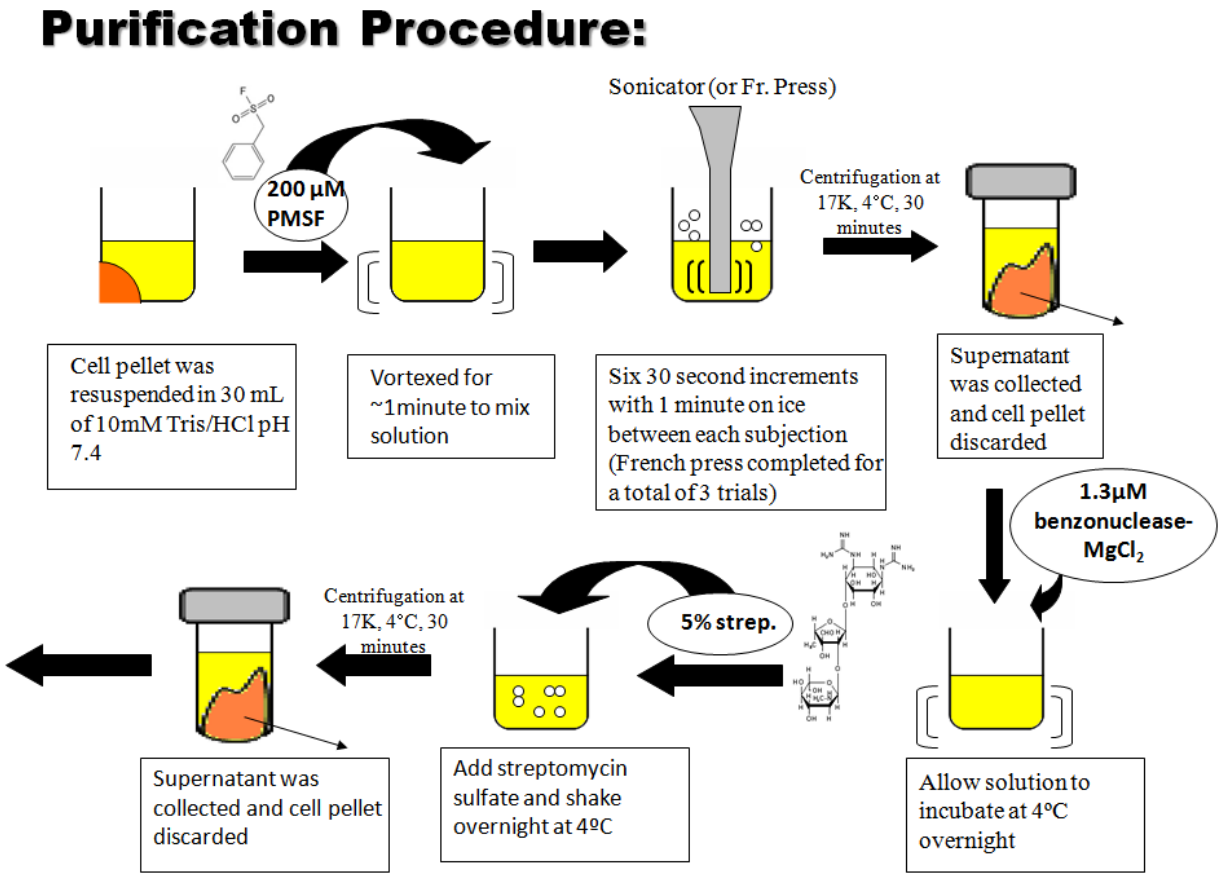

Figure 2.3. Summary of ProCA3 Purification Procedures.

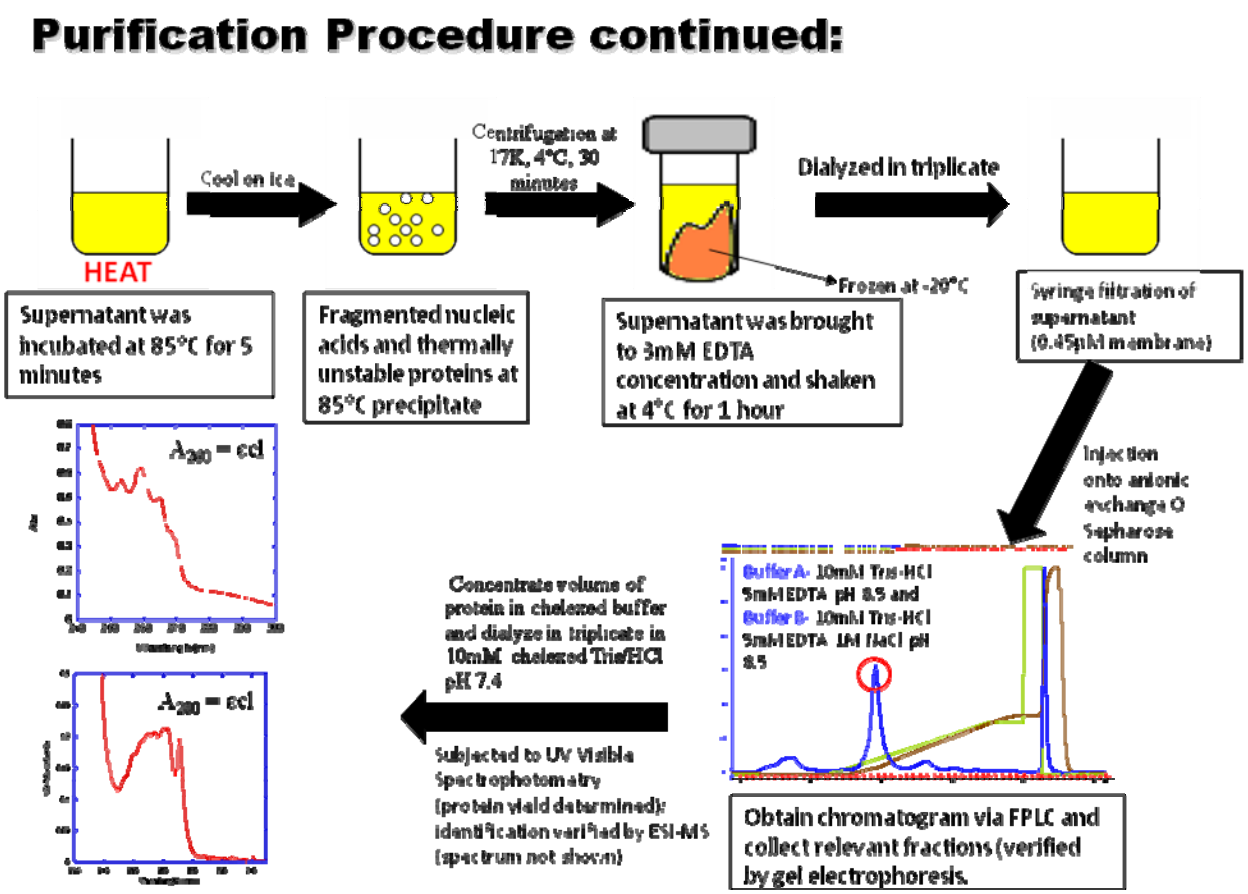

Figure 2.4. Summary of Purification Procedures Continued.

2.3.4. Protein Concentration Calculation

The UV absorbance of the concentrated protein was measured at its characteristic wavelength (previously mentioned) to calculate the final yield of protein and to verify its purity by comparing the spectra obtained to that of published data concerning the wildtype protein and F103W mutant. The concentration was calculated through use of the Beer-Lambert law,

$$A = \epsilon c l, \qquad \text{(Equation 2.1)}$$

where A is the measured absorbance at 260nm (phenylalanine characteristic absorbance) for ProCA-30 and at 280nm (tryptophan characteristic absorbance) for ProCA-31, ProCA-32, and ProCA-33, c is the protein concentration, and l is the path length of the cell (1cm). The molar

extinction coefficient for ProCA-30 is 1600 cm^{-1} while that of the remaining members of Class ProCA-3 is 7200 cm^{-1} [25, 34]. The protein was then stored at -20ºC.

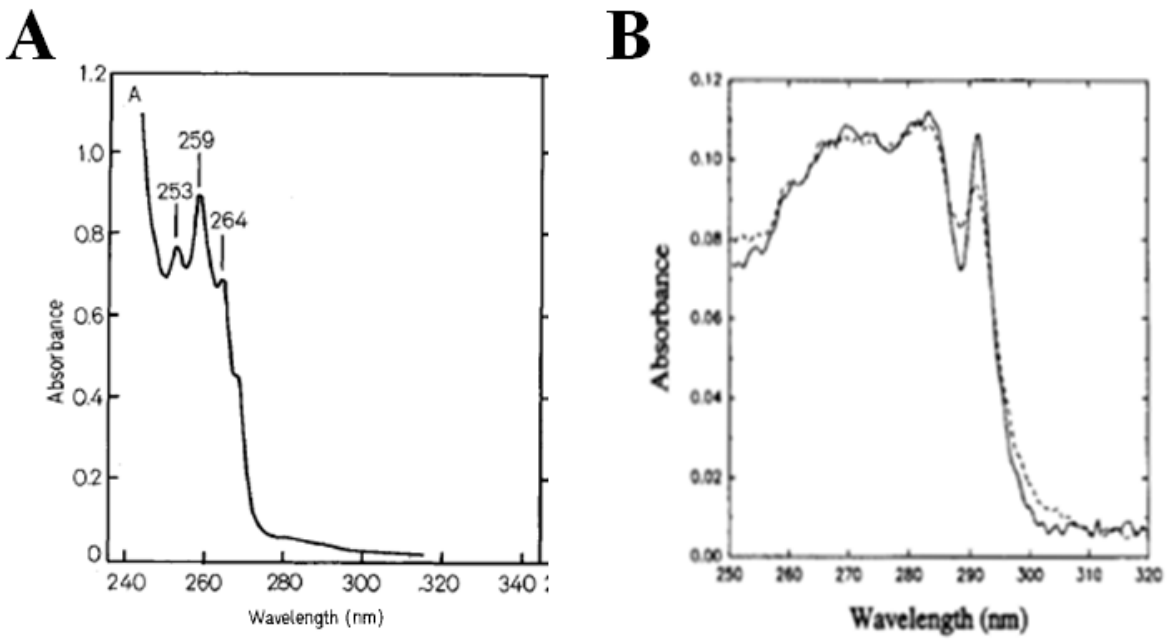

Figure 2.5.Published UV spectrum of Parvalbumin. (A) Wildtype. (B) Parvalbumin-F103W; Dashed line, metal-free form; solid line, Ca2+ loaded form [25, 35].

2.4. Circular Dichroism

Circular Dichroism (CD) is termed as the difference in the absorption of left- and right-handed circularly polarized light of a molecule containing one or more chiral light-absorbing groups [36]. CD measured as a function of wavelength is termed CD spectroscopy. Circular polarized light is converted from linearly polarized light, the sum of two linearly polarized states (horizontal and vertical) at right angles to each other confined to a single plane, using a quarter-wave plate [36]. This birefringent plate allows for the distinction between the refractive indices seen by horizontally and vertically polarized light, slowing one of the linear components of the beam with respect to the other so that they are one quarter-wave out of phase [36]. This produces a beam of either left- or right-circularly polarized light, due to variances in their speed

propagation in the medium. Projection of the resulting amplitude of the beam yields an ellipse instead of the usual line [36].

The chiral character of the molecules measured relies on their existence as non-superimposable pairs of mirror images (enantiomers) [36]. Though the physical and chemical properties of a pair of enantiomers are the same, their optical activity varies and thus allows for delineation between the two using CD spectroscopy. Measurements carried out by the spectrometer in the near and far ultraviolet regions of the electromagnetic spectrum monitor electronic transitions of each chiral chromophore state of a molecule. Thus, the signal will vary as a function of wavelength and reflects an average of the entire molecular population [36]. The CD signal is positive if the left-circularly polarized light is absorbed to a greater extent than the right-circularly polarized light. The signal is negative if the reverse occurs.

Though CD spectroscopy has been widely used in the study of various sizes of chiral molecules, it has been extensively implemented in the study of large biomolecules. More specifically, its role in secondary and tertiary structure determination of proteins has allowed researchers to observe conformational changes due to variations in environmental conditions such as temperature, pH, or interactions with other molecules such as metal ions. The secondary structure is observed in the far ultraviolet range of 250 to 190 nm while the packing interactions of the tertiary fold are observed in the near ultraviolet range of 350 to 250 nm [36]. An alpha-helix absorbs negatively at 208nm and 222 nm and positively at 192 nm while a beta-sheet structure absorbs negative at 218 nm and positive at 196 nm and a random coil absorbs positive at 212 nm and negative at 195 nm [36].

Proteins are composed of amino acids and 19 of the 20 naturally occurring amino acids (exception is glycine) are chiral and thus allow for observation via CD spectroscopy. Protein

chromophores are divided into three classes: the peptide bond, the amino acid sidechains, and any prosthetic groups [36]. For example, disulfide group of cysteine is an inherently asymmetric chromophore as it prefers a gauche conformation with a broad CD absorption around 250 nm. Additionally, the three aromatic side chains that occur in proteins (phenyl group of Phe, phenolic group of Tyr, and indole group of Trp) also have absorption bands in the ultraviolet spectrum. However, in proteins, their contribution to the CD spectra in the far UV (where secondary structural information is located) is usually negligible [36]. Aromatic residues, if unusually abundant, can have significant effects on the CD spectra in the region < 230 nm, complicating analysis.

Changes in CD signal stem from changes in protein structure. These changes are often observed in the presence of various metal ions. For example, previous studies conducted by A. Szent-Gyorgyi investigate the citric acid (oxygen metabolism) cycle (1941) in which subsequent electron transfers occur in eight proteins, which lead to the hypothesis that proteins act as conductors [37]. A group of researchers isolated and purified metal-doped (Cu_2O, CdO and PbO) muscle protein from fish (*Clarious batracus* Lin.) and characterized its potential as semiconducting biopolymer [37]. Initial characterization studies observed secondary structure changes of the isolated protein in the presence of Cd, Pb, and Cu using CD (Figure 2.6).

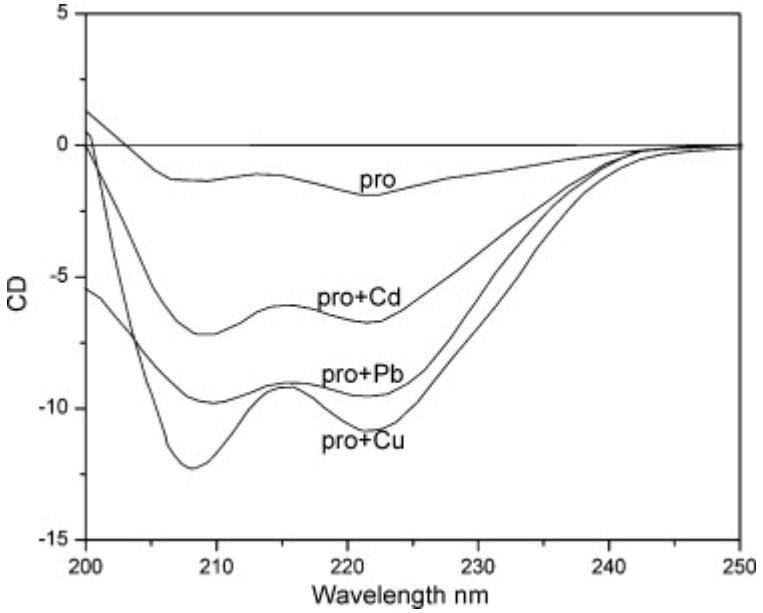

Figure 2.6. CD spectrum of protein with and without metal-doped (a) pro, (b) pro-Cd, (c) pro-Pb and (d) pro-Cu [37].

The scientists wanted to ensure the structural dependence of the protein with the metal ion. From the figure, one can observe that helicity decreased as the metals of increasing size were added to the protein. The authors attributed this phenomenon to the slight weakening of the hydrogen bonds caused by the insertion of larger metal ions [37]. This figure indicates that the protein has undergone a simple transformation from twisted coil to alpha-helix. From this study and countless others, one can see the usefulness of CD as a tool to probe changes in protein structure. More specifically, this spectroscopic technique can be used to evaluate structural changes induced by the binding of the ProCA3 agents to various metals.

The secondary structural changes, if any, of each agent in the presence of magnesium, calcium, gadolinium, and terbium were analyzed. The parameters for the CD instrument were set as follows: 0.5 nm data pitch, continuous scanning mode, 100 nm/min scanning speed, 1 sec response, 1 nm band width, 7 accumulation for the scans. Initially, the buffer 10 mM Tris/HCl (100 mM NaCl) chelex pH 7.4 was scanned. This spectrum was subtracted from the UV spectra

to follow. The second sample scanned consisted of the previous buffer system of the first sample containing 5 to 10 μM protein. The characteristic absorption of this alpha-helical protein was noted. The addition of calcium, gadolinium, terbium, or magnesium in this system for the consecutive samples was completed to observe any spectral changes in conformation. Appropriate background absorptions were subtracted for the samples with added metal. Analysis of the stability of the protein's structure as well as its conformational behavior in the presence of varying metal environments can be analyzed.

2.5. Fluorescence Spectroscopy

The length of time necessary for each member of Class ProCA-3 to equilibrate with gadolinium for accurate measurement of relaxation times was unknown. Thus, fluorescence spectroscopy was used to determine the appropriate metal equilibration time for preparing the relaxivity samples for measurement. It is well known that the length of time required is heavily dependent upon the binding affinity of the protein to gadolinium. Assuming that the member of Class ProCA-3 displaying the weakest binding affinity to gadolinium will require the longest amount of time to reach metal equilibration, ProCA-31 was chosen as the test subject. *It is important to note here that all dissociation constants were measured via terbium fluorescent metal competition experiments by Sr. PhD researcher David Xue.*

The parameters for an emission scan using the fluorimeter were set as follows: digital configuration, λ_{exc}- 552 nm (per manufacturer's recommendation), $\lambda_{em.}$- 560-650 nm (per manufacturer's recommendation), length: 90 nm, step size: 1 nm, integration: 0.2 seconds, averages: 1, and slit widths: excitation- 0.32 and emission-0.50. A stock sample of 100μM of ProCA-31 and 200μM of gadolinium was incubated at 37˚C over the following time points: 30

minutes, 3 hours, and overnight. Separately, a 10µM stock of Rhodamine-5N tripotassium salt, a weak calcium dye, was prepared in 100mM Tris/HCl 100mM NaCl chelex pH 7.44 (Figure 2.7).

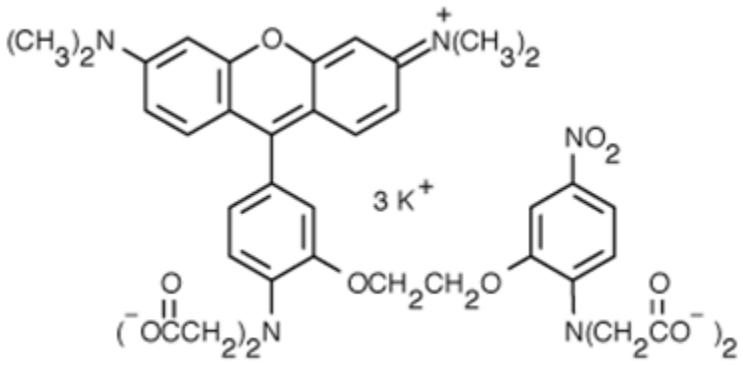

Figure 2.7. Chemical structure of rhodamine-5N tripotassium salt used in fluorescence titrations [38].

At the start of each time point, the fluorescent signal intensity of free 10µM Rhodamine-5N was measured. Then, a calculated volume of ProCA-31-Gd^{3+} from the stock sample was mixed with the 10µM Rhodamine-5N to yield a final concentration of 20µM ProCA-31 to 40µM gadolinium concentration in an 800µL volume. A subsequent scan of this sample's increased fluorescent signal was measured (Figure 2.8). Next, increasing amounts of gadolinium was titrated into the system until free Rhodamine-5N became saturated, as indicated by the absence of change in increasing fluorescence intensity. Then, a predetermined concentration of EGTA was added to the system to chelate the metal bound both to Rhodamine-5N and protein and decrease the fluorescent signal back to the baseline of fluorescent intensity (Figure 2.8).

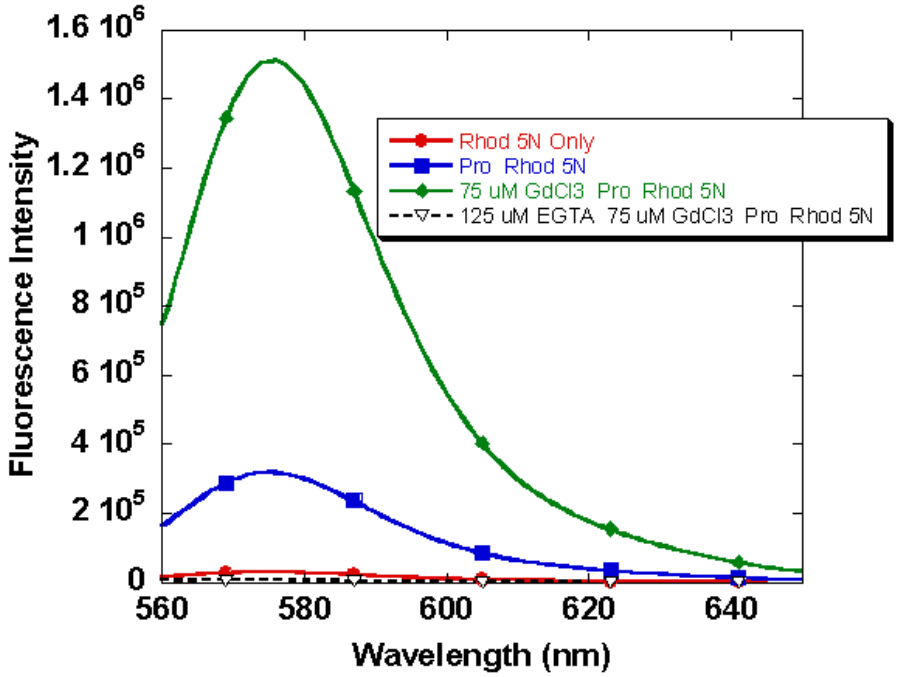

Figure 2.8. Fluorescence spectrum of free metal titration experiment.

The pH of the dye stock sample, the stock sample, and the EGTA added sample was monitored to ensure that the pH values remained close to the original conditions of 7.44. The maximum intensity of each scan was recorded and substituted into the following equation to yield the concentration of free metal remaining in solution:

$$[M]_{free,}\, M = K_d(F - F_0)/ (F_{max} - F) \quad [38], \qquad \text{(Equation 2.2)}$$

where K_d represents the binding affinity of ProCA-31 to gadolinium (previously determined to be 1.04×10^{-11}), F represents the maximum fluorescence intensity of the peak corresponding to the ProCA-31-Gd^{3+} complex and dye, F_0 represents the EGTA treated sample that returns the signal to baseline, and F_{max} represents the maximum intensity of the peak corresponding to the ProCA-31-Gd^{3+} complex and dye saturated with gadolinium [38]. The incubation time yielding the lowest concentration of free metal was chosen to be the standard time allowed for metal equilibration of future relaxivity samples.

2.6. Relaxometry

The T1 and T2 values of protein and/or metal samples were measured using a Bruker Minispec combined with an mq60 NMR Analyzer at 37ºC, a temperature monitored and controlled by a digitally operated water bath, at 60MHz or 1.5 Tesla. Verification of the temperature was also obtained manually using an alcohol thermometer. The samples to be measured consisted of either a 10mM Tris/HCl chelex pH 7.4 (low salt) or 10mM Tris/HCl 100mM NaCl chelex pH 7.4 (high salt) buffering system, in which varying concentrations (10 to 50μM) of a desired protein was suspended. An amount of metal, either calcium or gadolinium, was added in a one to one or one to two concentration relative to the protein concentration to observe changes in relaxivity. Additionally, experiments were conducted using a fixed concentration of gadolinium and varying ProCA-3 concentration to determine whether the binding of the metal to ProCA-3 is one to one or one to two. The average relaxivity from this experiment is taken as the average of the relaxivity of ratios located in the plateau portion of the curve. The following equation was used to calculate the relaxivity with respect to each relaxation time:

$$1/T_{1,2} = (1/T_{1,2\ \text{sample}} - 1/T_{1,2\ \text{buffer}})/\ [Gd^{3+}] \quad [10]. \qquad \text{(Equation 2.3)}$$

Using a Bruker Minispec application program, basic instrumental parameters were checked using a mineral oil sample. Following a daily check of the instrumental parameters (to be performed once per day of use), the instrumental gain was tuned using a buffer only sample. The gain value obtained for the T2 program was used for the T1 program. Each sample was measured in the following fashion: T2 first and then T1, with a 5 minute warming time for each sample at 37ºC prior to measurement. Following collection of data, the percent of T1 and T2 signals were plotted in Kaleidagraph 3.5 as a function of time to chart the change in relaxation signal over

time. For fixed ratio experiments, the data obtained was plotted in Kaleidagraph 3.5 as protein concentration vs. 1/T1 or 1/T2 to yield R1 and R2 values. For varying ratio experiments at a fixed concentration of gadolinium, the data obtained was plotted in Kaleidagraph 3.5 as protein concentration vs. 1/T1 or 1/T2, yielding averaged R1 and R2 values from the plateau portion of the curve and allowing one to infer the binding mode of the contrast agent to gadolinium: 1 to 1 or 1 to 2. By nature of design, we anticipate that the binding mode is 1 to 2.

3. EXPRESSION AND PURIFICATION RESULTS

3.1. Background

To obtain a large quantity of contrast agent for animal model studies and future clinical trials, it is extremely important to have a time-effective, cost conscientious, well established protocol for achieving a high yield of purified Class ProCA-3 agents. In this chapter, the expression results will reveal that each designed contrast agent of this class was successfully overexpressed using the aforementioned expression protocol in the chapter 2. Following improvements and modifications made to the established protocol for parvalbumin expression and purification, it will be later shown that members of Class ProCA-3 can be effectively isolated and purified. Studies were performed to improve the product yield by overcoming the limitations associated with the isolation of a tagless protein from nucleic acids coexisting in the supernatant following cell lysis.

3.2. Expression Results

As discussed in section 2.2.1, pilot expression procedures were implemented to analyze the cell strain and IPTG concentration optimal for overexpression of protein. Figure 3.1 indicates that the cells of all tested strains grew fairly well in LB media. Here, it's evident that BL-21(De3) pLysS and Tuner (De3) pLac I cell strains grew best prior to overnight incubation. After overnight growth, there seems to be no considerable difference in cellular growth amongst the different strains. Additionally, the varied concentrations of IPTG appear to have little to no effect on cell growth for all tested cell strains.

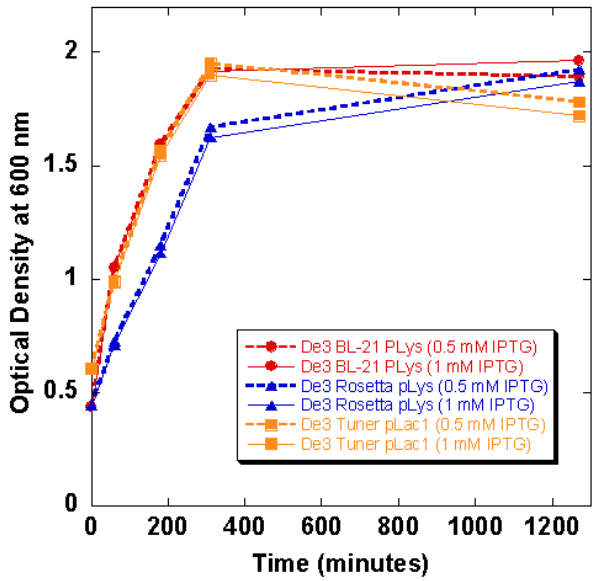

Figure 3.1. Cellular growth curve of pilot expression results.

Unlike previous expression experiments, SDS-PAGE analysis reveals that the BL-21 (De3) pLys strain did not overexpress the protein very well (Figure 3.2). The Rosetta pLysS expressed ProCA-30 at an intermediate level of expression compared to the enhanced overexpression in the Tuner pLacI strain. There appears to be little preference for overexpression between the two varying IPTG concentrations.

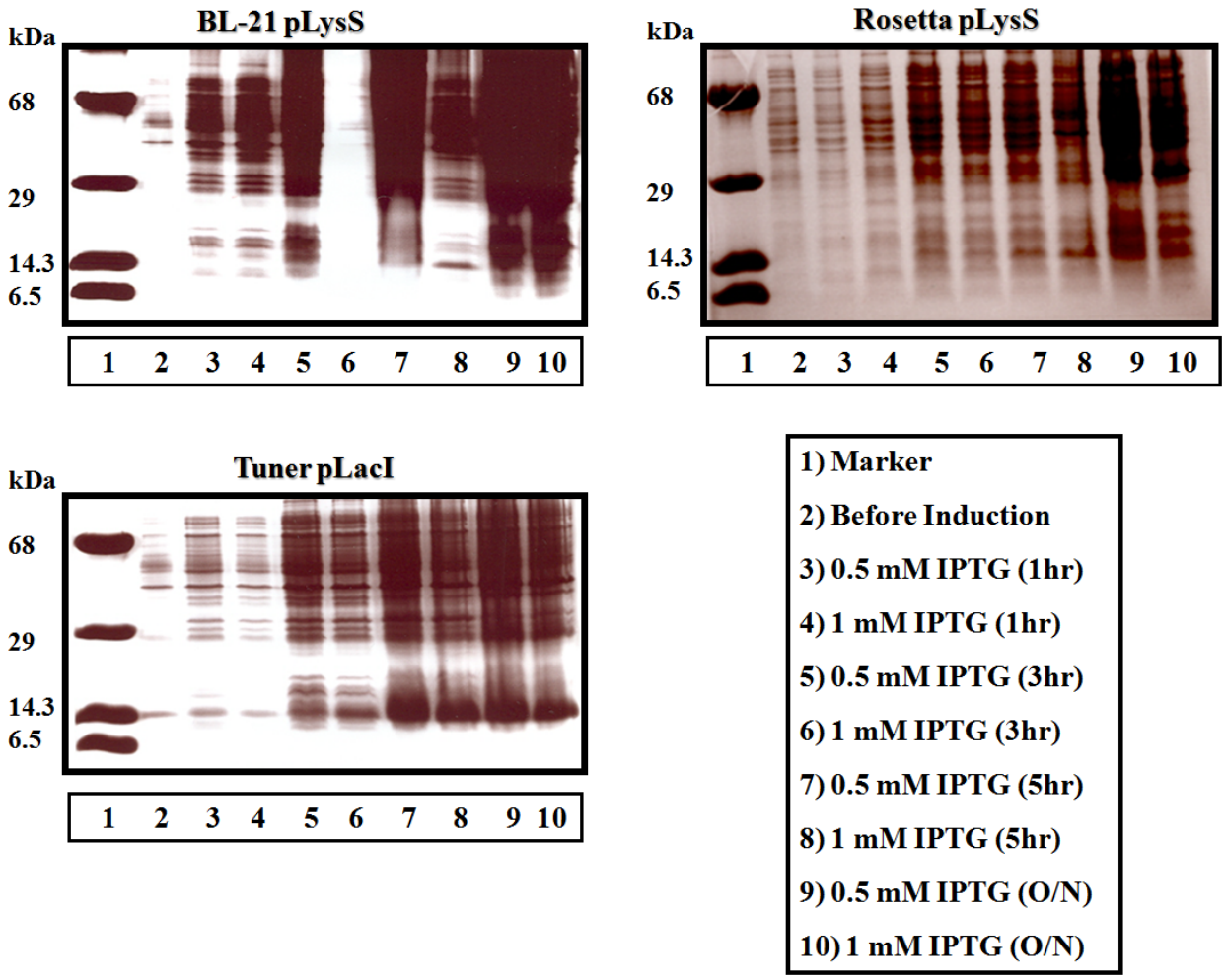

Figure 3.2. SDS-PAGE gel pilot expression results.

Taking into account the previous expression experiments of ProCA-30, the BL-21 pLys (De3) strain at 1mM IPTG allows for expression exclusively in the supernatant. The Tuner strain allowed for expression both in the supernatant and inclusion bodies (Figure 3.3). This condition is not favorable as the protein from each location will have to be purified separately. Protein expressed in the supernatant will be in a soluble form and likely folded properly. The protein expressed in the inclusion bodies will likely not be properly folded. The Rosetta pLys strain did not yield any protein in the supernatant. It was decided to continue expression in the BL-21 pLys (De3) strain to simplify purification of the tagless protein.

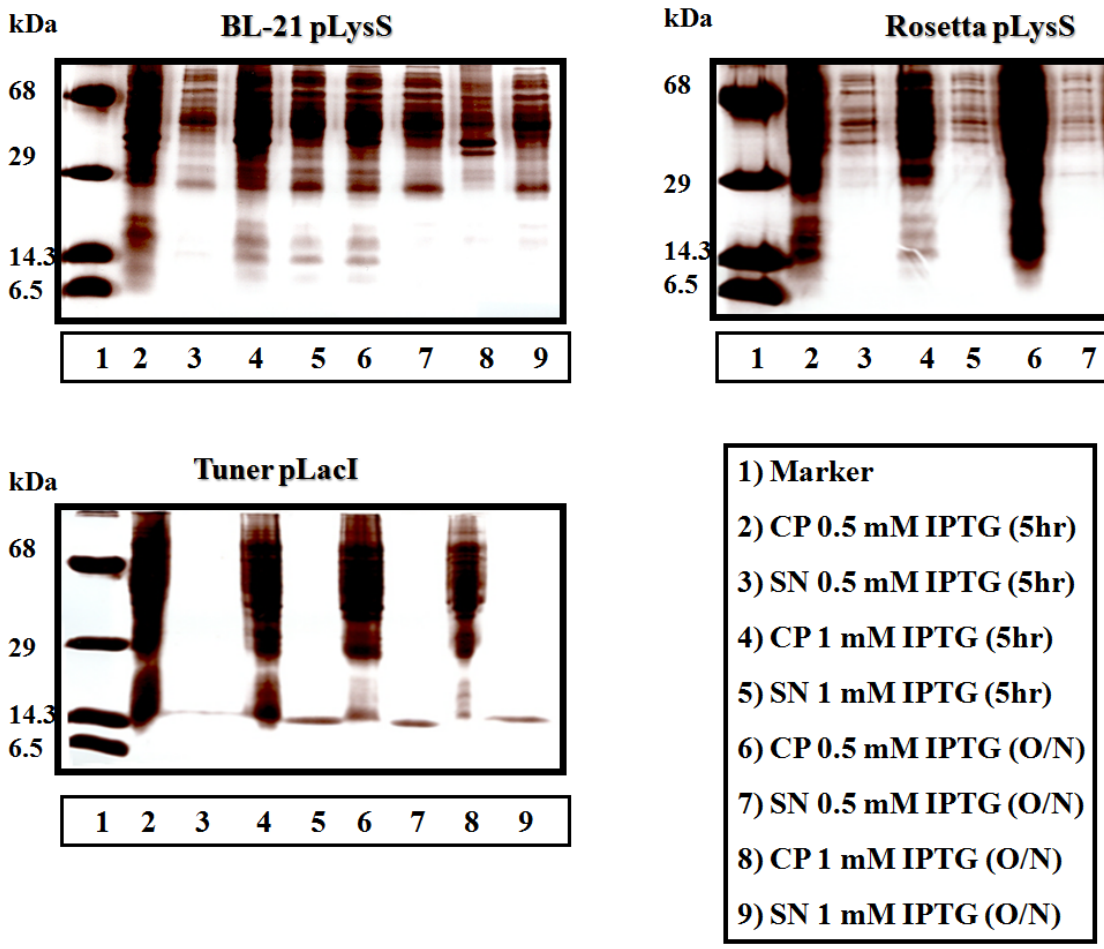

Figure 3.3. SDS-PAGE gel results following pilot expression cell fractionation.

ProCA-30

Following successful transformation of pET-22b(+)-ProCA-30 into BL-21 pLys cells, the procedures implemented for expression were identical to those described in the materials and methods section. According to the increasing optical density of cell culture, the cloned cells containing the gene encoding for ProCA-30 grew very well (Figure 3.4A). This observation was further evidenced by the increasingly "cloudy" appearance of the cell culture as incubation time increased. SDS-PAGE gel analysis indicates that there was little desired ProCA-30 expressed prior to induction with IPTG (Figure 3.4B). Following induction, it is clear that the heavier bands on the gel for samples after IPTG addition as compared to the one before induction

indicate that not only did the cells receive the signal to begin expressing the variant in high yield but a significant amount of protein was overexpressed. There was only a slight difference in the density of bands on the gel before and after overnight growth following induction. This indicates that overnight growth at a reduced temperature did little to significantly enhance the overexpression of ProCA-30. However, this effect observed is not sufficient to modify the procedure and eliminate overnight growth. Further expression of ProCA-30 and its variants are necessary to make such a conclusive decision.

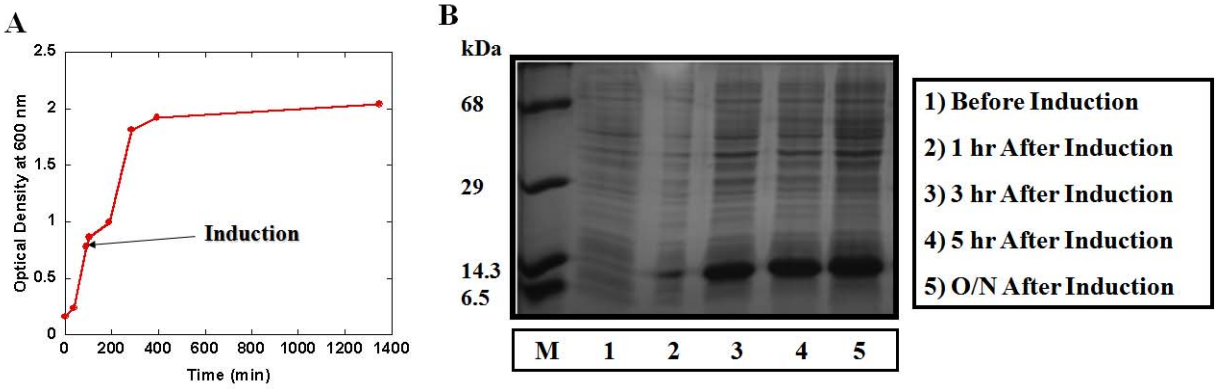

Figure 3.4. ProCA-30 Overexpression. (A) E. Coli ProCA-30 cellular growth curve. (B) ProCA-30 overexpression in E. Coli BL-21 pLys (DE3) cells in LB media.

ProCA-31

Following successful transformation gene of pET-22b(+)-ProCA-31 into BL-21 pLys cells, the contrast agent was expressed according to the methods described in the materials and methods section. According to the increasing optical density of cell culture, the cloned cells containing the gene encoding for ProCA-31 grew very well (Figure 3.5A). Like the expression of ProCA-30, this observation was further evidenced by the increasingly "cloudy" appearance of the cell culture as incubation time increased. It appears that a small amount of ProCA-31 was expressed prior to induction. To provide an explanation for the faint bands in lanes 2 and 3 of the SDS-PAGE gel, it is important to note that the top closing the eppendorf tubes of samples from 1

and 3 hours after induction were not secure (Figure 3.5B). Therefore, these samples were diluted during the boiling step prior to running SDS-PAGE. Following induction, the heavier bands on the gel for 5 hr and overnight samples indicate that a significant amount of protein was overexpressed. There was little difference in the density of bands on the gel before and after overnight growth following induction. This indicates that overnight growth at a reduced temperature did little to significantly enhance the overexpression of ProCA-30. Still, this effect observed is not sufficient to modify the procedure and eliminate overnight growth. Further expression of ProCA-31 and the remaining members of Class ProCA-3 are necessary to make such a conclusive decision.

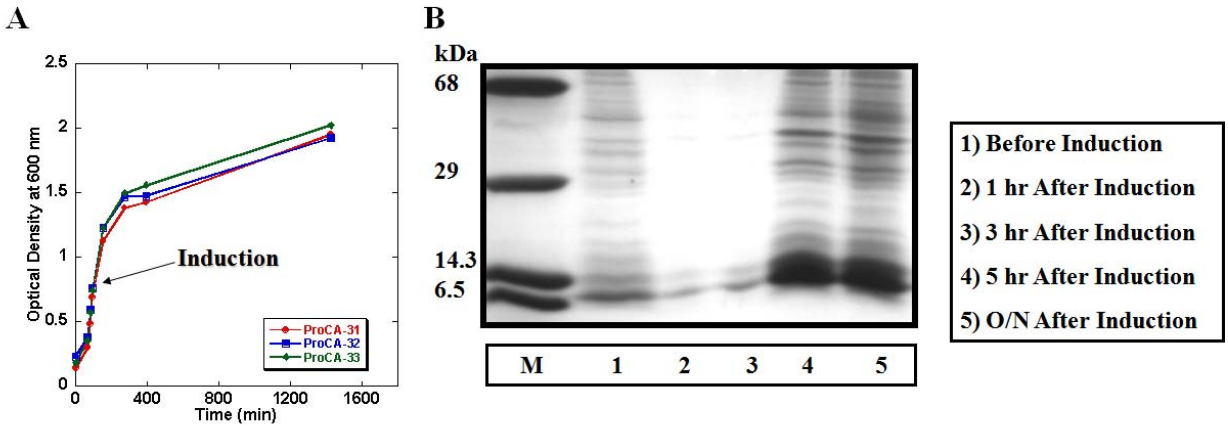

Figure 3.5. ProCA-31 Overexpression. (A) *E.* Coli ProCA-31cellular growth curve. (B) ProCA-31 overexpression in *E. Coli* BL-21 pLys (DE3) cells in LB media.

ProCA-32

pET-22b(+)-ProCA-32 was transformed into BL-21 pLys cells and expressed according to the procedures described in the materials and methods section. According to the increasing optical density of cell culture, the cloned cells containing the gene encoding for ProCA-32 grew very well (Figure 3.6A). SDS-PAGE gel analysis indicates that there was a fair amount of protein expressed prior to induction with IPTG (Figure 3.6B). There is little difference between 1

and 3 hour induced states. Furthermore, provided an equal amount of each sample was loaded onto the gel, overnight condition after induction yields slightly more desired protein when compared to 5 hours following induction. Overall, it is clear that a significant amount of protein was overexpressed during this expression experiment.

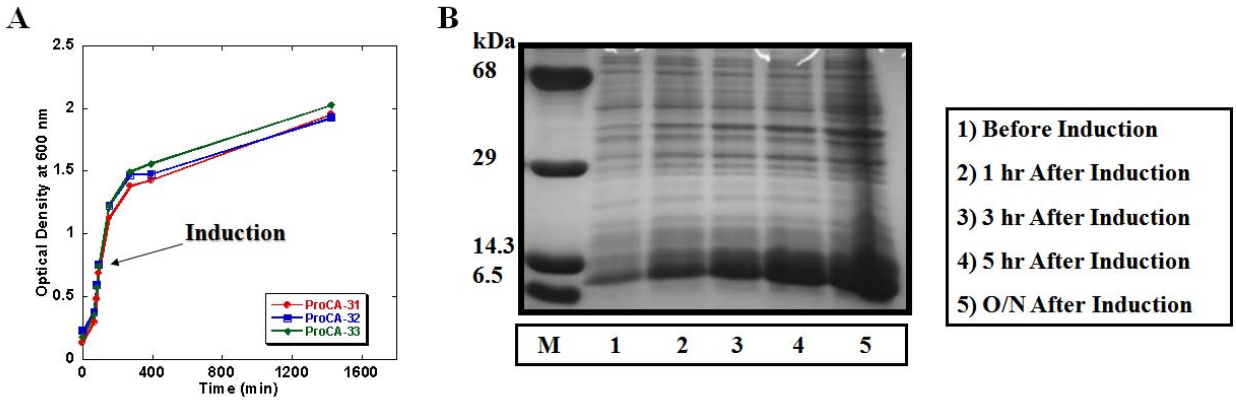

Figure 3.6. ProCA-32 Overexpression. (A) E. Coli ProCA-32 cellular growth curve. (B) ProCA-32 overexpression in E. Coli BL-21 pLys (DE3) cells in LB media.

ProCA-33

pET-22b(+)-ProCA-33 was successfully transformed into BL-21 pLys cells. The procedures for expression were identical to those described in the materials and methods section. According to the increasing optical density of cell culture and the increasingly "cloudy" appearance of the cell culture as incubation time increased, the cloned cells containing the gene encoding for ProCA-33 grew very well (Figure 3.7A). Although SDS-PAGE gel analysis indicates that there was a small amount of protein expressed prior to induction, the increased density of bands on the gel for samples following induction indicate that a significant amount of protein was overexpressed (Figure 3.7B). Like ProCA-32 overexpression, there was a notable difference in the density of bands on the gel for 5 hour and overnight growth after induction.

This indicates that overnight growth at a reduced temperature enhances the overexpression of ProCA-33.

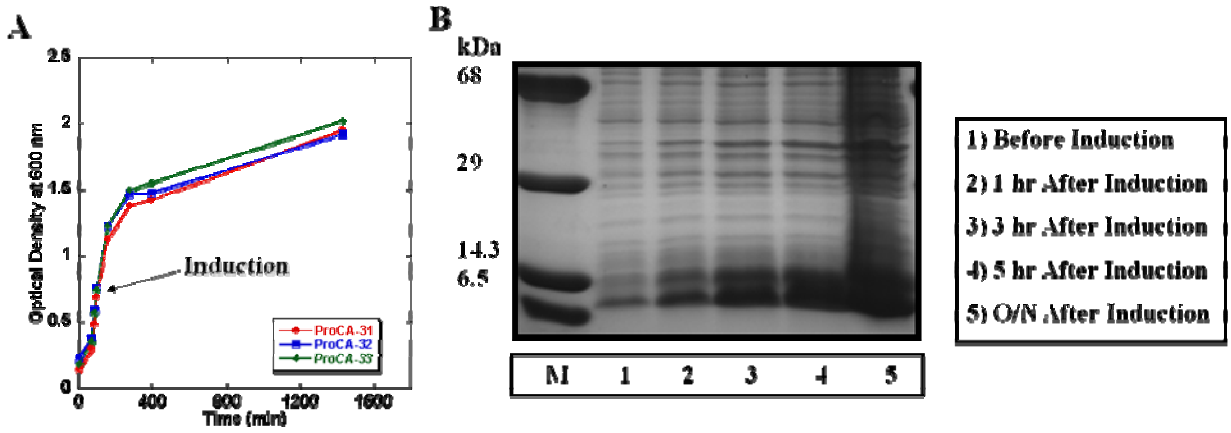

Figure 3.7. ProCA-33 Overexpression. (A) E. Coli ProCA-33 cellular growth curve. (B) ProCA-33 overexpression in E. Coli BL-21 pLys (DE3) cells in LB media.

3.3. Optimizing the Purification Protocol

3.3.1. Old Purification Method and Its Limitations

The original purification protocol was identical to the current protocol with the following exceptions: a 1% streptomycin sulfate concentration was used, there was no dialysis step introduced prior to injection of the supernatant onto the Q-column, the pH of the FPLC buffers was 7.4, the program for FPLC separation was not optimized, and a second FPLC run using another set of buffers introducing calcium into the system was introduced (Figure 3.8).

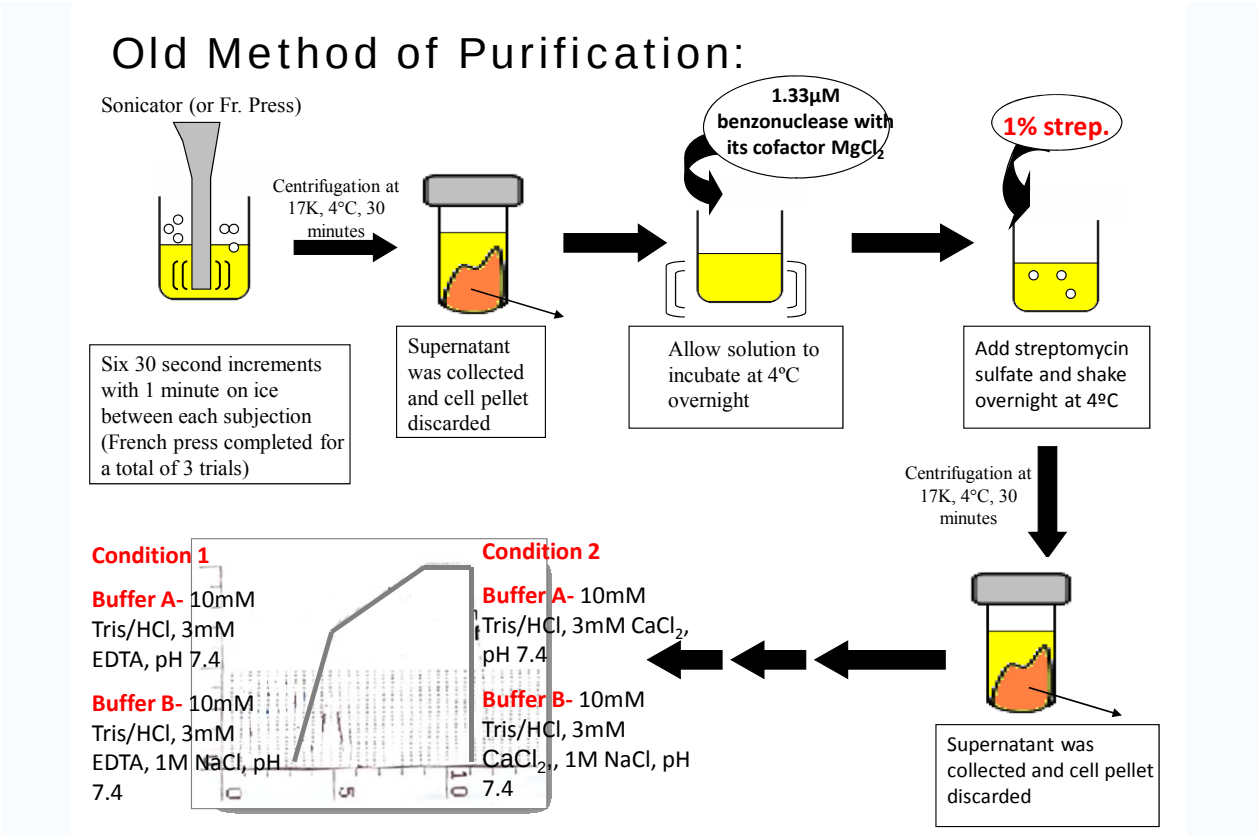

Figure 3.8. Original purification protocol prior to modifications.

For simplification purposes, the expression gels pertaining to the purification results using the older protocol are not depicted. However, it's important to note that the expression results from these experiments were comparable to those mentioned in the previous section. The results for each ProCA-3 member purified according to the original purification methods described in Figure 3.8 are as follows:

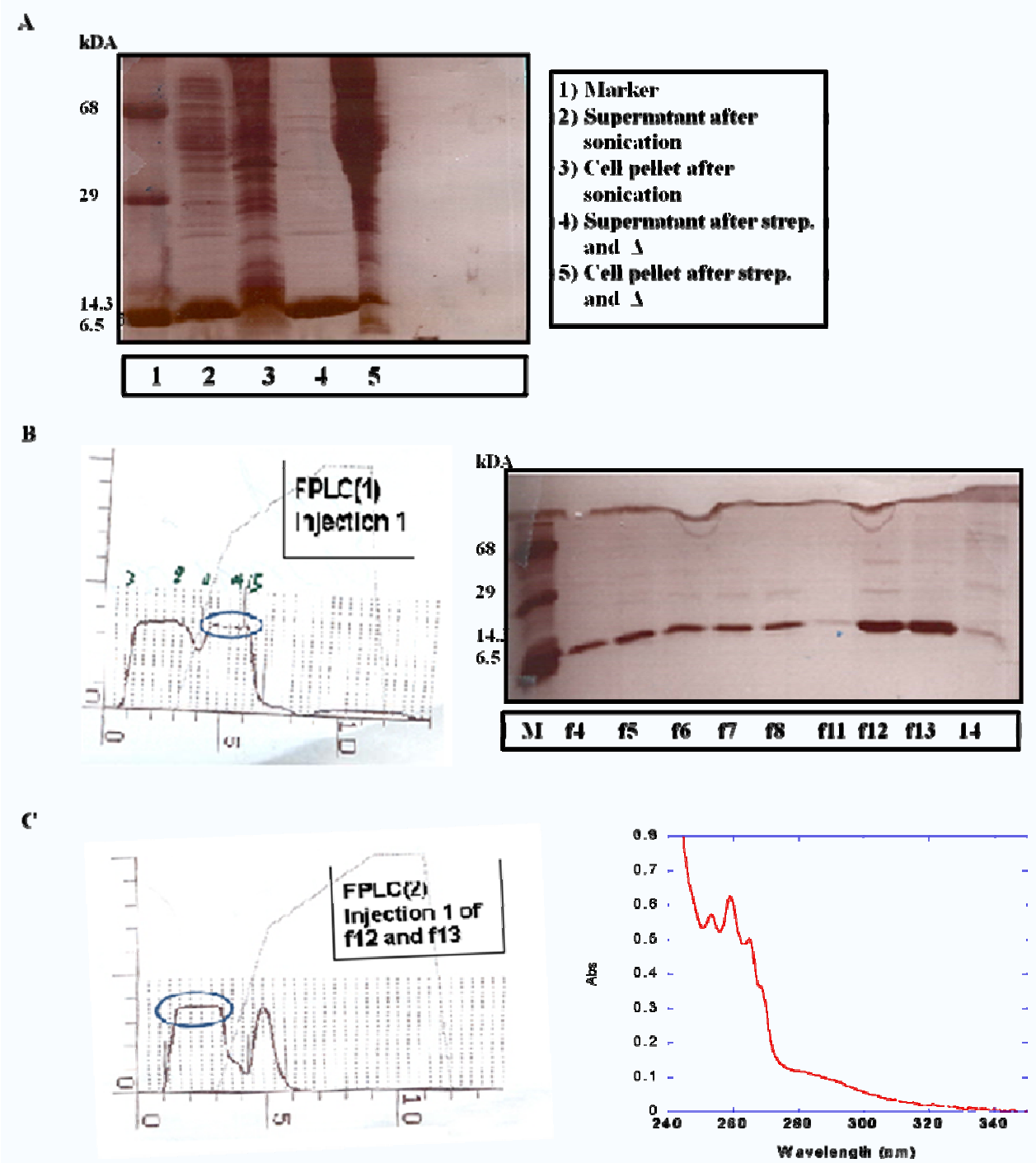

Figure 3.9. ProCA-30 Old Purification Protocol Results. (A) SDS-PAGE from purification. (B) FPLC Condition 1 in the absence of calcium. (C) Left to Right: FPLC Condition 2 results in the presence of calcium and UV-Spectrum results of collected fractions.

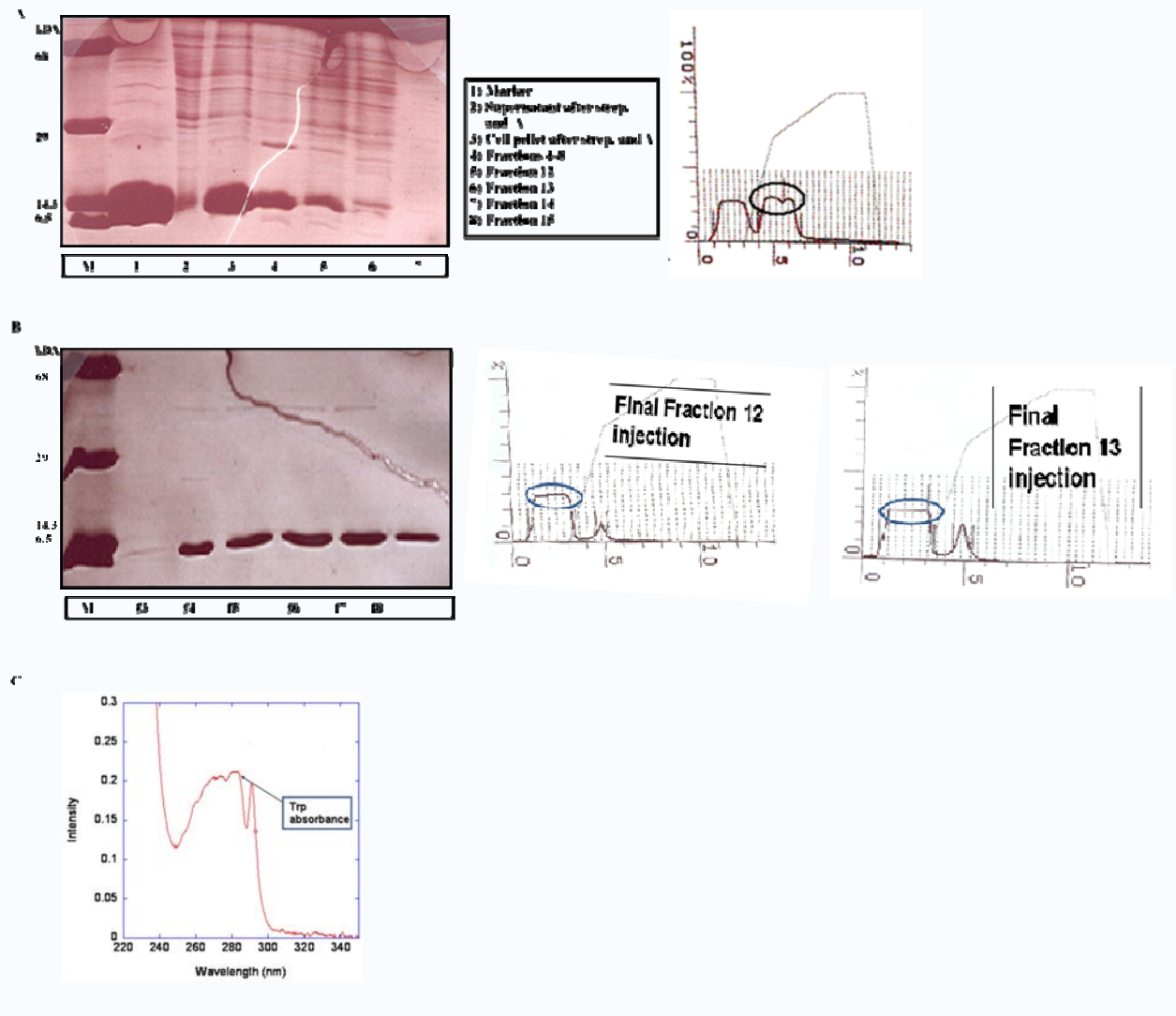

Figure 3.10. ProCA-31 Old Purification Protocol Results. (A) SDS-PAGE from purification and FPLC Condition 1 in the absence of calcium. (B) FPLC Condition 2 results in the presence of calcium. (C) UV-Spectrum results of collected fractions.

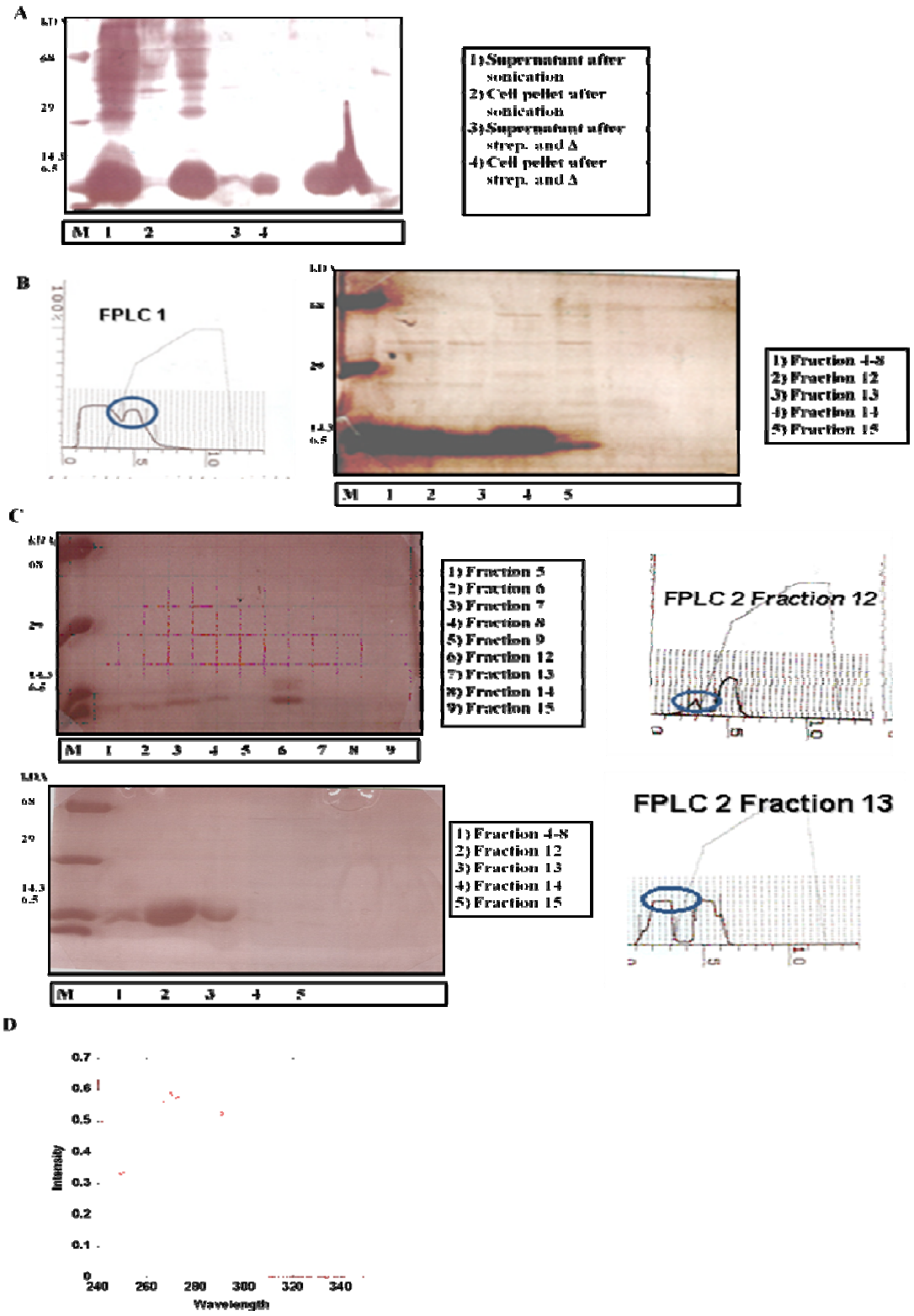

Figure 3.11. ProCA-32 Old Purification Protocol Results. (A) SDS-PAGE from purification. (B) FPLC Condition 1 in the absence of calcium. (C) FPLC Condition 2 results in the presence of calcium. (D) UV-Spectrum results of collected fractions.

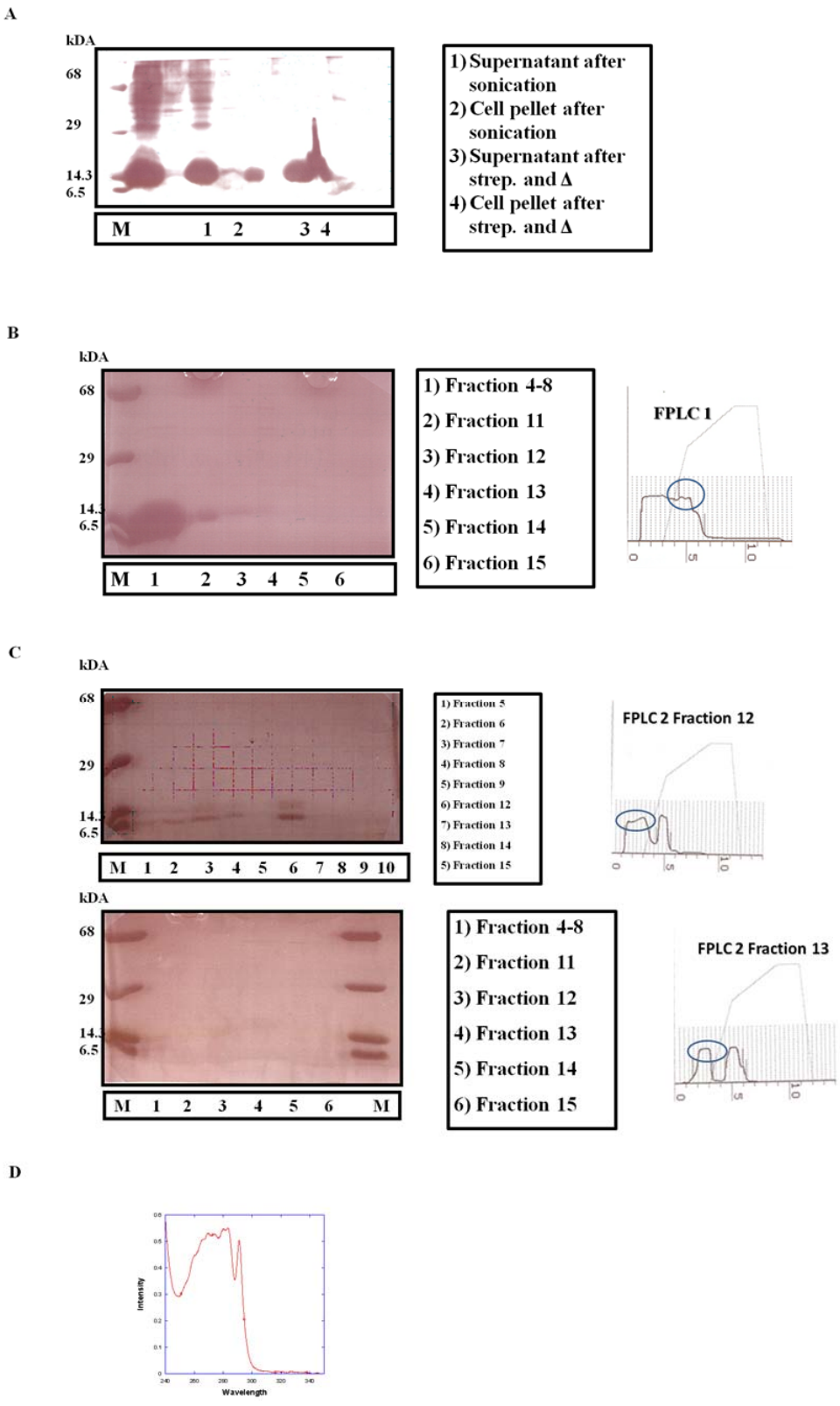

Figure 3.12. ProCA-33 Old Purification Protocol Results. (A) SDS-PAGE from purification. (B) FPLC Condition 1 in the absence of calcium. (C) FPLC Condition 2 results in the presence of calcium. (D) UV-Spectrum results of collected fractions.

There are several limitations to the old purification methods used to extract Class ProCA-3 agents from an *E.Coli* cell pellet: Q-column overloading, high concentration of nucleic acids present in supernatant, inability to separate protein from nucleic acid due to inefficient FPLC salt gradient method, and loss of protein during the second FPLC condition when calcium is introduced into the system. As one can infer from Figures 3.9 -3.12, the purification gels reveal that the predominant protein injected onto the Q-column is the desired overexpressed variant. Prior to FPLC injection, there is little undesired protein present in the supernatant. At this stage, it was assumed that the predominant biomolecules present in the supernatant were the desired contrast agent and nucleic acids (verified by UV-spectrum). However, FPLC condition 1 (no calcium) and condition 2 (in presence of calcium) chromatograms clearly indicate that the proteins are not binding to the column well, eluting from the column before the salt gradient is introduced for both conditions 1 and 2 FPLC injections. This is also evidenced by the bands pertaining to the collected fractions at approximately 12 kDa on the SDS Page gels. Because nucleic acids are negatively charged in solution at pH 7.4, they have a higher affinity for anionic Q-column than the contrast agents. It's possible that the column efficiency was reduced due to the inability of 1% streptomycin sulfate, supplemented with heat, to precipitate the substantial concentration of nucleic acids that coexist with the desired contrast agent in the supernatant prior to FPLC injection. Thus, the column became saturated with the high concentration of nucleic acids remaining in the supernatant and reduced the column's capacity to bind the contrast agents. Additionally, it's evident that the FPLC salt gradient may not be optimal for separation. It increases sharply to 70% NaCl and steadily to 100% NaCl. Because the members of Class ProCA-3 bind calcium very strongly, on the order of 10^{-9}M, it is very difficult to achieve the apo-form of the variants for future analysis. Therefore, other than the consequential loss of

protein associated with an increase in subsequent purification steps, the second FPLC condition introducing calcium into the purification system is not ideal. Thus, modifications to this protocol will be devoted to increasing column capacity by cleaning the Q-column more efficiently with a combination of ethanol, 1M NaCl, deionized water, and Buffer A prior to injection and by decreasing the amount of nucleic acids coexisting in the supernatant. Furthermore, diluting the highly concentrated supernatant before FPLC injection and modifying the salt gradient of the FPLC program to allow for effective isolation of the desired contrast agent will significantly improve the purification yield.

3.3.2. Streptomycin Variation to Reduce Nucleic Acid Concentration in the Supernatant

The members of Class ProCA-3 agents are soluble variants that typically lie in the supernatant following cell lysis. It is well known that nucleic acids are also very soluble and lie in the supernatant. Because both nucleic acids and the variants of this class are negatively charged in solution, the primary goal is to isolate a pure, functional form of each contrast agent devoid of any "contamination," including nucleic acids. More specifically, it was thought that the presence of a high concentration of similarly negatively charged nucleic acids in the supernatant injected onto the Q-column could possibly saturate the positively charged column and decrease its efficiency by interfering with the proteins' optimal binding. For the purposes of this thesis, three variants of ProCA-30 were arbitrarily chosen reducing the concentration of nucleic acids in the supernatant: PV-S56D, PV-E60D, and PV-G99D.

Prior to streptomycin treatment for purification, a 1mL sample of each mutant was treated with 1%, 3%, 5%, and 10% streptomycin sulfate to observe which concentration was optimal for the removal of nucleic acids and other proteins not thermally stable at high temperatures. The effects of concentrations of streptomycin sulfate above 10% were not investigated in efforts to

reduce the amount of "impurities" introduced into the purification schemes. Following treatment with streptomycin sulfate, the samples were incubated overnight at 4˚C per the purification protocol, and agarose and SDS gels were run on the samples the following day. Because SDS gel electrophoresis requires that samples be boiled with a loading buffer before loading onto the gel, the SDS-PAGE results are post boiling while the agarose gel samples were taken and run before boiling. The intensity of the agarose gel bands should be the same for each condition. However, the migration distance will vary with different streptomycin sulfate concentrations based upon how efficiently streptomycin sulfate binds the nucleic acids in the sample. SDS-PAGE results allow one to infer the degree of precipitation of thermally unstable proteins present in each sample. Using these tools, the optimal concentration of streptomycin sulfate used during the purification process can be approximated.

PV-S56D and PV-E60D were overexpressed again according to previous expression protocols and were very successful. Once streptomycin sulfate was added, samples of PV-S56D and PV-E60D were analyzed (Figure 3.13).

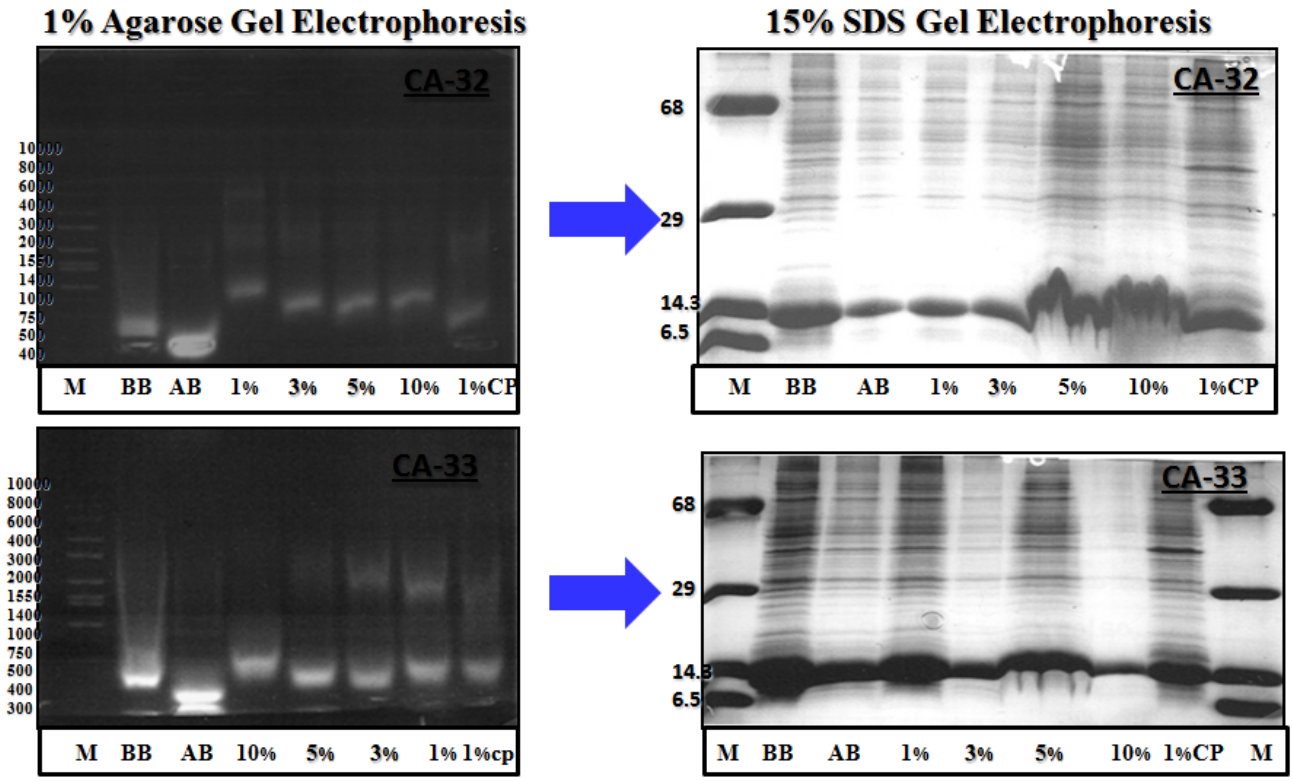

Figure 3.13. Varying Strep. Treatment Conditions to S56D and E60D. (A) PV-S56D results. (B) PV-E60D results.

Agarose gel results of PV-S56D reveal that the treatment of the supernatant before benzonuclease (BB) versus after the treatment (AB) yields a slight increase in fragmentation of the nucleic acids as evidenced by the more migrated band in the AB lane (Figure 3.13A). SDS-PAGE analysis of these samples yields slightly less protein following the addition of benzonuclease because the boiling of samples required for SDS gel analysis may have facilitated the precipitation of thermally unstable proteins. It is important to note here that the striated bands on the SDS gel for 5% and 10% streptomycin treatment are typical results associated with SDS-streptomycin sulfate experiments due to heat-facilitated precipitation of sample components. This pattern likely occurs at higher concentrations of streptomycin sulfate because more proteins are precipitated, making it more difficult for the bands to pull down during electrophoresis. To allow for more conclusions to be drawn from SDS gel analysis, the supernatant isolated from

centrifugation of these samples should have been run on the gel to avoid the negative effects associated with significant protein precipitation during SDS-PAGE.

It appears that 1% streptomycin sulfate is optimal for PV-S56D nucleic acid precipitation because its band has a higher molecular weight than that of the other tested streptomycin sulfate concentrations (streptomycin binds to DNA yielding a higher molecular weight) shown in the agarose gel and it appears to have a reduced amount of undesired proteins (SDS gel) present in the supernatant following heat. Furthermore, the 1% cell pellet isolated from centrifuging the 1% streptomycin sulfate sample contains a comparable amount of nucleic acids, though at a smaller molecular weight. Due to a flaw in experimental design, the concentration of nucleic acids in the cell pellets from other tested streptomycin sulfate concentrations were not run on the gel and thus cannot be compared to the 1% cell pellet. This will be later addressed with PV-G99D experiments. Because the SDS gel results are not conclusive this experiment was repeated with a different variant of ProCA-30, PV-E60D.

Like PV-S56D, the treatment of PV-E60D supernatant before benzonuclease (BB) versus after the treatment (AB) yields a slight increase in fragmentation of the nucleic acids as evidenced by the more migrated band in the AB lane (Figure 3.13B). It is unclear why SDS-PAGE analysis of these samples yields slightly less protein following the addition of benzonuclease. Furthermore, it is unclear why the amount of nucleic acid for each streptomycin concentration sample differs. While nucleic acid concentration appears to be inconsistent for 5% and 10%, 1% and 3% appear to maintain comparable concentrations of nucleic acids. This may be due to human sample loading error. Nevertheless, based solely on the reduced distance of band migration for agarose gel electrophoresis and the reduced amount of undesired proteins (SDS gel) present in the supernatant following heat, it appears that 3% streptomycin sulfate is

optimal for nucleic acid removal. The absence of "band striations" at 10% streptomycin sulfate for this variant compared to that of PV-S56D may be related to the heterogeneous nature of the samples run on the SDS gel.

PV-G99D was overexpressed very well and subjected to the varying streptomycin sulfate concentration experiment (Figure 3.14). Using a similar method of analysis as achieved with PV-S56D and PV-E60D but implementing the boiling and centrifugation steps prior to gel analysis, it appears that 5% streptomycin sulfate is optimal for DNA precipitation from the supernatant of G99D (Figure 3.14). The reduction of nucleic acids present in the supernatant before and after heating and centrifugation is most significant at 5% streptomycin sulfate (lanes 8 and 9). Furthermore, the 5% cell pellet contains the highest concentration of nucleic acid isolated from the supernatant following heat and centrifugation. It's important to note that heat significantly facilitates the precipitation of nucleic acids removed by precipitation.

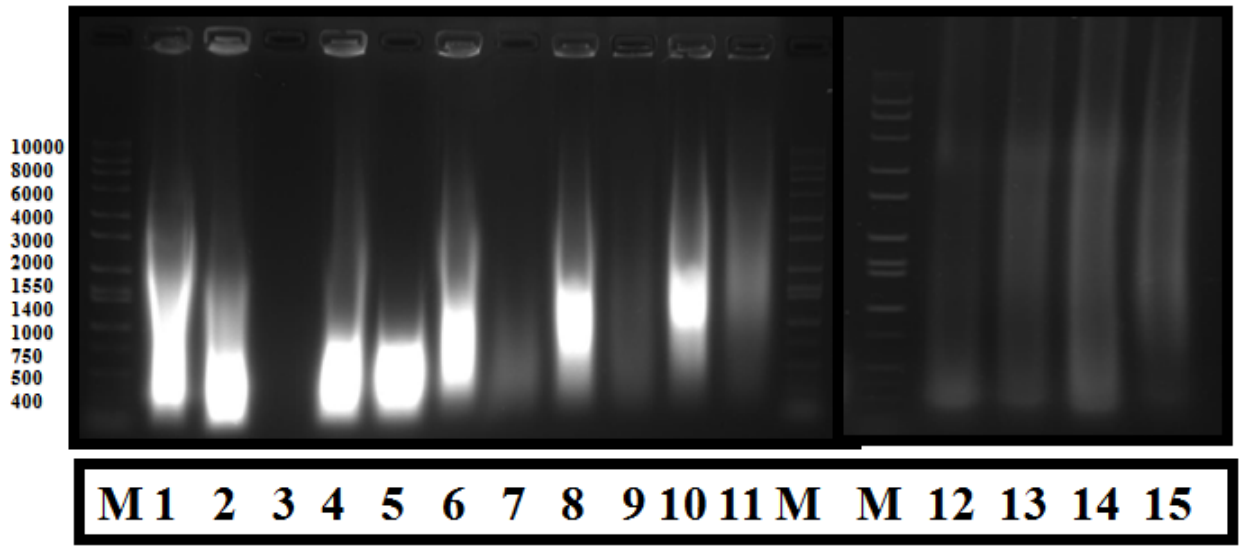

1) Before benzonuclease
2) After benzonuclease
3) 30% Strep
4) 1% Strep before heat
5) 1% Strep after heat
6) 3% Strep before heat
7) 3% Strep after heat
8) 5% Strep before heat
9) 5% Strep after heat
10) 10% Strep before heat
11) 10% Strep after heat
12) 1% Cell pellet
13) 3% Cell pellet
14) 5% Cell pellet
15) 10% Cell pellet

Figure 3.14. PV-G99D varying streptomycin sulfate treatment agarose gel results. (A) Streptomycin screening for optimal conditions. (B) Changes in nucleic acid concentration at 5% streptomycin sulfate.

Overall, it appears that the streptomycin sulfate precipitation method is effective at reducing the concentration of nucleic acids in the supernatant. While the data from PV-S56D and PV-E60D insinuates that 1-3% streptomycin sulfate is optimal for binding to nucleic acids in the supernatant and facilitating their precipitation, it does not incorporate the use of heat and centrifugation into agarose gel analysis, which has shown to significantly decrease the concentration of nucleic acids in the experiment using PV-G99D. From the G99D experiment, it was found that 5% streptomycin sulfate concentration is optimal for nucleic acid precipitation from the protein supernatant following overnight cleavage of nucleic acids with benzonuclease.

This is evidenced by the reduced concentration of nucleic acids present in the supernatant following heating and centrifugation and the increase of nucleic acids present in the 5% cell pellet conditions. Therefore, the purification protocol was modified to use 5% streptomycin sulfate process for nucleic acid precipitation.

3.3.3. Modified FPLC Program

Previous FPLC experimental conditions allowed for a second FPLC run during which Buffers A and B contained 3mM Ca instead of EDTA. However, this step was eliminated to reduce the number of steps required to isolate the apo-form of the proteins for metal analysis via circular dichroism, relaxivity, and fluorescence. It is well known that the native form of ProCA-30 binds calcium with a high affinity and it is difficult and time-consuming to remove the metal ions at such a high concentration of calcium previously used. Additionally, with each successive step of the purification process, there are consequential subsequent losses of protein. Thus, the elimination of this step along with an optimal salt gradient of separation, may allow for isolation of a higher quantity of protein.

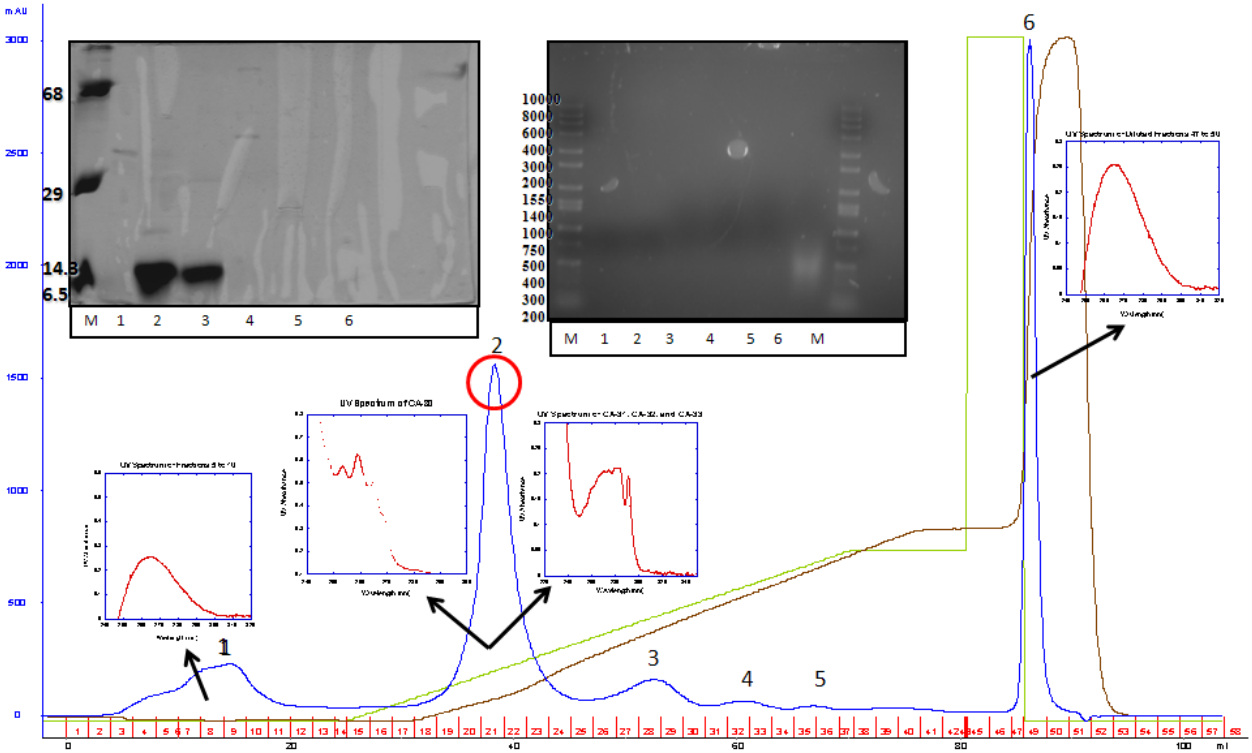

Figure 3.15. Typical FPLC chromatogram of ProCA-3 agents by Q-column separation and the UV absorbance of each fraction.

Figure 3.15 depicts the characteristic chromatogram and UV absorbance spectra resulting from Q-column FPLC separation of ProCA-3 agents cell lysate. Each labeled peak directly corresponds to the numbers used to label the lanes on both the SDS-PAGE gel and the agarose gel. Here, the FPLC gradient was modified from a sharp increase to 70% NaCl and steady increase to 100% NaCl (old protocol) to final program specifications of column washing with 15mL of Buffer A, a steady increase to 25% NaCl and then holding that concentration for three column volumes (15mL) before a sharp increase to 100% NaCl to elute any bound proteins or nucleic acids to the Q-column. This program was implemented on ProCA-30, ProCA-31, ProCA-32, and ProCA-33 (Figures 3.17-3.20). As one can infer from the broad peak at 260nm of the UV-spectrum corresponding to peak 1 and the absence of a band on the SDS-PAGE gel, peak 1 is likely smaller fragments of nucleic acids and to a lesser degree of undesired protein that did

not bind to the column. Because the concentration of fragmented nucleic acids was low, it did not show on the agarose gel. Peak 2 is the isolated variant and likely corresponds to the apo-form of N-formyl methionine-cleaved ProCA-3. This is confirmed by SDS-PAGE gel, agarose gel, and mass spectrometry data (Figure 3.15, Figure 3.16).

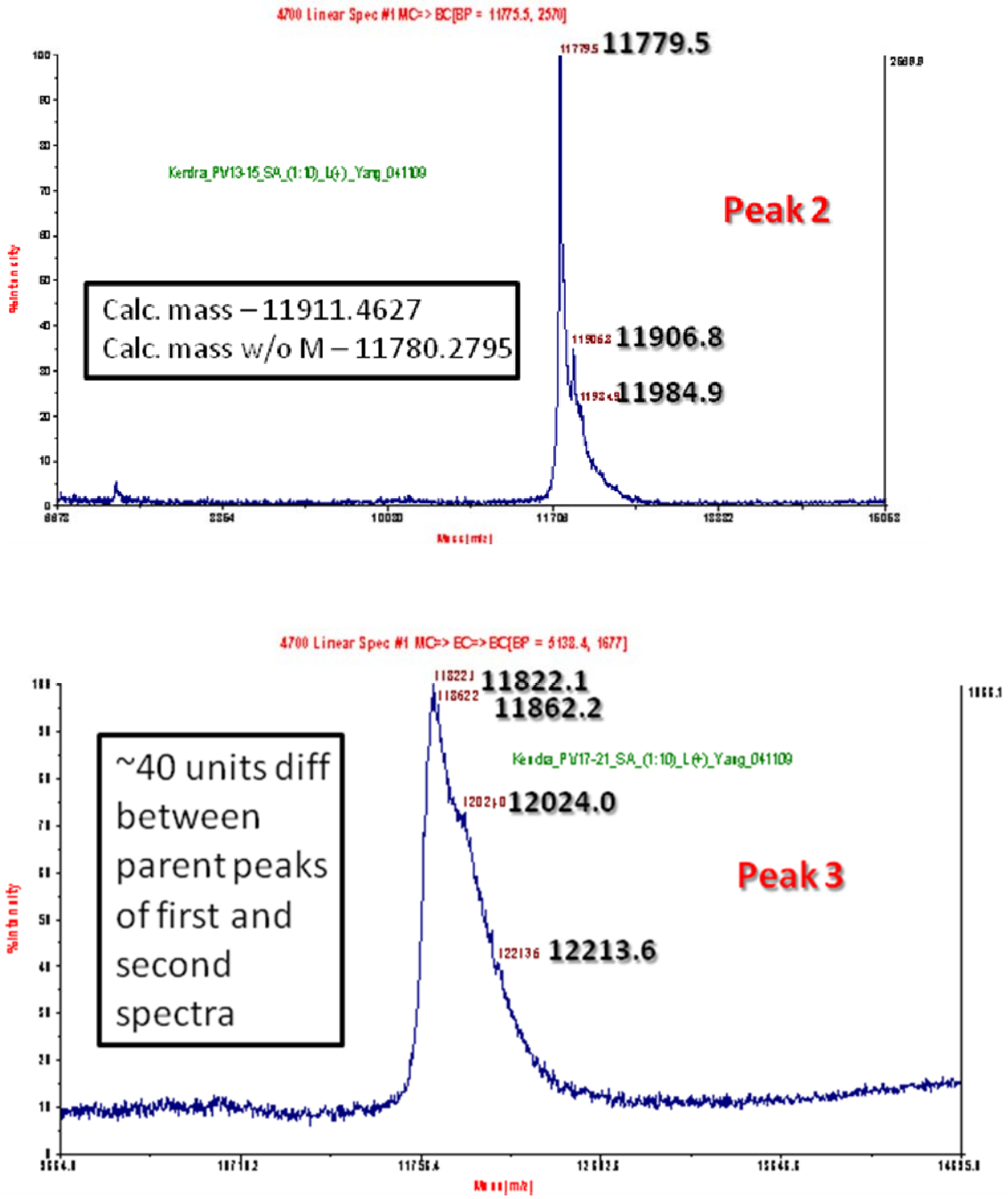

Figure 3.16. Mass spectrometry results of peaks 2 and 3 from the modified purification protocol.

Peaks 3, 4, and 5 are believed to be the holo-forms of methionine-cleaved ProCA-3 agents. SDS-PAGE gel, agarose gel, and mass spectrometry data confirms the speculations of peak 3 identification (Figure 3.15, Figure 3.16). Summarizing the results, the modified FPLC program yields a significant improvement in the overall yield of protein to a high degree of purity compared to the old methodology (Table 3.1).

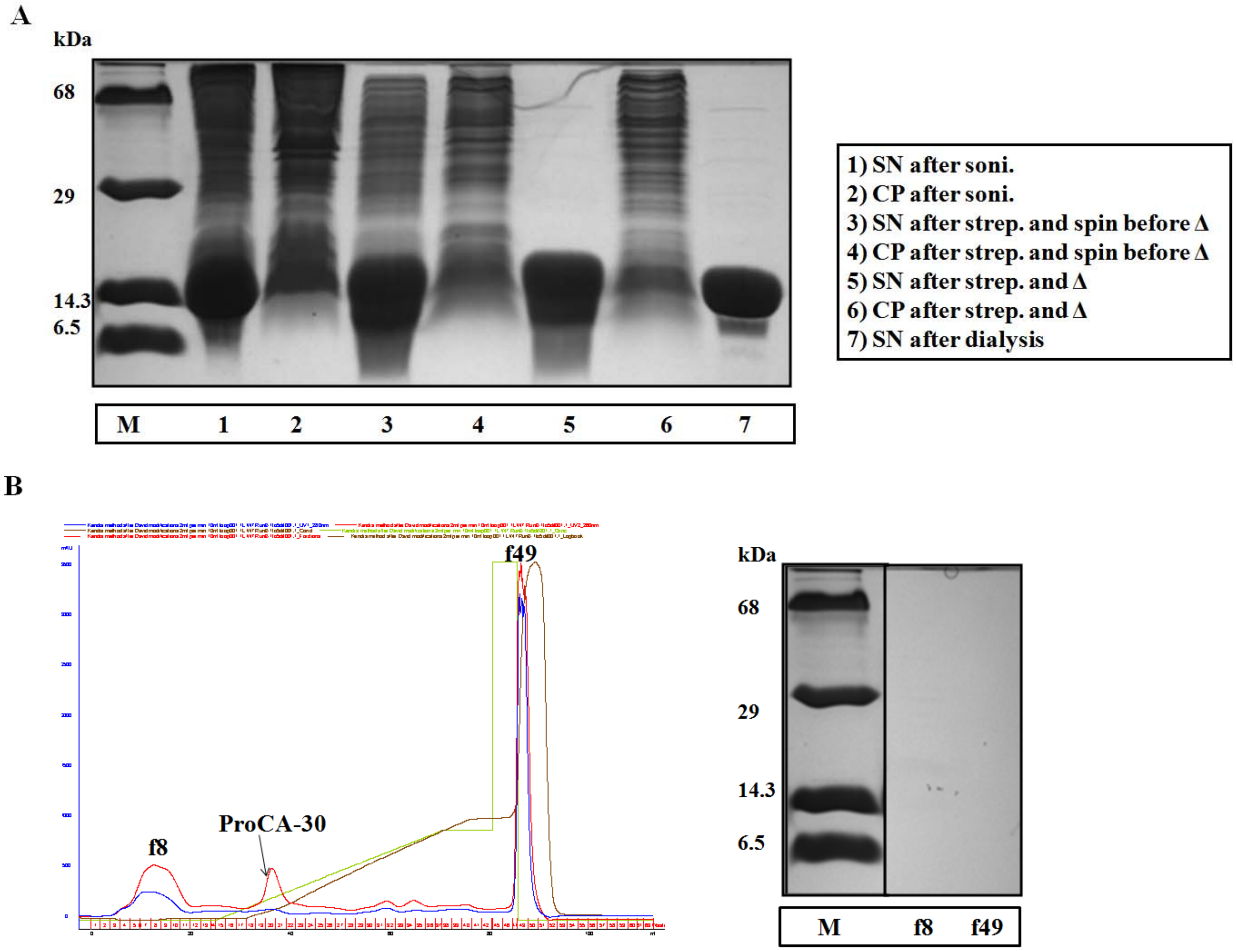

Figure 3.17. ProCA-30 Purification. (A) SDS-Page results of purification process. (B) FPLC chromatogram depicting isolation of target variant.

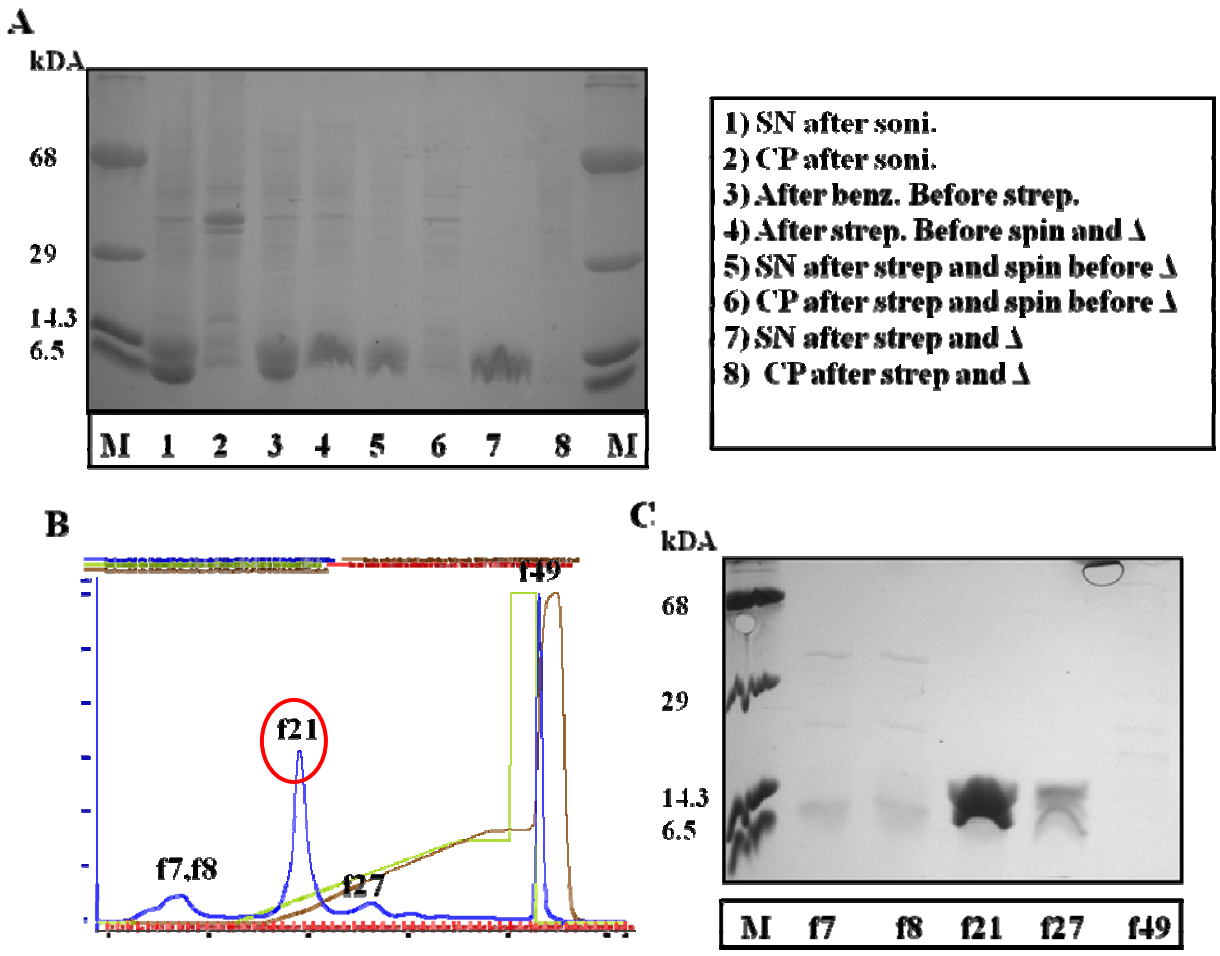

Figure 3.18. ProCA-31 Purification. (A) SDS-Page results of purification process. (B) FPLC chromatogram depicting isolation of target variant. (C) Relevant SDS Page results from FPLC separation.

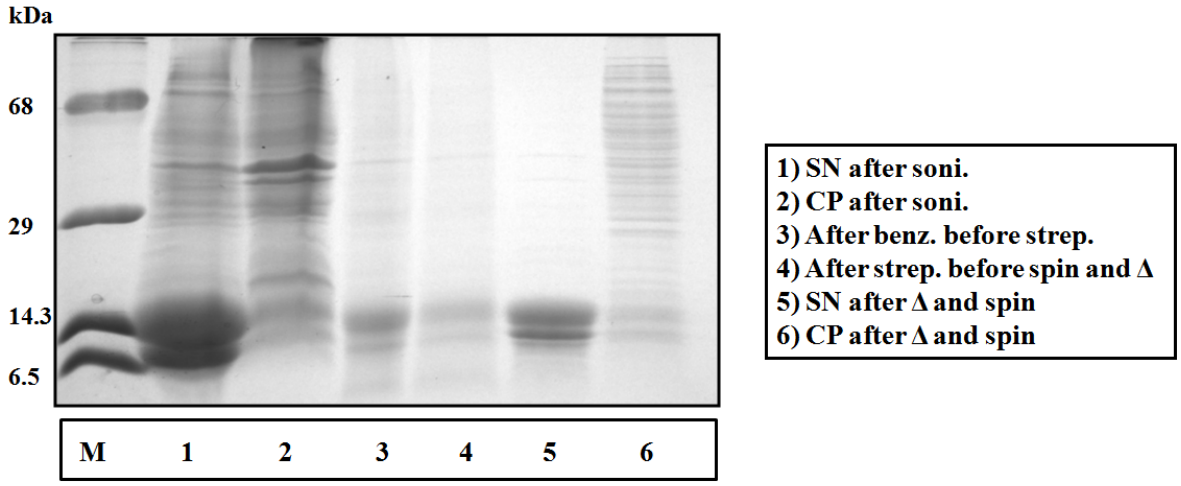

B

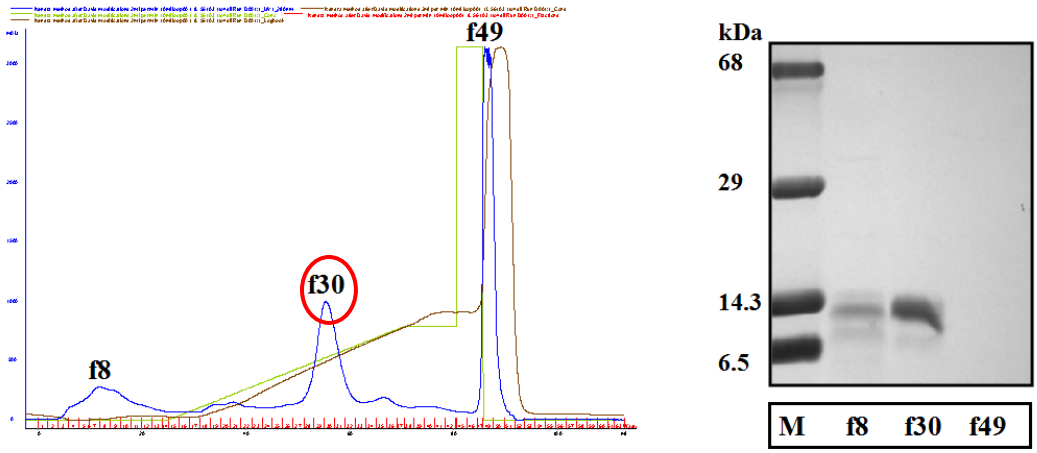

Figure 3.19. ProCA-32 Purification. (A) SDS-Page results of purification process. (B) FPLC chromatogram depicting isolation of target variant and relevant SDS Page results from FPLC separation.

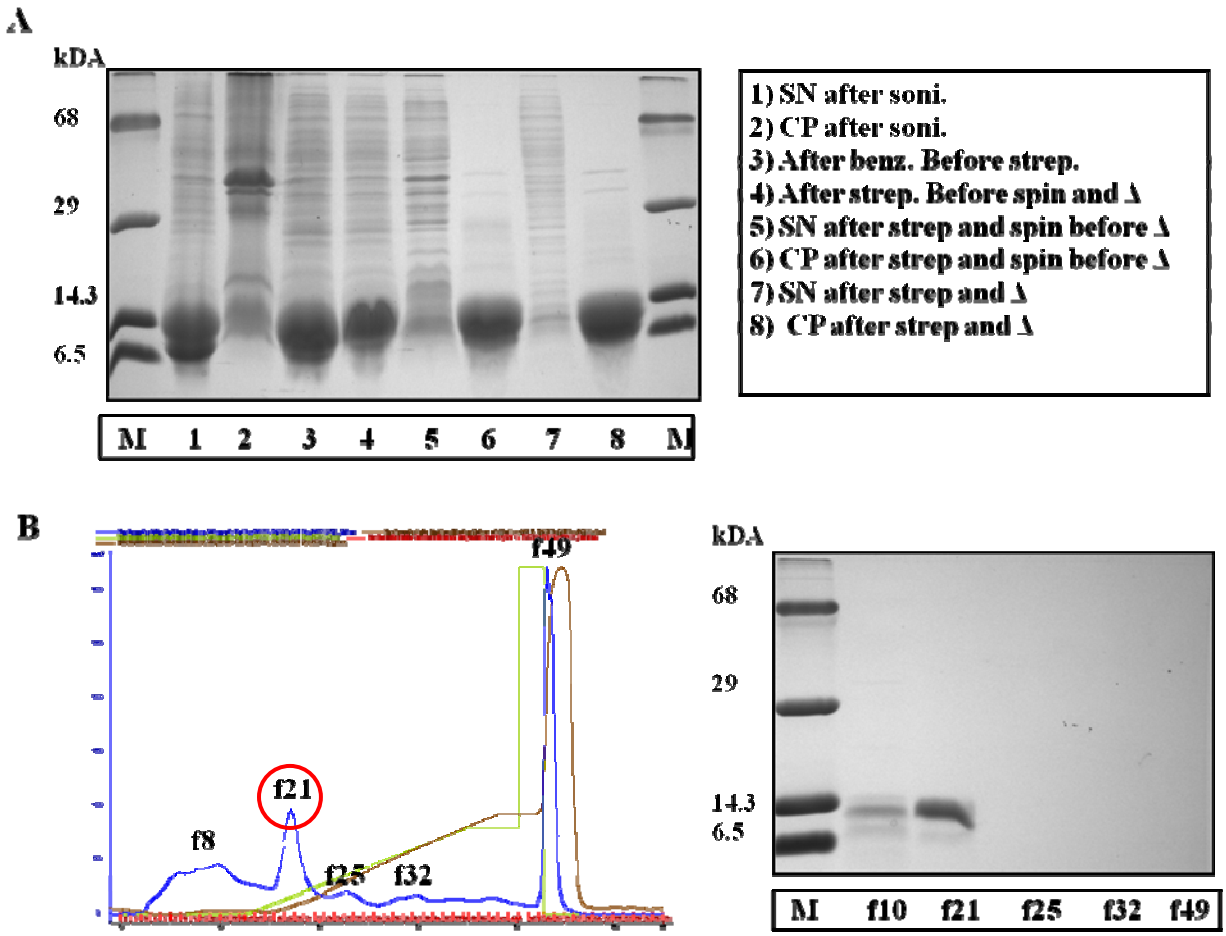

Figure 3.20. ProCA-33 Purification. (A) SDS-Page results of purification process. (B) FPLC chromatogram depicting isolation of target variant and relevant SDS Page results from FPLC separation.

3.4. Final Yield

Summarizing the aforementioned results of his chapter, the unrevised purification protocol closely resembles that of the current protocol. However, there were a few minor changes made that have drastically increased the purification yield. Incorporating the use of an optimal streptomycin sulfate concentration and modifying the FPLC salt gradient for separation, the yields of all members of Class ProCA-3 agents have increased nearly four to six times compared to the old methods with the exception of ProCA-33. Figures 3.21 and 3.22 further confirm the purity of contrast agent isolated. The UV spectra obtained are closely related to that

of the published expected spectra (see section 2.3). The yield of ProCA-33 was 39.41 mg and did not significantly increase compared to the implementation of the old purification protocol due to the inefficiency of the contrast agent binding to the Q-column. This is evidenced by the low resolution observed between the first two peaks in the FPLC chromatogram (Figure 3.15). This inefficacy is related to insufficient cleaning of the column and was due to human error.

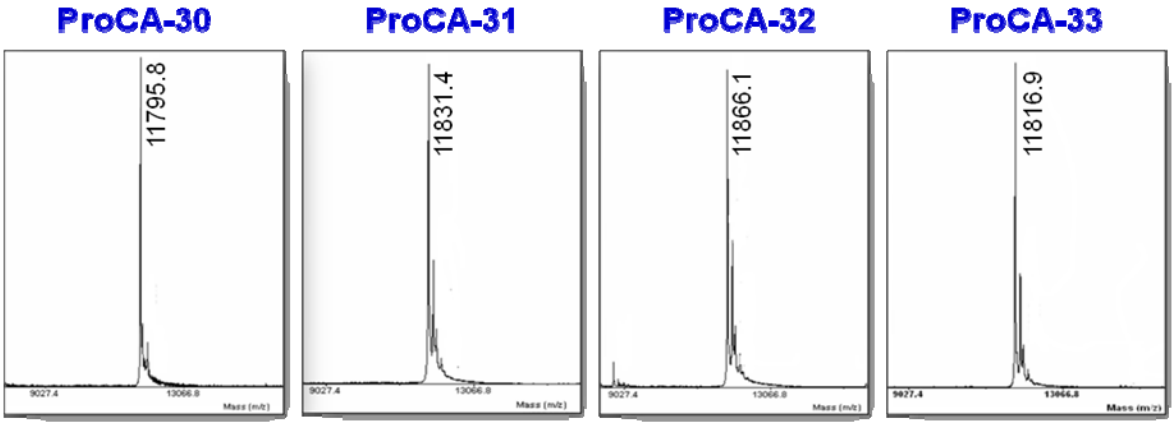

Figure 3.21. Maldi-TOF results confirming identity and purity of isolated members of Class ProCA-3 agents.

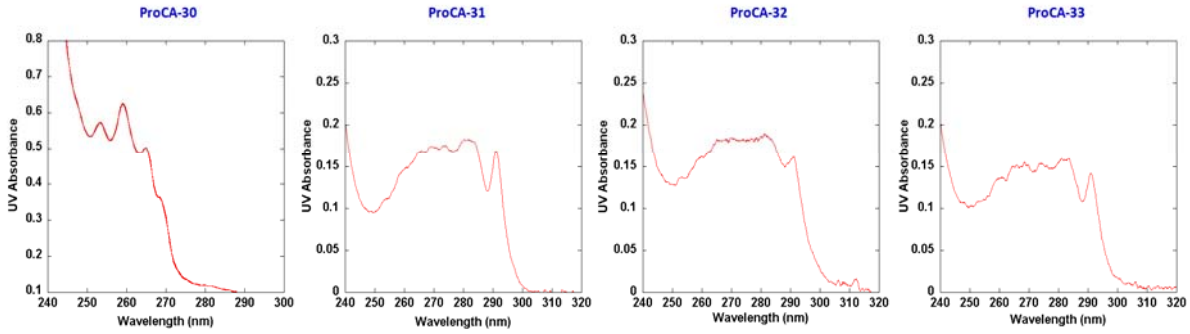

Figure 3.22. Final UV absorbance spectra of class ProCA-3 agents.

Table 3.1. ProCA-3 Purification Yields

ProCA-3	ProCA-30	ProCA-31	ProCA-32	ProCA-33
Old Yield from 2L LB media	31.70 mg	37.50 mg	32.60 mg	41.50 mg
New Yield from 1L LB media	109.12 mg	76.16 mg	60.21 mg	39.41 mg*

*Due to human error, there was no significant increase in yield due to loss of protein during the FPLC injection stage.

4. CONFORMATIONAL ANALYSIS AND METAL STUDIES

4.1. Background

It is of crucial importance that the structural integrity of the designed protein-based contrast agents of Class ProCA-3 maintains the native structure of parvalbumin, the scaffold protein. Maintenance of the characteristic alpha-helical structure allows one to draw the conclusion that the introduction of mutations into the skeletal structure does not significantly alter or perturb the proteins secondary structure, providing insight into their relative stabilities. Figure 4.1 depicts the published Far-UV spectrum of parvalbumin in the presence and absence of calcium.

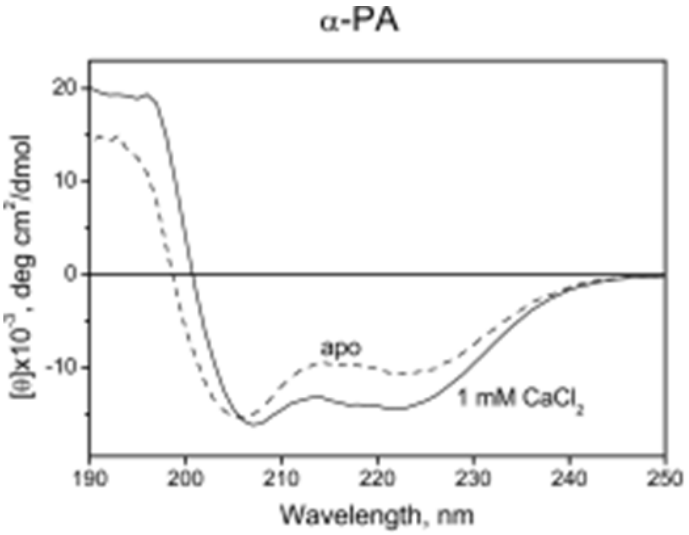

Figure 4.1.Published Far-UV spectrum of wildtype parvalbumin; Dashed line, metal-free form; solid line, Ca^{2+} loaded form [39].

Using circular dichroism to measure the Far-UV region absorptions, one is able to detect changes in secondary structure alone. It is important to note here that this technique does not allow one to draw conclusions about the intrinsic stability of the gadolinium binding site as a result of the introduced mutations in ProCA-31, ProCA-32, or ProCA-33. Furthermore, measuring the optical absorptions in the Far-UV CD region does not provide any indication of

potential changes in the globular or tertiary structure of the designed agents. To detect tertiary structural changes of the agents, the Near-UV spectrum, instead of the Far-UV region, must be examined using circular dichroism. However, for the purposes of this thesis, only the Far-UV CD region was observed.

Not only is the maintenance of the secondary structure following the introduction of mutations important, but it is also of crucial importance to investigate the effects of increasing concentrations of physiological metal ions and high salt on the stability of the structure. For the purposes of this discussion, the effects of magnesium, calcium, gadolinium, and terbium will be examined.

4.2. Magnesium-Induced Structural Effects

Magnesium is a divalent metal that plays a major role in a number of biological processes. Under normal physiological conditions, the extracellular concentration of magnesium is 1-2mM. Native parvalbumin acts as a cytosolic buffering protein, respectively binding both calcium and magnesium, on the orders of 10^{-9}M and 10^{-6}M [25]. Therefore, at a fixed 6μM concentration of protein, the spectral changes associated with the addition of magnesium chloride to each contrast agent of Class ProCA-3 was observed at a 1:1 protein to Mg^{2+} concentration ratio, 1:2 protein to Mg^{2+} concentration ratio, 1mM Mg^{2+} , and an excessive amount of 5mM Mg^{2+}. The metal-induced structural changes were observed under both low and high salt conditions. A major assumption drawn for these experiments is that the background metals and EDTA from purification present in the buffer system are below the micromolar range. However, this must be further verified. Nevertheless, some conclusions can be drawn.

4.2.1. ProCA-30

ProCA-30 secondary structure changes under varying concentrations of magnesium were observed. At low salt concentrations, the protein maintains its native α-helical character with slight decreases in its helicity for the holo forms (Figure 4.2). Under high salt conditions, the reverse is true up to 1mM additional magnesium. At 5mM calcium, the helicity decreases. Here, it's safe to assume that the presence of high salt helps to stabilize ProCA-30 up to 1mM magnesium. As will be later explained, more pronounced spectral differences are primarily seen between the low and high salt forms of the protein in the presence of calcium.

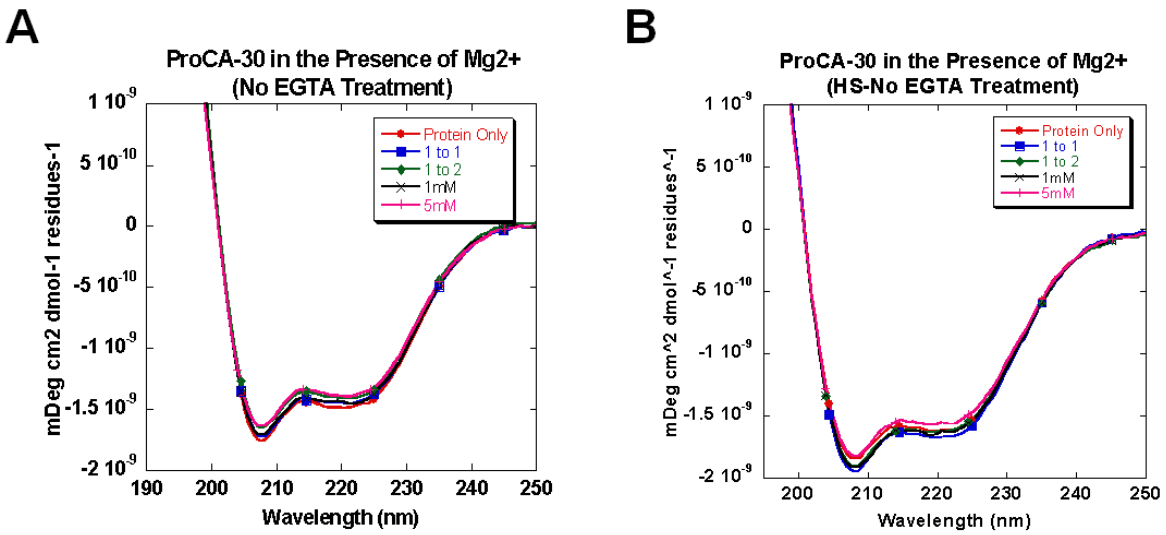

Figure 4.2. Far UV spectra of 6 μM ProCA-30 in the presence varying protein to magnesium ratios. (A) Low salt conditions. (B) High salt conditions. A buffer of 10mM Tris/HCl chelex pH 7.4 100mM NaCl was used.

4.2.2. ProCA-31

ProCA-31 yields characteristic alpha-helix wavelength absorbencies at 209 nm and 222 nm in the absence of additional added metals and in the presence of increasing concentration of magnesium under both low and high salt conditions (Figure 4.3). Thus the introduction of a F103W mutation does not significantly alter the secondary structure of the protein. For varying

ratios of magnesium, like ProCA-30, ProCA-31 decreases in helical character as the concentration of added magnesium increases under low salt conditions. The same can be said for high salt conditions, though more pronounced spectral differences were noted. Here, the presence of high salt has little effect on the stability of ProCA-31 in the presence of magnesium.

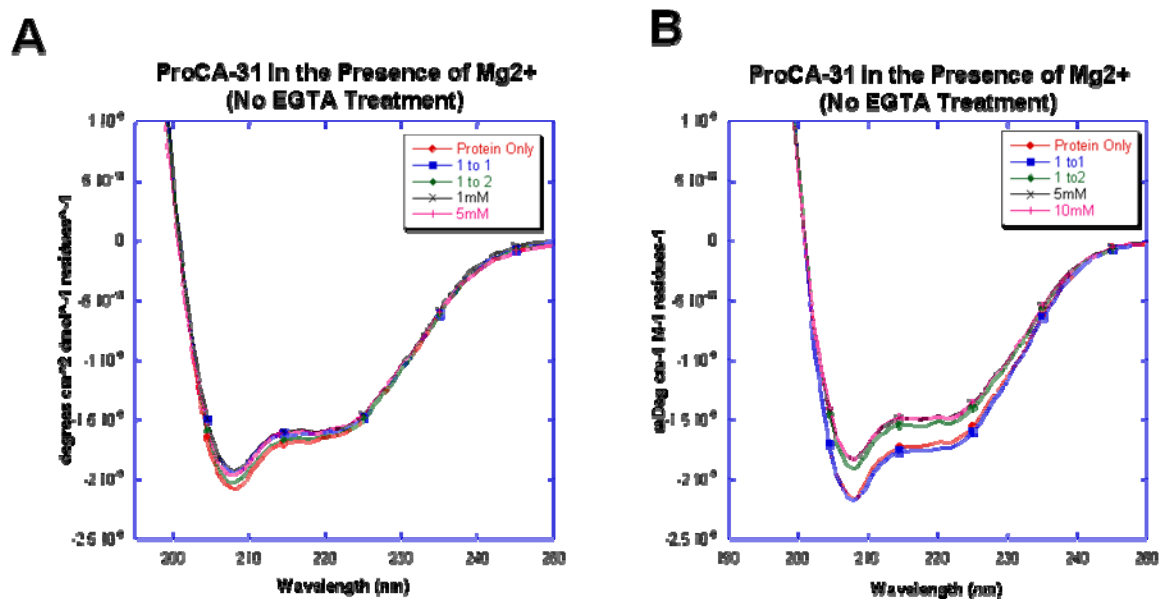

Figure 4.3. Far UV spectra of 6 µM ProCA-31 in the presence varying protein to magnesium ratios. (A) Low salt conditions. (B) High salt conditions. A buffer of 10mM Tris/HCl chelex pH 7.4 (100 mM NaCl) was used.

4.2.3. ProCA-32

Under the subjection to circularly polarized light, the Far-UV CD spectrum of 6µM ProCA-32 yields characteristic alpha-helix wavelength absorbencies at 209 nm and 222 nm in the presence of increasing concentrations of magnesium (Figure 4.4). This indicates that the mutation does not significantly alter the secondary structure of the protein. The helical content of the protein appears to slightly increase in the presence of magnesium under low salt conditions, implying enhanced stability. There are little notable spectral differences with increasing

concentration of magnesium under high salt conditions, indicating that ProCA-32 is fairly stable under comparable extracellular conditions.

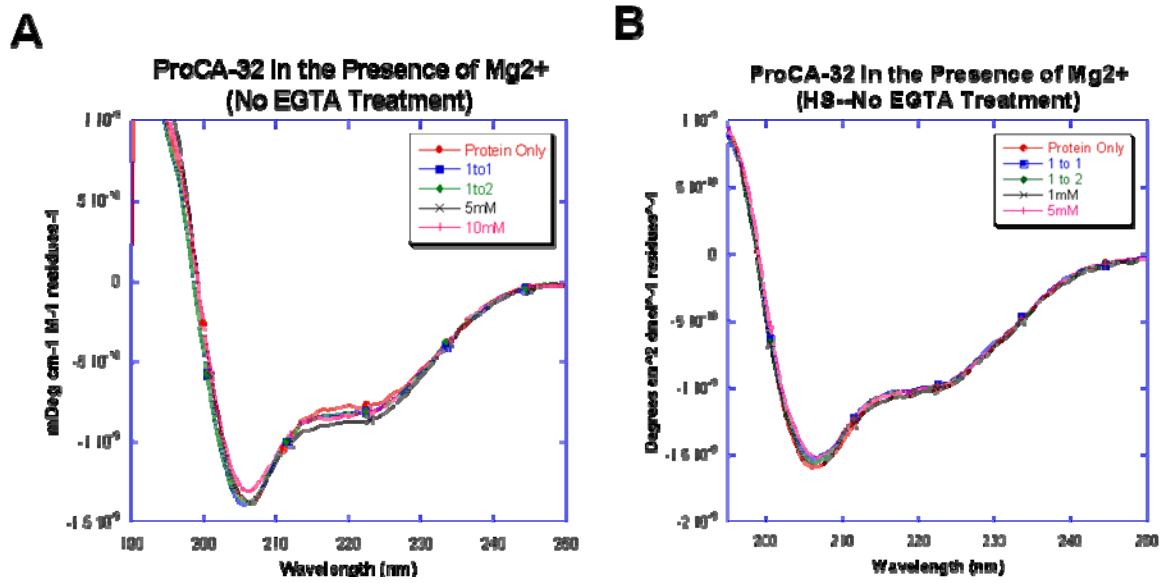

Figure 4.4. Far UV spectra of 6 µM ProCA-32 in the presence varying protein to magnesium ratios. (A) Low salt conditions. (B) High salt conditions. A buffer of 10mM Tris/HCl chelex pH 7.4 (100 mM NaCl) was used.

4.2.4. ProCA-33

It is unclear whether the introduction of an aspartic acid in place of glutamic acid at position 60 located in the CD site and a tryptophan in lieu of phenylalanine at position 103 located just outside of the EF site will significantly alter the secondary structure of the native skeletal design of the contrast agent. Furthermore, we are not certain of the metal-induced structural effects of this contrast agent. For varying concentrations of magnesium in a low salt buffer, ProCA-33 helical content is enhanced with increasing concentrations of magnesium (Figure 4.5A). With the exception of a slight decrease in helicity at 5mM magnesium, the helical content under high salt conditions remains fairly consistent, indicating that high salt plays little role in secondary structure destabilization of ProCA-33 in the presence of magnesium (Figure 4.5B).

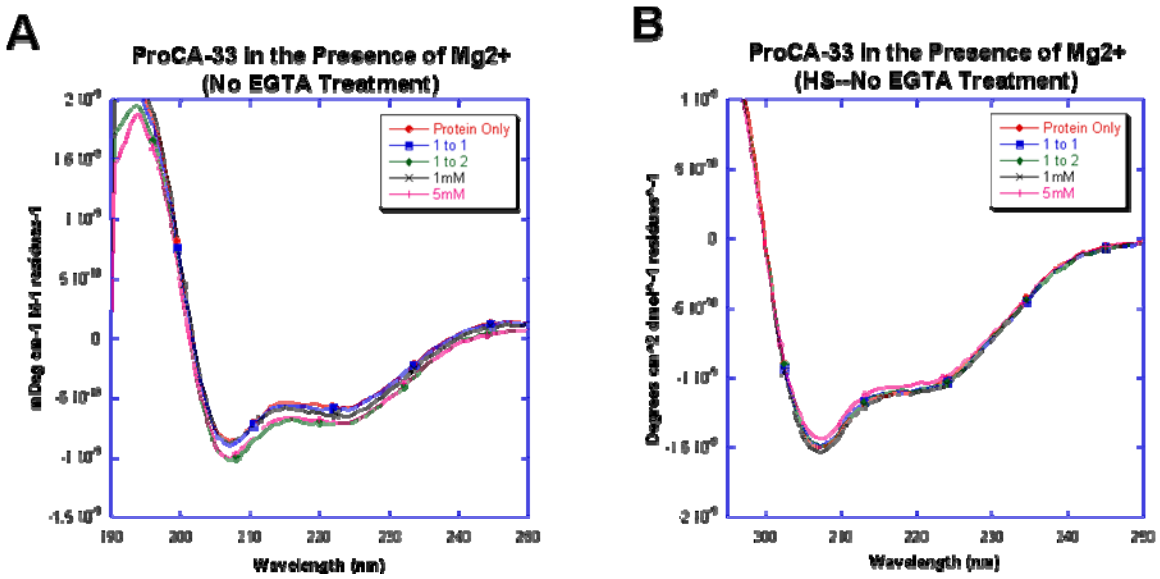

Figure 4.5. Far UV spectra of 6 μM ProCA-33 in the presence varying protein to magnesium ratios. (A) Low salt conditions. (B) High salt conditions. A buffer of 10mM Tris/HCl chelex pH 7.4 (100 mM NaCl) was used.

4.3. Calcium-Induced Structural Effects

Calcium ions are one of the most abundant minerals in the human body and is essential for living organisms, particularly in cell physiology [40-41]. Though its concentration is 10^4 to 10^6-fold less than that of magnesium and potassium intracellulary, respectively, calcium is not only "an essential structural component in the biomineralization of teeth, bones, and shells but also a 'second messenger' that controls numerous cellular processes such cell division and growth, secretion, ion transport, and muscle contraction through calcium-induced conformational change" [28]. More specifically, calcium-binding proteins with varying affinities for this metal mediate and regulate both extracellular and intracellular calcium-dependent functions [28]. Because their metal selectivity over other metal ions is closely related to many physiological processes and diseases, understanding the key factors in their selectivity and conformational change allows for a more in depth analysis of calcium signaling [28, 42].

4.3.1. ProCA-30

Pronounced spectral differences are primarily seen between the low and high salt forms of the protein in the presence of calcium (Figure 4.6). Under low salt conditions, ProCA-30 is destabilized as the concentration of calcium increases. Under high salt conditions, there are little notable differences with increasing concentrations of calcium with the exception of a decrease in helicity at 5mM calcium. Here, one can draw the conclusion that the presence of salt does little to perturb the structure up to 1mM calcium.

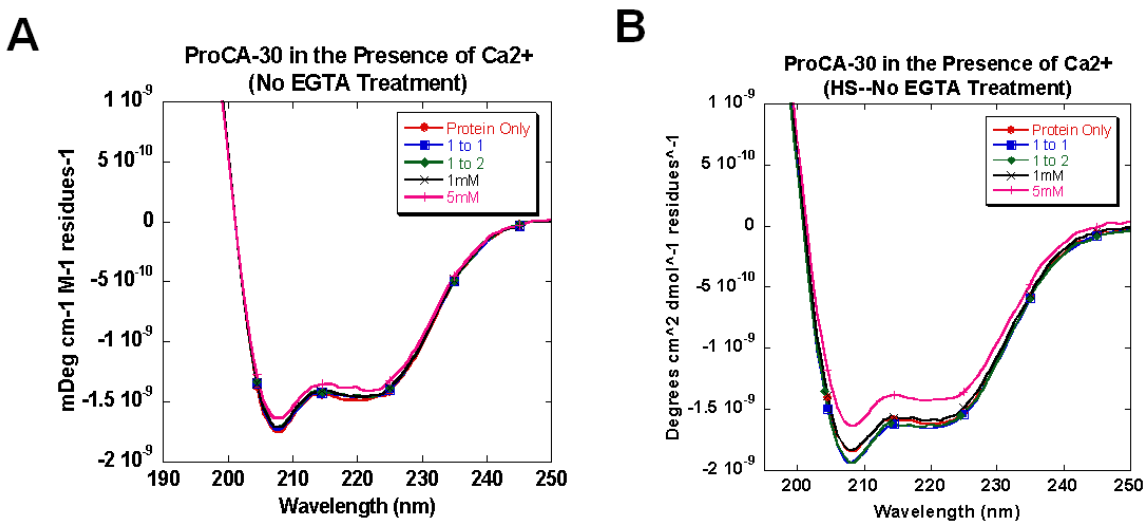

Figure 4.6. Far UV spectra of 6 µM ProCA-30 in the presence varying protein to calcium ratios. (A) Low salt conditions. (B) High salt conditions. A buffer of 10mM Tris/HCl chelex pH 7.4 (100 mM NaCl) was used.

4.3.2. ProCA-31

Because the alpha-helical structure is maintained, one can assume that the introduction of a F103W mutation just outside of the EF binding site does not significantly perturb the secondary structure of the protein (Figure 4.7). For varying ratios of calcium, more pronounced spectral changes between the different ratios of magnesium predominately occur under low salt

conditions (Figure 4.7). Under high salt conditions, there are little notable changes in the helical content, indicating that the ProCA-31 is stable under applicable *in vivo* salt concentrations.

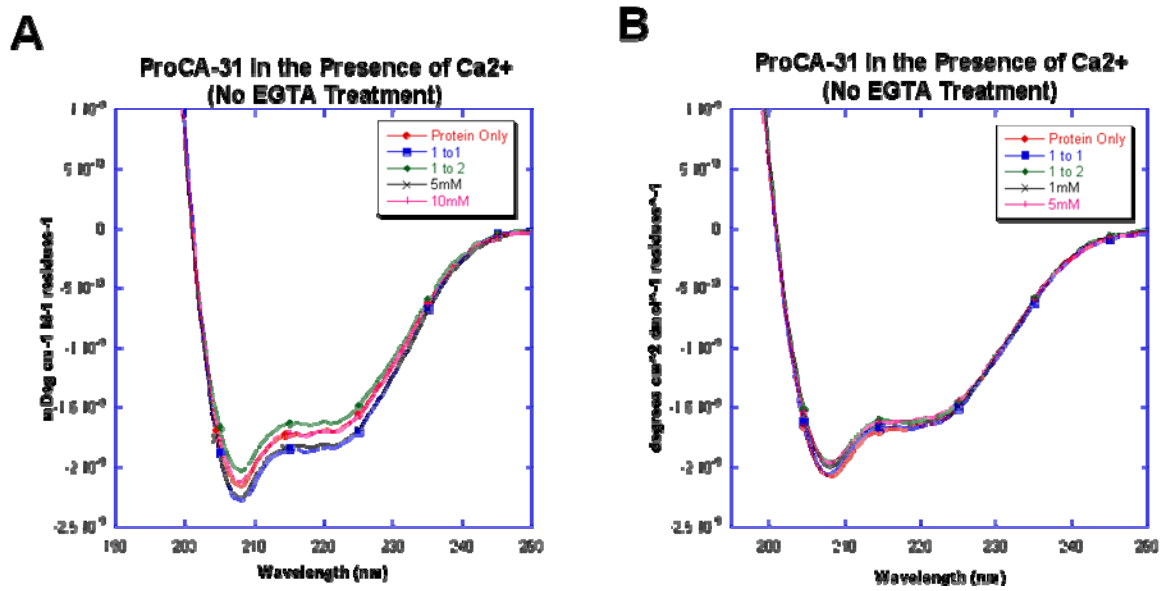

Figure 4.7. Far UV spectra of 6 µM ProCA-31 in the presence varying protein to calcium ratios. (A) Low salt conditions. (B) High salt conditions. A buffer of 10mM Tris/HCl chelex pH 7.4 (100 mM NaCl) was used.

4.3.3. ProCA-32

The alpha-helical fold of ProCA-32 is maintained with introduction of a S56D mutation in the CD site of wildtype parvalbumin, indicating that the mutation does not significantly alter the secondary structure of the protein (Figure 4.8). In the presence of varying metal ratios in the absence of EGTA treatment at low and high salt concentrations, the protein maintains its native α-helical character (Figure 4.8). For varying ratios of calcium under both low and high salt conditions, ProCA-32 increases in helical character for all ratios and concentrations of metal added. Thus, ProCA-32 is a stable variant and the presence of high salt does little to destabilize the secondary structure.

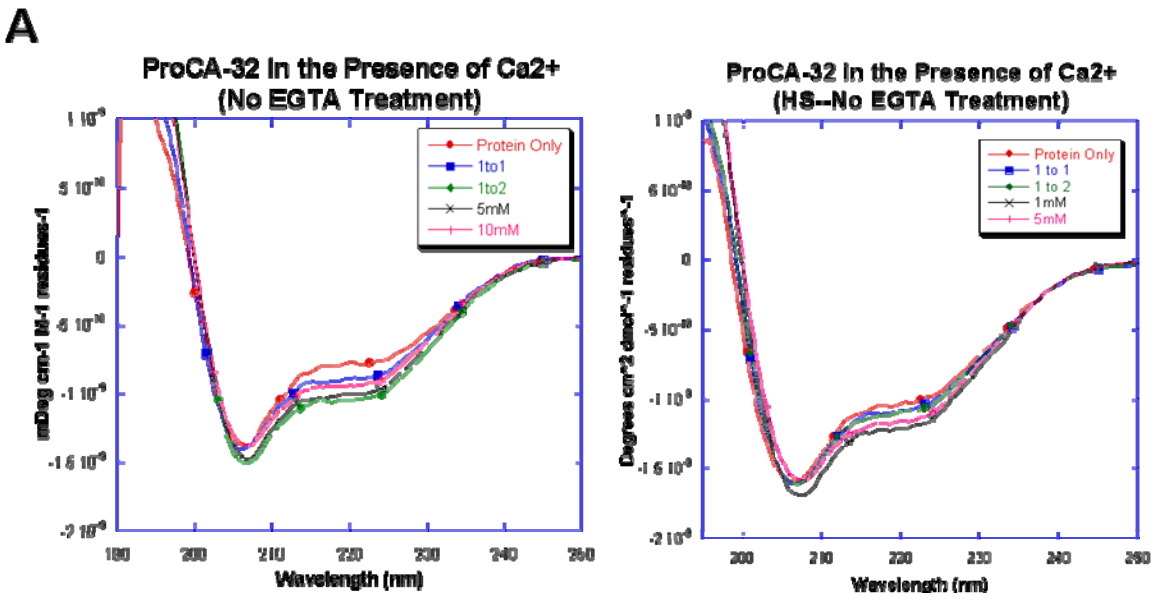

Figure 4.8. Far UV spectra of 6 μM ProCA-32 in the presence varying protein to calcium ratios. (A) Low salt conditions. (B) High salt conditions. A buffer of 10mM Tris/HCl chelex pH 7.4 (100 mM NaCl) was used.

4.3.4. ProCA-33

The alpha-helical fold of ProCA-33 is maintained with introduction of an E60D mutation in the CD site of wildtype parvalbumin, indicating that the mutation does not significantly alter the secondary structure of the protein. In the presence of varying metal ratios in the absence of EGTA treatment at low and high salt concentrations, the protein maintains its native α-helical character (Figure 4.9). For varying ratios of calcium, dominant spectral changes are more visible under low salt conditions. The helical content increases for all concentrations of added calcium under low salt while there are little to no spectral changes under high salt conditions. Like the aforementioned members of Class ProCA-3 in the presence of calcium, the presence of high salt does little to destabilize the secondary structure of the designed contrast agents.

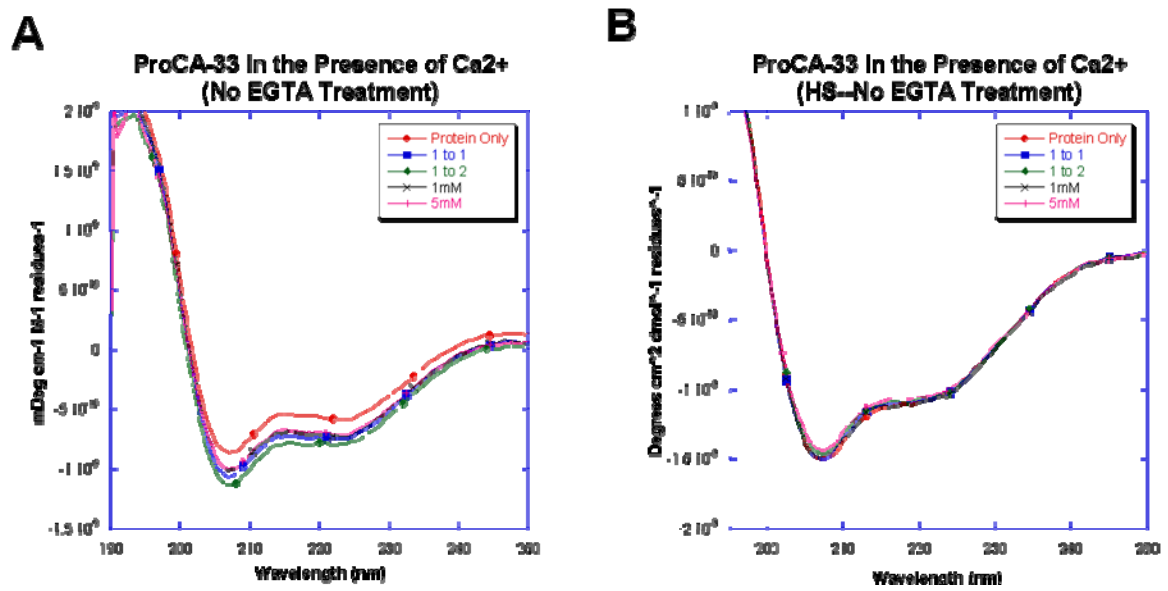

Figure 4.9. Far UV spectra of 6 µM ProCA-33 in the presence varying protein to calcium ratios. (A) Low salt conditions. (B) High salt conditions. A buffer of 10mM Tris/HCl chelex pH 7.4 (100 mM NaCl) was used.

4.4. Gadolinium-Induced Structural Effects

Gadolinium is a paramagnetic metal whose local magnetic field perturbs the relaxation of water protons located on its surface. Once again, the members of Class ProCA-3 are expected to bind gadolinium in a 1 to 2 fashion. Here, we want to observe how the binding of gadolinium affects the secondary structure of the protein.

4.4.1. ProCA-30

Under both low and high salt conditions, the helical content of ProCA-30 appears to decrease for all added concentrations of gadolinium (Figure 4.10). This indicates that gadolinium is able to competitively displace “background metals” from the CD and EF binding sites, even at low concentrations of 6µM (1 to 1) and 12µM (1 to 2) gadolinium. However, this also indicates that gadolinium slightly destabilizes the secondary structure of ProCA-30 under both low and

high salt conditions. The presence of a high concentration of salt does little to perturb the structural changes associated with gadolinium-binding.

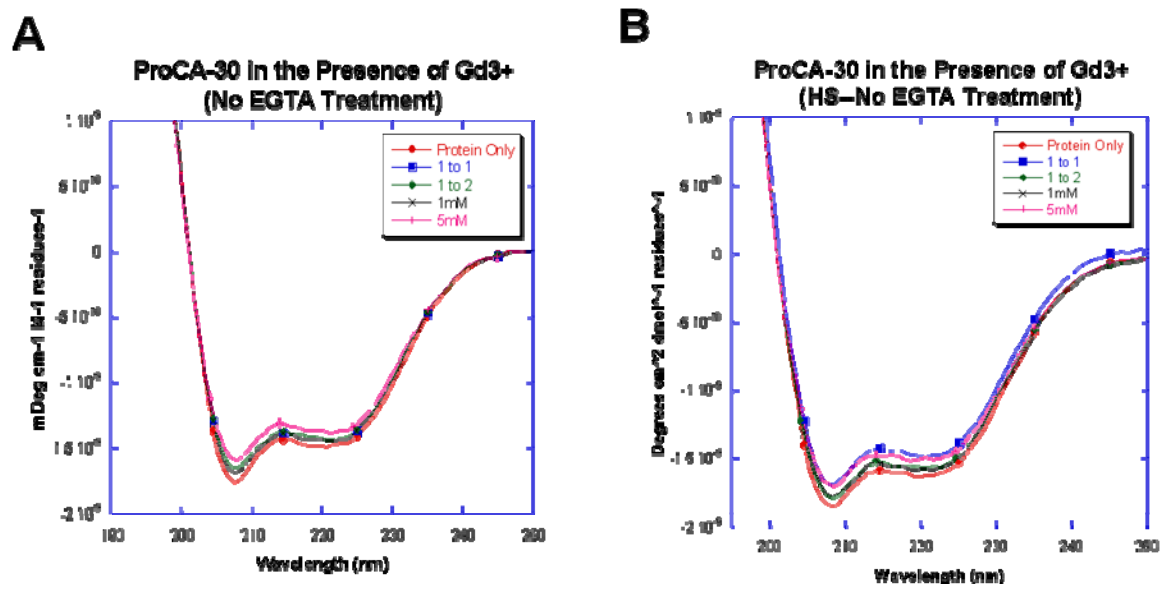

Figure 4.10. Far UV spectra of 6 µM ProCA-30 in the presence varying protein to gadolinium ratios. (A) Low salt conditions. (B) High salt conditions. A buffer of 10mM Tris/HCl chelex pH 7.4 (100 mM NaCl) was used.

4.4.2. ProCA-31

Because the native alpha-helical structure is maintained, it appears that the F103W mutation does not significantly alter the secondary structure of ProCA-31. For various added concentrations of gadolinium, ProCA-31 is destabilized because the helical character decreases for all ratios and concentrations (Figure 4.11). More pronounced spectral differences are associated with low levels of salt. There were only minor decreases in the helical content as increasing concentrations of gadolinium was added under high salt conditions. Thus, one can assert that the presence of high salt plays a nominal role in stabilizing the structure compared to low salt conditions. Nevertheless, as one can infer from Figure 4.11, the native structure of the ProCA-31 is maintained in the presence of gadolinium.

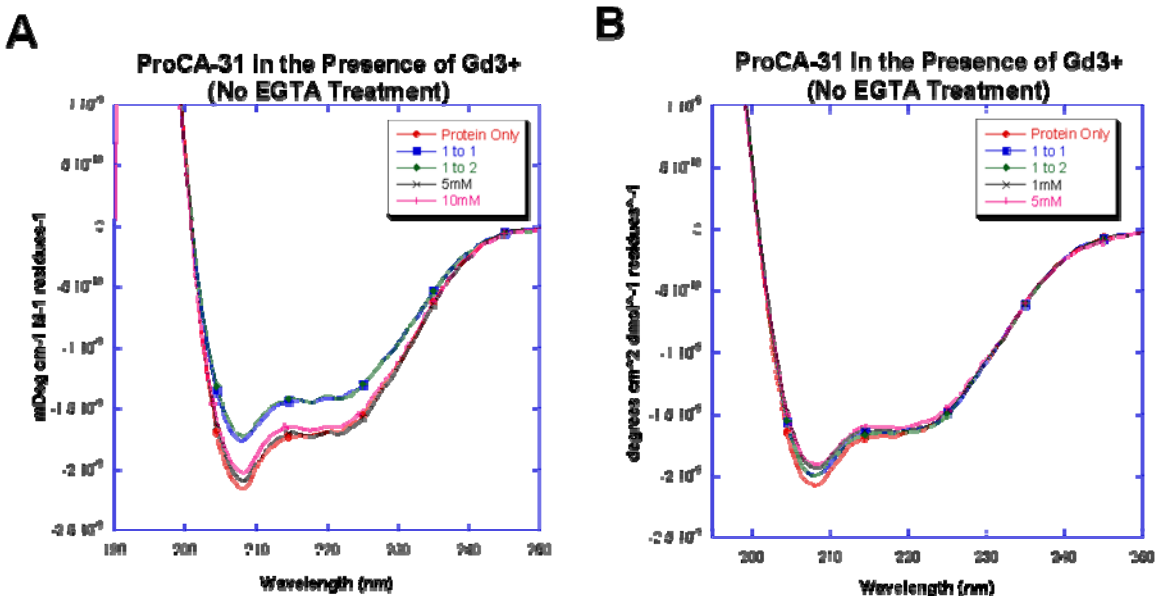

Figure 4.11. Far UV spectra of 6 µM ProCA-31 in the presence varying protein to gadolinium ratios. (A) Low salt conditions. (B) High salt conditions. A buffer of 10mM Tris/HCl chelex pH 7.4 (100 mM NaCl) was used.

4.4.3. ProCA-32

The alpha-helical fold of ProCA-32 is maintained with introduction of a S56D mutation in the CD site of wildtype parvalbumin, indicating that the mutation does not significantly alter the secondary structure of the protein (Figure 4.12). For varying ratios of gadolinium, the helical character increases for almost all ratios and concentrations of added metal under both low and high salt conditions (Figure 4.12). Slightly less spectral differences were noted under high salt conditions, indicating that the presence of 100mM NaCl marginally enhances ProCA-32 stability. Nevertheless, the ProCA-32 alpha-helical content retains the native structure in the presence of gadolinium.

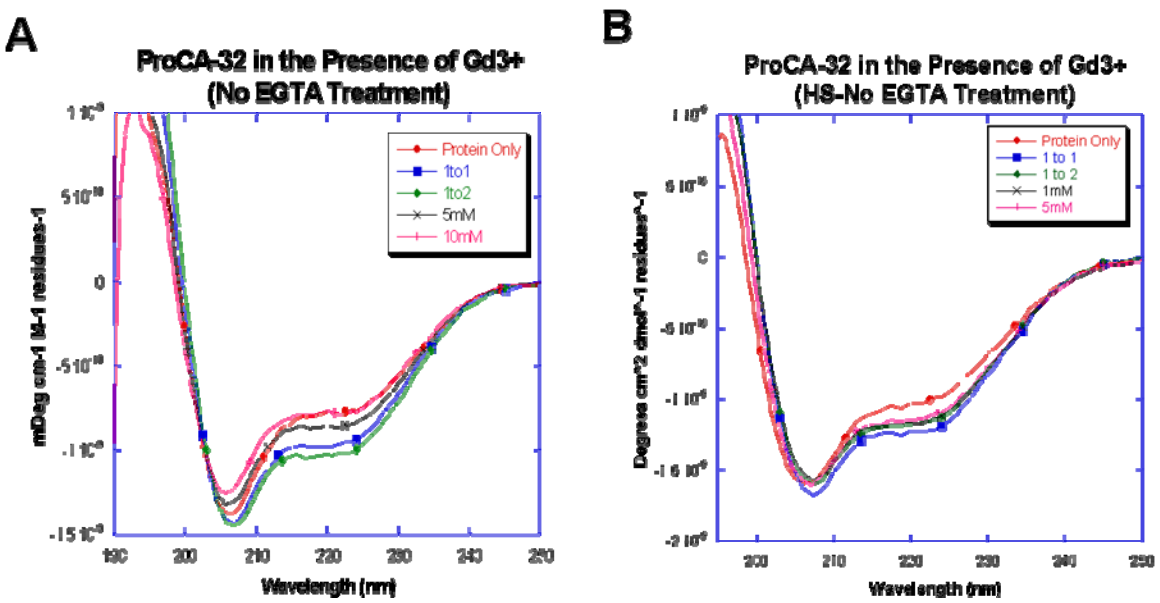

Figure 4.12. Far UV spectra of 6 µM ProCA-32 in the presence varying protein to gadolinium ratios. (A) Low salt conditions. (B) High salt conditions. A buffer of 10mM Tris/HCl chelex pH 7.4 (100 mM NaCl) was used.

4.4.4. ProCA-33

The alpha-helical fold of ProCA-33 is maintained with introduction of an E60D mutation in the CD site of wildtype parvalbumin (Figure 4.13). In the presence of varying gadolinium ratios in the absence of EGTA treatment at low and high salt concentrations, the protein maintains its native α-helical character (Figure 4.13). For varying ratios of gadolinium, the helical content increases for all ratios and concentrations under low salt conditions. Minimal spectral changes were observed under high salt conditions indicating that the presence of salt ions help to stabilize the secondary structure of ProCA-33.

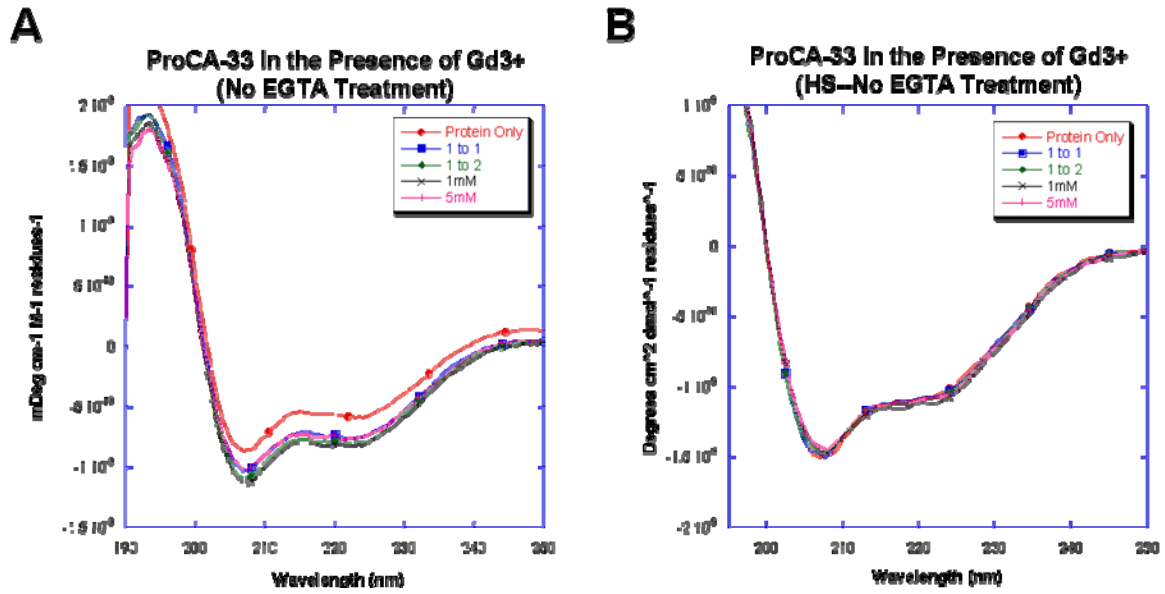

Figure 4.13. Far UV spectra of 6 µM ProCA-33 in the presence varying protein to gadolinium ratios. (A) Low salt conditions. (B) High salt conditions. A buffer of 10mM Tris/HCl chelex pH 7.4 (100 mM NaCl) was used.

4.5. Terbium-Induced Structural Effects

Terbium is a trivalent metal ion used in fluorescent spectroscopy studies to probe the intrinsic properties of metal binding sites within biomolecules. Studies of this sort can provide information concerning the stability of the metal binding site and also contribute to quantifying the binding affinity of a biomolecule to a metal. Although these experiments were not discussed in this thesis, they will be performed in the near future. Thus, it was of importance to examine the secondary structural changes associated with increasing concentration of this metal.

4.5.1. ProCA-30

ProCA-30 maintains an alpha-helical structure like that of wildtype parvalbumin. More specifically, the structure is maintained with increasing concentrations of terbium (Figure 4.14). The spectral differences associated with the low salt spectrum were slightly greater than that of the high salt spectrum. Terbium appears to slightly destabilize the secondary structure of ProCA-

30 under both low and to a nearly negligible degree of high salt conditions. Nevertheless, the native structure is maintained as the concentration of terbium increases.

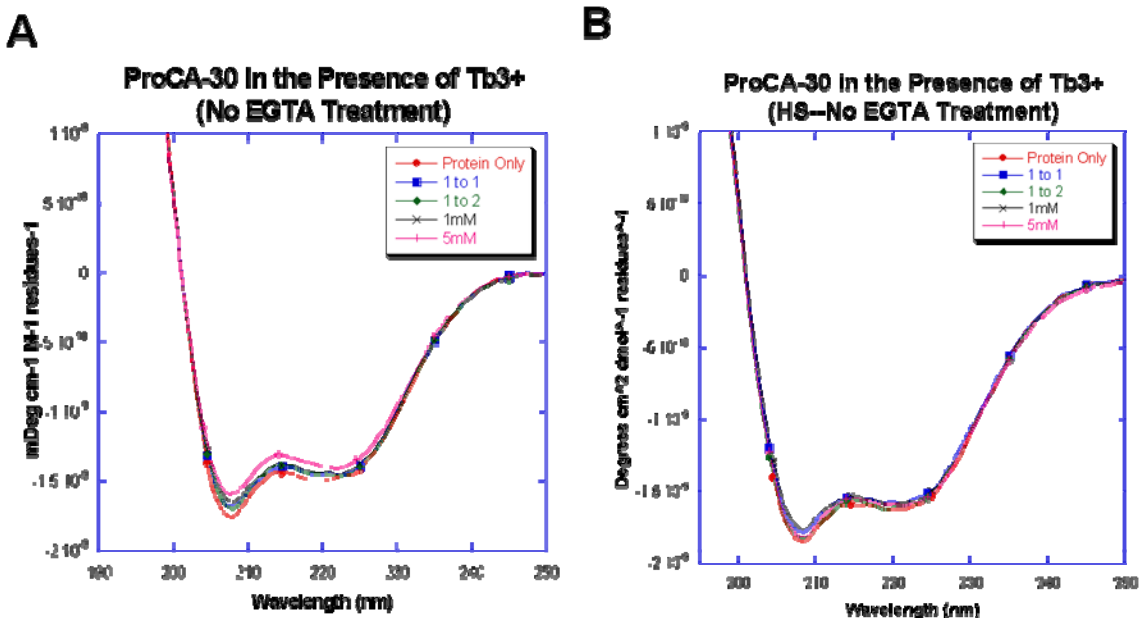

Figure 4.14. Far UV spectra of 6 µM ProCA-30 in the presence varying protein to terbium ratios. (A) Low salt conditions. (B) High salt conditions. A buffer of 10mM Tris/HCl chelex pH 7.4 (100 mM NaCl) was used.

4.5.2. ProCA-31

As mentioned previously, the effects of F103W mutation on the fold of the protein are minor (Figure 4.15). For increasing ratios of terbium, the helical character decreases for all ratios and concentrations. Like ProCA-30, there are nominal spectral differences associated with increasing concentrations of terbium under high salt conditions compared to low salt conditions. Although the helicity is destabilized under both conditions, high salt helps to counter this destabilization. Still, one can conclude that the secondary structure is maintained in the presence of terbium at the tested concentrations.

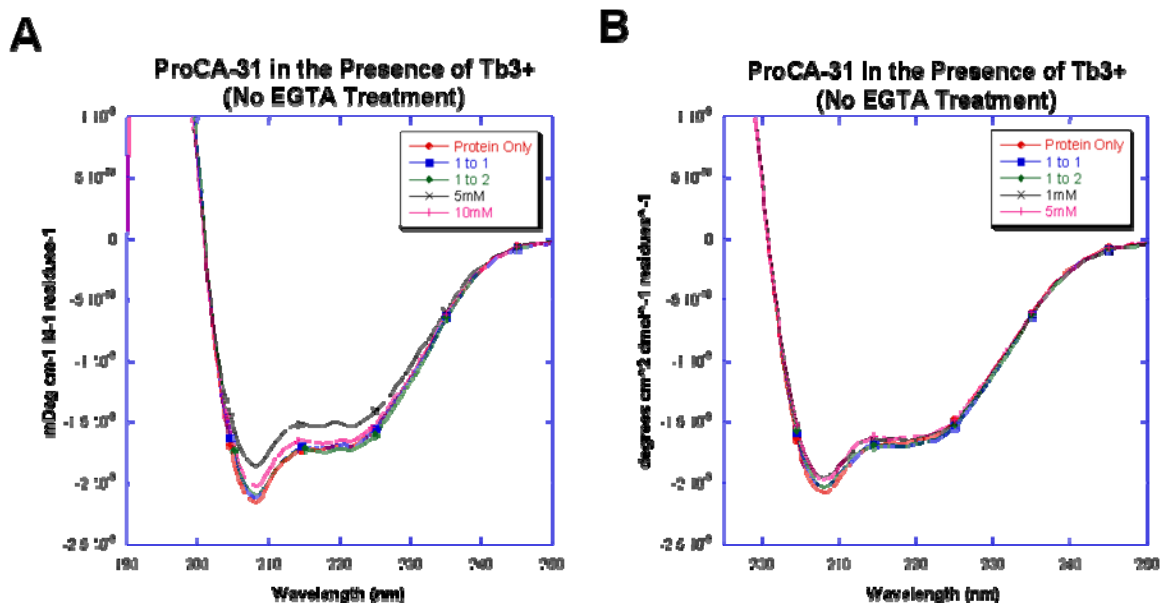

Figure 4.15. Far UV spectra of 6 µM ProCA-31 in the presence varying protein to terbium ratios. (A) Low salt conditions. (B) High salt conditions. A buffer of 10mM Tris/HCl chelex pH 7.4 (100 mM NaCl) was used.

4.5.3. ProCA-32

Once again, the alpha-helical fold of ProCA-32 is maintained with introduction of a S56D mutation in the CD site of wildtype parvalbumin, indicating that the mutation does not significantly alter the secondary structure of the protein (Figure 4.16). For varying ratios of terbium, the helical character increases for concentrations up to 5mM terbium under low and high salt conditions. Thus, though terbium appears to increase the stability of ProCA-32, salt plays little role in affecting the stabilization.

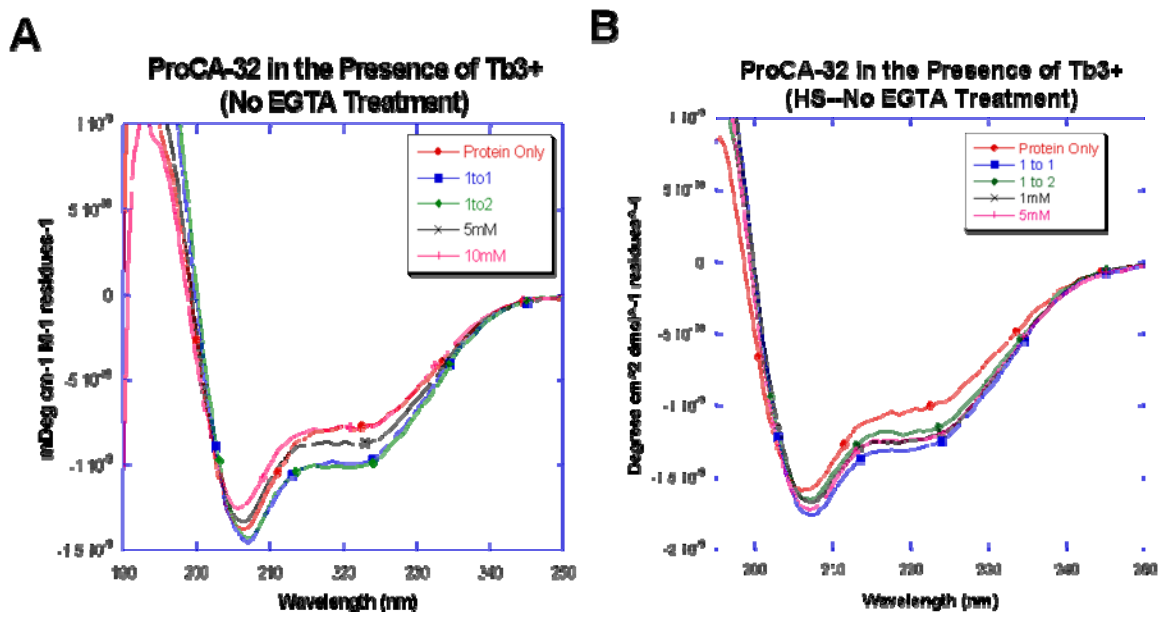

Figure 4.16. Far UV spectra of 6 µM ProCA-32 in the presence varying protein to terbium ratios. (A) Low salt conditions. (B) High salt conditions. A buffer of 10mM Tris/HCl chelex pH 7.4 (100 mM NaCl) was used.

4.5.4. ProCA-33

It has been well established that the alpha-helical fold of ProCA-33 is maintained with introduction of an E60D mutation in the CD site of wildtype parvalbumin (Figure 4.17). In the presence of increasing ratios of terbium in the absence of EGTA treatment at low and high salt concentrations, the protein maintains its native α-helical character (Figure 4.17). For varying ratios of terbium, the helical content increases for all ratios and concentrations under low salt conditions. Only minor spectral changes are associated with high salt conditions indicating that the presence of high salt helps to stabilize the secondary structure of the protein in the presence of increasing concentrations of terbium.

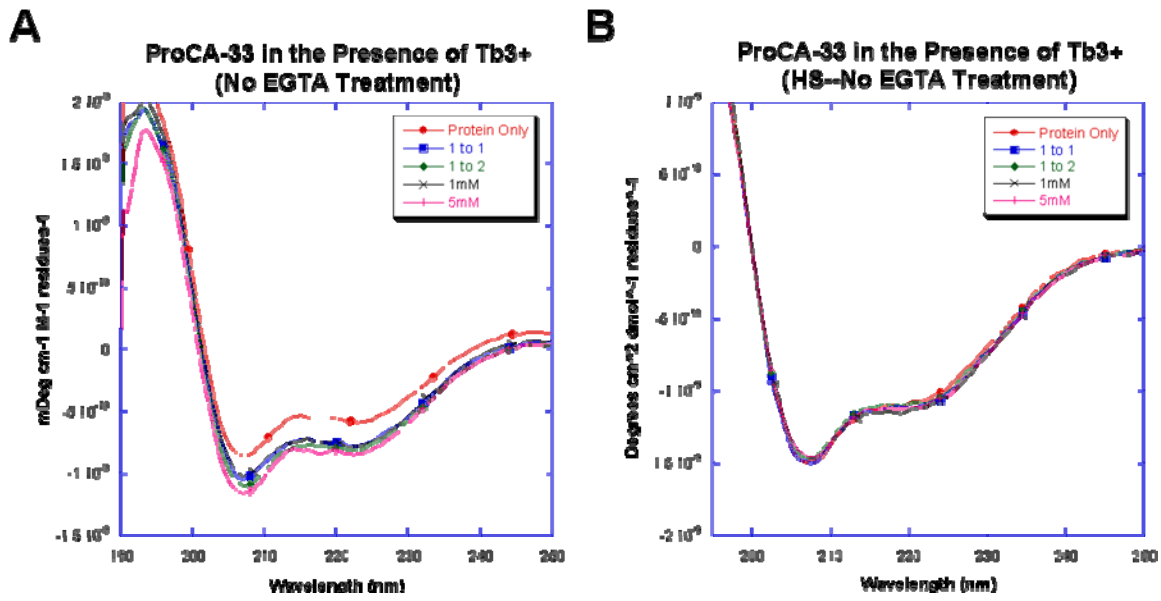

Figure 4.17. Far UV spectra of 6 µM ProCA-33 in the presence varying protein to terbium ratios. (A) Low salt conditions. (B) High salt conditions. A buffer of 10mM Tris/HCl chelex pH 7.4 (100 mM NaCl) was used.

4.6. Summary of Metal-Dependent Secondary Structural Changes

It has been established that ProCA-30 maintains its native secondary structure following bacterial overexpression and purification. This is also confirmed by published CD spectra of ProCA-30 [39]. It was then investigated how the secondary structure of ProCA-31, ProCA-32, and ProCA-33 changed under extremely high concentrations of varying metals (Figure 4.18-4.20).

.

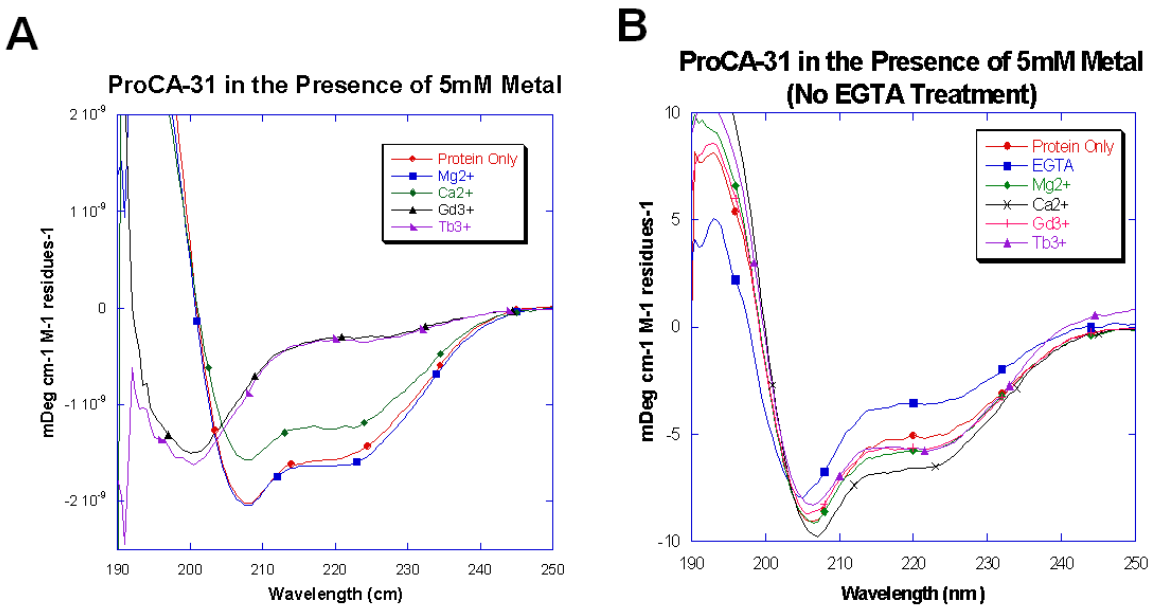

Figure 4.18**.** CD Spectrum of 6 µM ProCA-31 in the Presence of 5mM Metals. (A) In the presence of 5mM EGTA. (B) No EGTA treatment.

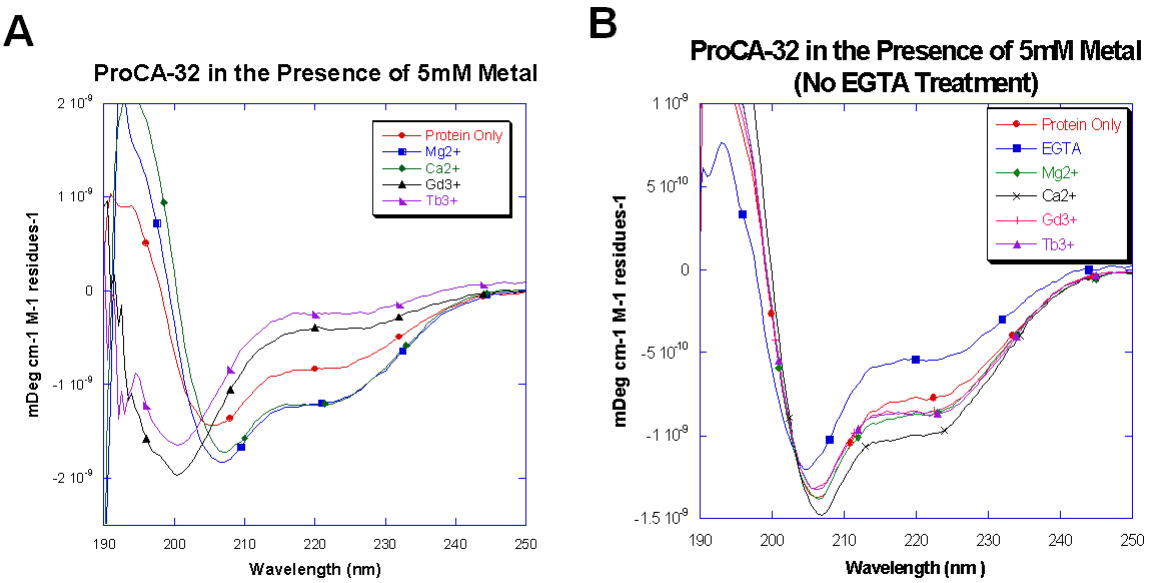

Figure 4.19. CD Spectrum of 6 µM ProCA-32 in the Presence of 5mM Metals. (A) In the presence of 5mM EGTA. (B) No EGTA treatment.

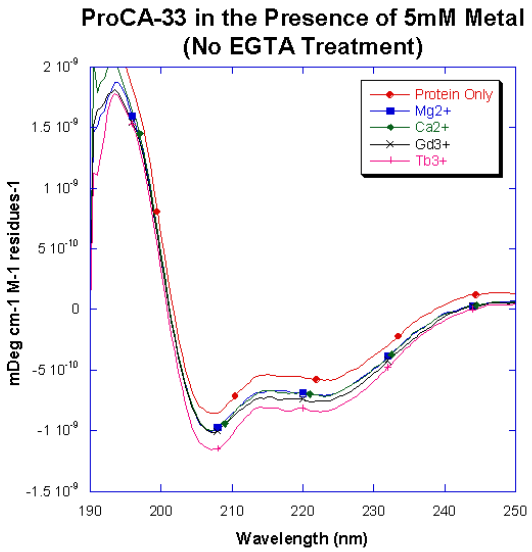

Figure 4.20. CD Spectrum of 6 μM ProCA-33 in the Presence of 5mM Metals in the absence of EGTA.

In the presence of 5mM EGTA and 5mM Tb^{3+} or Gd^{3+}, the α-helical content of ProCA-31 and ProCA-32 decreases in helicity and the spectrum shifts to a random coil (Figures 4.18-4.20). No protein precipitation was noted. There are a number of possible explanations for the random coil formation noted for ProCA-31 and ProCA-32 the presence of 5mM gadolinium and terbium The first may be due to nonspecific binding of metal ions to various sites on the protein, disrupting the hydrogen bonds helping to maintain the protein's native structure. The second explanation may be due to pH effects induced as EGTA binds the metal ions (Table 4.1). For every EGTA that binds a metal ion, four protons are released, decreasing the pH of the system. Though the CD samples are immersed in a buffering system of 10mM Tris/HCl, the 10mM concentration of Tris/HCl may not be sufficient to balance or maintain the pH environment of the sample at pH 7.4. If the conformation of the protein changes from an alpha helix to a random coil at 5mM concentration of these two metals in the absence of EGTA, one can safely assume

that the induction of conformational change was due to nonspecific binding of the metal ion to the protein instead of due to pH changes. This in fact proved to be the case.

At 5mM Mg^{2+}, Ca^{2+}, Tb^{3+}, or Gd^{3+} in the absence of EGTA, the ProCA-31, ProCA-32, and ProCA-33 maintain the native structure. The helical content of ProCA-31 appears to decrease in the presence of calcium and increase in the presence of magnesium. Possible explanations for these phenomena are not well understood. One would anticipate that the helicity of ProCA-31 would increase in the presence of calcium since it has a much stronger binding affinity to this particular metal than magnesium. The helical content of ProCA-33 appears to increase in the presence of all tested metals at 5mM concentration and decrease in the presence of EGTA. One can draw the presumption that the presence of the tested metals enhances the structural stability of ProCA-33.

Table 4.1. pH Effects Observed Before and After the Addition of EGTA.

	ProCA-30		**ProCA-31**		**ProCA-32**		**ProCA-33**	
	10mM metal	**10mM metal and 5mM EGTA**	**10mM metal**	**10mM metal and 5mM EGTA**	**10mM metal**	**10mM metal and 5mM EGTA**	**10mM metal**	**10mM metal and 5mM EGTA**
Mg^{2+}	7.51	6.77	7.50	6.80	7.49	6.86	7.46	6.85
Ca^{2+}	7.36	4.53	7.39	4.39	7.41	4.42	7.42	4.42
Tb^{3+}	6.49	2.23	6.65	2.29	6.60	2.33	6.63	2.27
Gd^{3+}	6.70	2.32	6.54	2.30	6.78	2.35	6.73	2.35

In the presence of varying metal ratios in the absence of EGTA treatment at low and high salt concentrations, the proteins maintain their native α-helical character. Pronounced spectral differences are primarily seen between the low and high salt forms of the protein. Significant structural changes were predominately noted at concentration of 1mM metal and higher. It's reasonable to assume that the background concentration or "contamination" of metals is likely

above 6μM. Therefore, although the buffer signals were subtracted from the metal-contrast agent signals, the added magnesium, calcium, gadolinium, and terbium for 1:1 and 1:2 protein to metal ratios may not be sufficient for displacing resting calcium or magnesium in the CD and EF binding sites. Thus, only minor spectral changes were noted.

In summary, one can conclude that all members of Class ProCA-3 retained the native alpha-helical fold. The introduction of mutations into the skeletal design of Class ProCA-3 did not significantly alter the secondary structure of the protein and the presence of high salt did little to destabilize the structure. Special attention should be paid for significant pH changes following the addition of high concentration of metals in the presence of EDTA. Furthermore, the members of this class exhibit strong secondary structure stability against high concentrations of Mg^{2+}, Ca^{2+}, Tb^{3+}, or Gd^{3+}, allowing one to infer that an excellent scaffold structure chosen for contrast agent design.

4.7. Determined Metal Binding Affinities of Class ProCA-3

For the purposes of presenting a more comprehensive study of the members of Class ProCA-3 agents, the binding affinity of each agent, with the exception of ProCA-30, to calcium, terbium, and gadolinium was determined by senior researcher David Xue. Using a competitive metal titration aided by fluorescence spectroscopy, 20μM of protein in 100mM Tris/HCl 100mM NaCl chelex pH 7.4 was initially saturated with terbium and the binding affinity (k_D) of the protein to terbium was calculated using the Hill equation. Then, terbium was competitively competed out by increasing concentrations of either calcium or gadolinium. Using the equation in Figure 4.21 below, the binding affinity of the protein to either calcium or gadolinium was approximated. ProCA-32 was found to have the highest affinity for gadolinium compared to the other members studied. The remaining k_D values for each agent are listed in Figure 4.22.

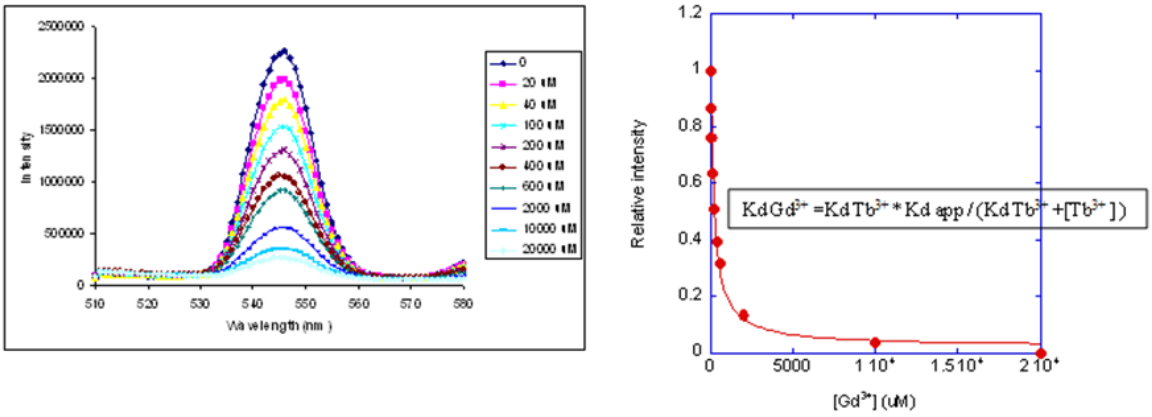

K_d	Ca^{2+} (M)	Tb^{3+} (M)	Gd^{3+} (M)
CA31	3.91 ± 0.96 E-09	4.50 ± 0.28 E-12	1.04E-11
CA32	3.57 ± 0.01 E-09	1.55 ± 0.29 E-18	3.60E-18
CA33	1.05 ± 0.09 E-08	5.34 ± 0.34 E-12	1.24E-11

The dissociation constant of Ca^{2+}, Tb^{3+} and Gd^{3+} to contrast agent were measured by fluorescence spectroscopy. To determine the Ca^{2+} dissociation constant, the intrinsic tryptophan of CA31, CA32, CA33 or tyrosine from CA20, CA22, CA23 fluorescence changes were used to monitor the binding process between contrast agent and metal.

Figure 4.21. Class ProCA-3 metal binding ability.

5. RELAXIVITY MEASURES

5.1. Introduction

As discussed in chapter 1 (section 1.1.2), relaxivity is a quantitative term used to reflect the intrinsic contrast capability of a contrast agent per gadolinium ion. The measured relaxivity is governed by the sample prep conditions and the relaxation properties of the agent discussed in chapter 1. Thus, it is important to determine the conditions for sample preparation. This chapter describes studies on the required sample volume, incubation time frame, and metal equilibration for accurate *in vitro* relaxation time measurements. Additionally, two different protocols for measuring relaxivity were implemented to determine how the relaxivity of the contrast agents change when bound to one gadolinium versus two and to accurately determine the maximum relaxivity and binding mode. The effect of salt on the measured relaxivity of the members of Class ProCA-3 was also investigated

The conditions for measuring relaxivity as they relate to the effect of sample volumetric changes, effect of sample incubation time, and extent of time required for metal equilibration were first determined. To determine the effect an increase in volume has on the relaxation times, the relaxation times of low concentrations of free gadolinium at 200μL and 400μL volumes were measured. Figure 5.1A illustrates that the differences in T1 relaxation times are within the range of fitting error (with the exception of 10μM gadolinium) while more notable differences were observed in T2 relaxation times. However, these results are not reliable, as they are within the range of residual background metal concentrations as later explained in the details outlining optimization of the fixed gadolinium protocol. Because less pronounced changes were noted in T1, it was decided to continue using 200μL volumes for relaxivity measurements.

To determine the effects of different incubation times at 37˚C on relaxation times, a sample of 50μM ProCA-32 and 100μM Gd^{3+} was arbitrarily chosen to note changes for 5 minutes, 4 hours, and overnight incubation. Figure 5.1B yields that there are only minor variances in the relaxation times as a function of incubation time. SDS-PAGE analysis indicates that the protein is stable over the measured incubation times. However, it is important to note the inconsistency in the density of the bands for lanes 1 and 2 of the gel in Figure 5.1C. This was likely due to a sample loading human error. Nevertheless, it appears that the length of incubation up to overnight conditions at 37˚C has no significant effect on the relaxation times.

To determine the extent of metal equilibration time necessary to measure accurate relaxation times, a ProCA-31 relaxivity sample, pseudo-form of ProCA-30, was chosen under the presumption that the contrast agent bearing the weakest binding affinity to gadolinium (found by Senior PhD researcher David Xue) would require the longest amount of time to bind the metal compared to ProCA-32 and ProCA-33. Therefore, ProCA-31 was prepared in a 1 to 2 ratio (50μM ProCA-31 and 100μM gadolinium) and the concentration of free metal following 30 minutes, 3 hours, and overnight equilibration was measured using a weak calcium-binding dye Rhodamine-5N (Figure 5.1C). Theoretically, the optimal equilibration time will have the lowest concentration of free metal. Of the observed time points, it was found that overnight equilibration yielded the lowest concentration of free metals. Therefore, it was determined that the relaxivity samples for future measure (fixed gadolinium experiments) would be equilibrated overnight.

A

Free Gd^{3+} → 200uL vs 400 µL Sample Volume				
$[Gd^{3+}]$ (mM)	T1 (ms) 200uL	T1 (ms) 400uL	T2 (ms) 200uL	T2 (ms) 400uL
0.001	3590 ± 20	3620 ± 30	2065 ± 1	1879 ± 3
0.005	3190 ± 30	3230 ± 20	1936 ± 1	1751 ± 3
0.01	2810 ± 30	2870 ± 20	1767 ± 1	1625 ± 3

B

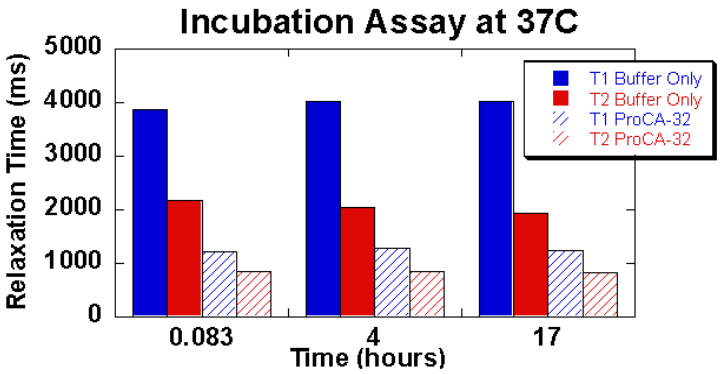

C

1) **Fresh: ProCa-31 only**
2) **Fresh: 20 µM ProCa-31 and 40 µM $GdCl_3$**
3) **30 minutes: 20 µM ProCa-31 and 40 µM $GdCl_3$**
4) **3 hours: 20 µM ProCa-31 and 40 µM $GdCl_3$**
5) **Overnight: 20 µM ProCa-31 and 40 µM $GdCl_3$**
6) **Marker**

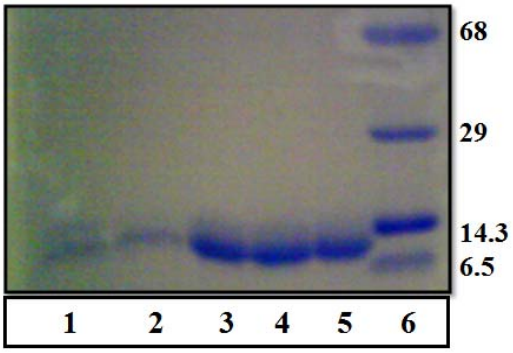

Time of Sample Equilibration	Trial 1 $[M]_{free}$, M	Trial 2 $[M]_{free}$, M	Average $[M]_{free}$, M
30 minutes	$2.833 \times 10^{-12} \pm 1.480 \times 10^{-13}$	$4.946 \times 10^{-12} \pm 6.114 \times 10^{-14}$	$3.890 \times 10^{-12} \pm 1.057 \times 10^{-12}$
3 hours	$2.580 \times 10^{-12} \pm 8.656 \times 10^{-14}$	$6.271 \times 10^{-12} \pm 2.520 \times 10^{-13}$	$4.426 \times 10^{-12} \pm 1.846 \times 10^{-12}$
Overnight	$2.423 \times 10^{-12} \pm 1.213 \times 10^{-12}$	$1.453 \times 10^{-11} \pm 1.219 \times 10^{-12}$	$8.477 \times 10^{-12} \pm 6.054 \times 10^{-12}$

5.1. Optimizing Relaxivity Sample Prep Conditions. (A) Volumetric observations. (B) Incubation time assay. (C) Metal equilibration schemes.

5.2. Determining Relaxivity Using Two Different Protocols

The parameter relaxivity is directly proportion to the amount of signal intensity visualized in an MR image. Therefore, the higher the relaxivity, the greater the signal intensity and thus a more improved differentiated image of normal versus diseased tissues. Here, we use two different methods to determine an accurate relaxivity value. The traditional method for measuring relaxivity is well established. It is commonly implemented to measure the relaxivity of commercially available contrast agents. Using this method, the relaxation times of different protein-gadolinium samples prepared at a fixed ratio were measured. The slope of the linear plots represents the relaxivity of the sample at the fixed ratio. The second method used involves fixing the gadolinium concentration and increasing the protein concentration. It was originally developed to design a novel way of using a relaxometer to measure the binding affinity of a protein to gadolinium. Details into extrapolating the dissociation constant from the relaxivity data are not discussed here. This newly developed method also allows one to eliminate effects on relaxivity associated with the interference of non-specific binding of gadolinium with the contrast agents at significantly high concentrations of gadolinium. Using this method, one can obtain the maximum relaxivity of the protein-gadolinium complex by averaging the relaxivity of ratios occurring in the plateau portion of the curve formed during the experiment. Furthermore, this method allows one to gain insight into the binding stoichiometry of developed contrast agents. The latter two uses for the newly developed protocol are discussed in this thesis.

5.3. Traditional Methods for Measurement

Class ProCA-3 Agents are multi-binding site contrast agents that can selectively bind a maximum of two metal ions, one in their CD and EF sites respectively. We assume that there is little to no nonspecific binding of gadolinium at the experimental concentrations used, as we do

not exceed a 1:2 protein to gadolinium ratio in our sample preparative methods. However, this must be further investigated. Though secondary structural analysis was performed, it is unclear at this time how increasing concentrations of metal affect the tertiary structure of the agents. Also, it has not been determined whether decreasing the ratio of protein to gadolinium in solution will lead to significant global structural changes. This also must be further investigated. Nevertheless, it has been proposed that increasing the number of gadolinium binding sites shortens the longitudinal and transverse relaxation times, thus increasing the relaxivity. For this reason, the relaxivity for the 1:2 ratio is expected to be higher than that of the 1:1 ratio. However, this phenomenon is not observed under low or high salt conditions (see section 2.6 for experimental details).

Using the traditional protocol mentioned in chapter 2 (section 2.6), the relaxation times T1 and T2 were measured at fixed protein to gadolinium ratios of 1:1 and 1:2 under low and high salt conditions. The concentration (μM) ratios of protein to gadolinium for the 1:1 experiment were as follows: 10:10, 20:20, 30:30, 40:40, and 50:50. The concentration (μM) ratios of protein to gadolinium for the 1:2 experiment were as follows: 10:20, 20:40, 30:60, 40:80, and 50:100. This concentration dependence assay allows for one to calculate the *in vitro* relaxivity as a function of protein concentration (or of gadolinium concentration for 1:1) by taking the slope of the line formed by the series of fixed protein to gadolinium ratios. To calculate the relaxivity of the 1:2 experiment as a function of gadolinium concentration, the slope of the line must be halved. Otherwise, the relaxivity as a function of the protein concentration for the 1:2 experiments can be taken from the slope of the line. Tables 5.1 and 5.2 reveal the calculated relaxivity values per gadolinium ion for the developed contrast agents discussed in this thesis.

Table 5.1. In vitro relaxivity of designed contrast agents under low salt conditions.

	1:1		1:2	
Developed Contrast Agent	R1 (mM^{-1} s^{-1})	R2 (mM^{-1} s^{-1})	R1 (mM^{-1} s^{-1})	R2 (mM^{-1} s^{-1})
Gd DTPA	3.8	4.5	3.8	4.5
ProCA-30	28.13 ± 1	36.75 ± 1	27.20 ± 1	35.42 ± 2
ProCA-31	28.10 ± 3	36.25 ± 4	31.87 ± 4	41.60 ± 4
ProCA-32	7.64 ± 0.2	10.04 ± 1	20.40 ± 6	26.64 ± 7
ProCA-33	5.07 ± 0.1	5.49 ± 1	8.08 ± 1	10.43 ± 1

The samples were prepared in 10mM Tris/HCl chelex pH 7.44.

Table 5.2. In vitro relaxivity of designed contrast agents under high salt conditions.

	1:1		1:2	
Developed Contrast Agent	R1 (mM^{-1} s^{-1})	R2 (mM^{-1} s^{-1})	R1 (mM^{-1} s^{-1})	R2 (mM^{-1} s^{-1})
Gd DTPA	3.8	4.5	3.8	4.5
ProCA-30	27.33 ± 2	36.11 ± 2	28.32 ± 1	33.36 ± 6
ProCA-31	31.38 ± 0.3	40.86 ± 1	28.32 ± 2	36.52 ± 7
ProCA-32	9.46 ± 0.3	12.17 ± 0.3	21.07 ± 1	27.52 ± 1
ProCA-33	5.05 ± 0.2	5.55 ± 1	7.82 ± 1	8.62 ± 2

The samples were prepared in 10mM Tris/HCl chelex 100mM NaCl pH 7.44.

As one can observe, the T1 and T2 times for ProCA-30 shorten as the protein to metal ratio increases for both low and high salt conditions (Figure 5.2).

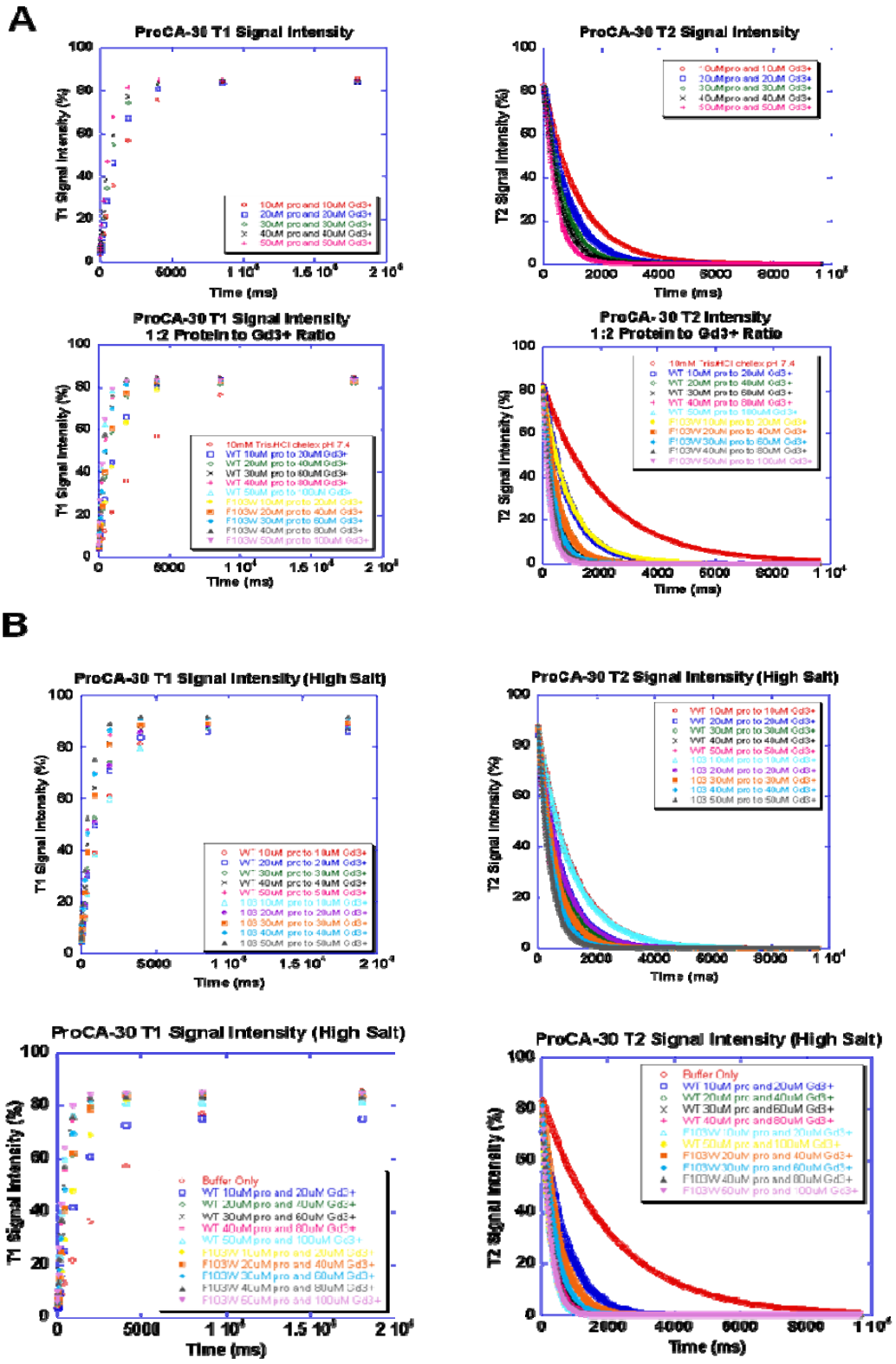

Figure 5.2. ProCA-30 T1 and T2 Signal Intensity Plots per traditional relaxivity methodology. (A) Signal intensity under low salt conditions. (B) Signal intensity under high salt conditions.

The average R1 and R2 values for ProCA-30 under low salt conditions for a 1:1 binding ratio are 28.13 ± 1 mM^{-1} s^{-1} and 36.75 ± 1 $mM^{-1}s^{-1}$, respectively while for a 1:2 binding ratio, the values are 27.20 ± 1 mM^{-1} s^{-1} and 35.42 ± 2 mM^{-1} s^{-1}, respectively. Similarly, the average R1 and R2 values or ProCA-30 under high salt conditions for a 1:1 binding ratio are 27.33 ± 2 mM^{-1} s^{-1} and 36.11 ± 2 mM^{-1} s^{-1}, respectively while for a 1:2 binding ratio, the average relaxivities are 28.32 mM^{-1} s^{-1} ± 1 and 33.36 ± 6 mM^{-1} s^{-1}, R1 and R2 respectively (Figure 5.3).

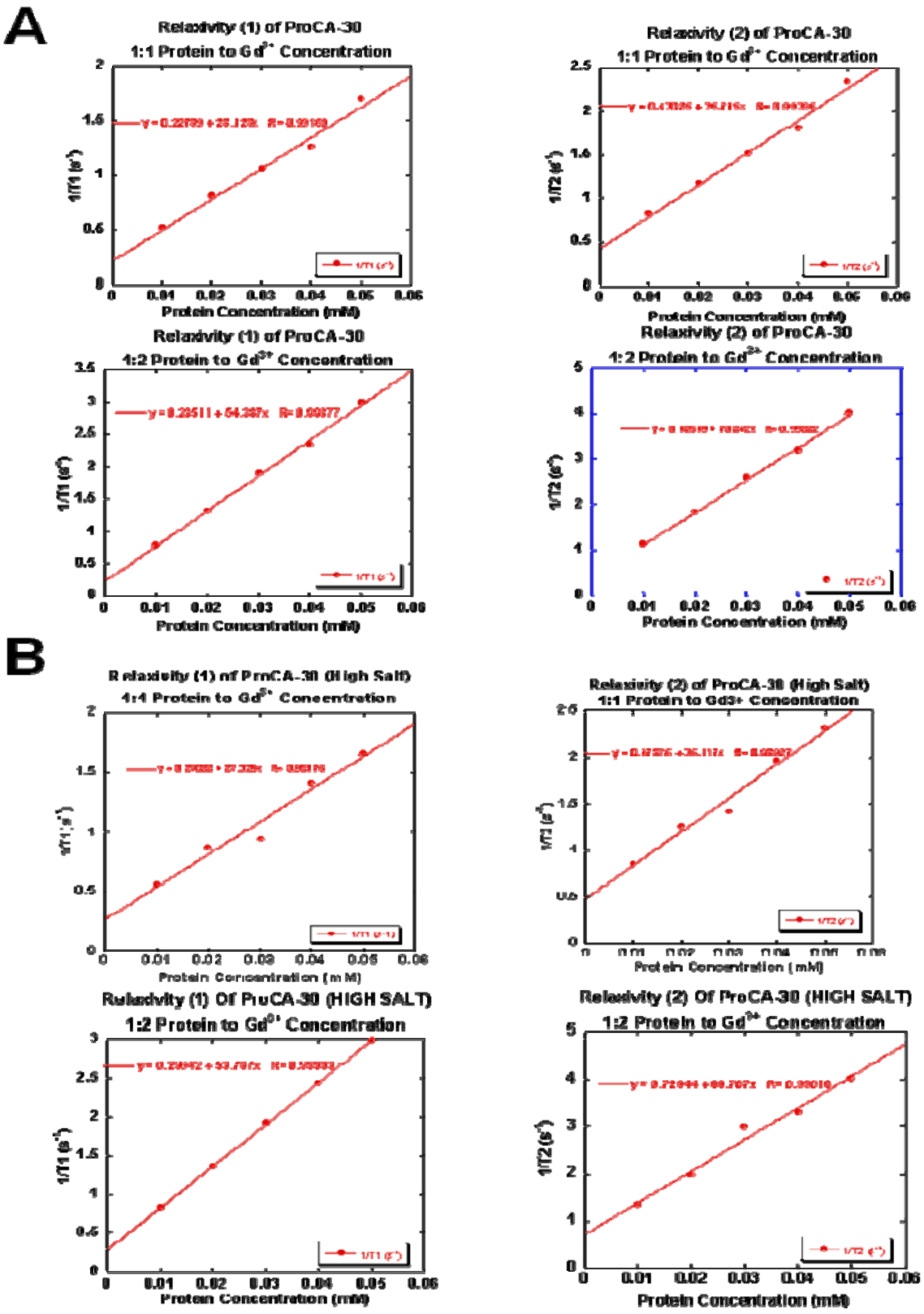

Figure 5.3. ProCA-30 R1 and R2 linear plots of $1/T_{1,2}$ vs. protein concentration. (A) Linear plots under low salt conditions. (B) Linear plots under high salt conditions.

There were little differences between the 1:1 and 1:2 ratios under both low and high salt conditions, indicating that the presence of high salt does little to significantly alter the relaxivity values. Furthermore, the saturation of both binding sites in ProCA-30 does not significantly enhance the relaxivity. Correlating this with the CD data in chapter 4 (section 4.4.1), although increasing concentrations of gadolinium appears to destabilize the secondary structure under both low and high salt conditions, the presence of high salt does little to disturb metal-dependent structural changes (Figure 4.10). Additionally, the nominal CD spectral differences associated with a 1 to 1 and 1 to 2 binding ratio are consistent with the little variance in relaxivity values for these ratios under both salt conditions. Moreover, these values yield exciting results, showing that the relaxivity 1 and 2 values of ProCA-30 are significantly higher than those of commercial Gd-DTPA of 3.8 mM^{-1} s^{-1} and 4.5 mM^{-1} s^{-1}, respectively.

Like that of ProCA-30, the T1 and T2 times of ProCA-31 shorten as the protein to metal ratio increases for both low and high salt conditions (Figure 5.4).

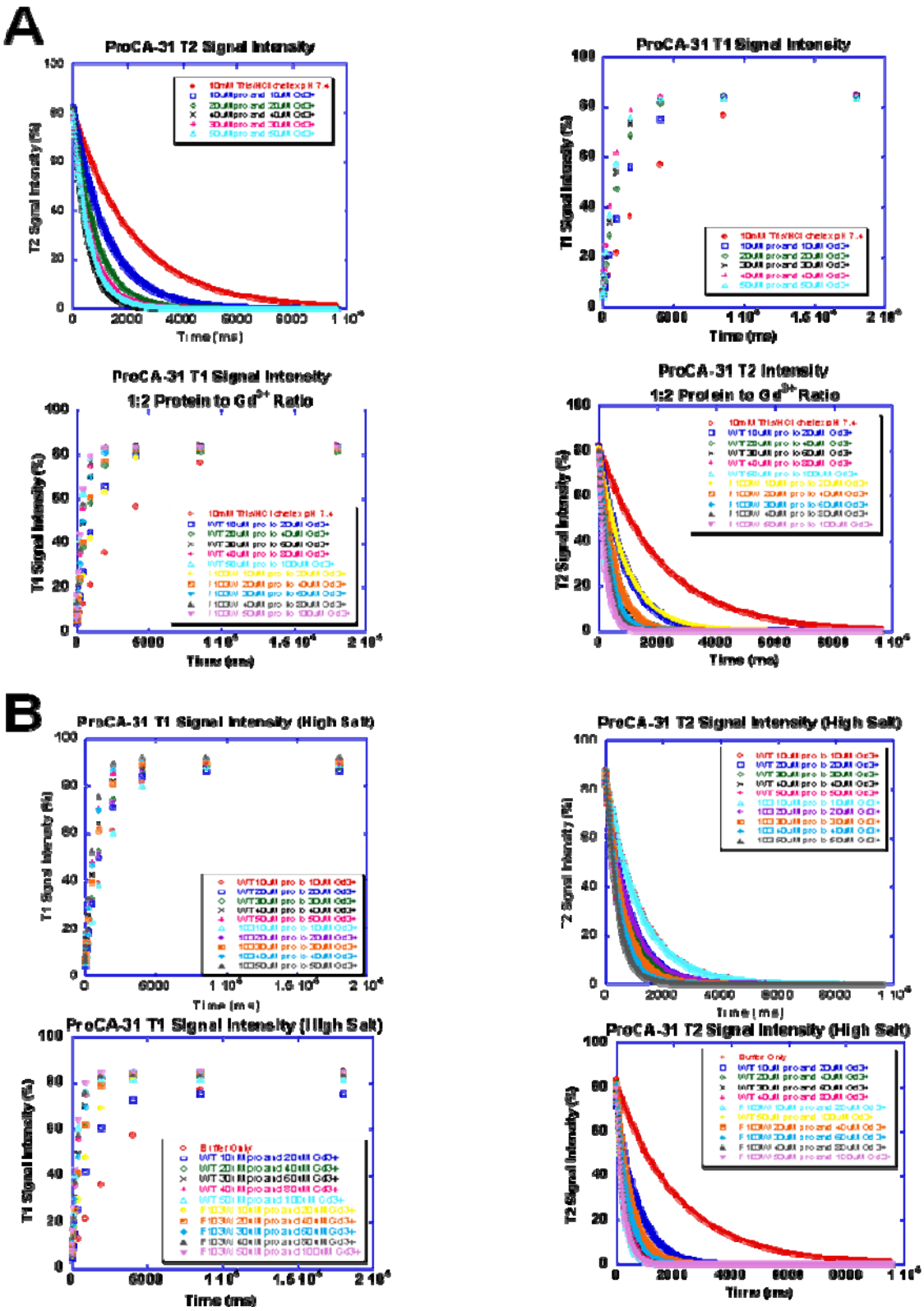

Figure 5.4. ProCA-31 T1 and T2 Signal Intensity Plots per traditional relaxivity methodology. (A) Signal intensity under low salt conditions. (B) Signal intensity under high salt conditions.

The average R1 and R2 values of ProCA-31 under low salt conditions for a 1:1 binding ratio are 28.10 ± 3 mM^{-1} s^{-1} and 36.32 ± 4 $mM^{-1}s^{-1}$, respectively while for a 1:2 binding ratio, the values are 31.87 ± 4 mM^{-1} s^{-1} and 41.60 ± 4 mM^{-1} s^{-1}, respectively. Under high salt conditions for a 1:1 binding ratio, the average R1 and R2 values are 31.38 ± 0.3 mM^{-1} s^{-1} and 40.86 ± 1 mM^{-1} s^{1}, respectively while for a 1:2 binding ratio under high salt conditions, the averaged R1 and R2 values are 28.32 ± 2 mM^{-1} s^{-1} and 36.52 ± 7 mM^{-1} s^{-1}, respectively (Figure 5.5). Like ProCA-30, the presence of high salt does not significantly alter the relaxation times. Correlating this with the CD data in chapter 4 (section 4.4.2), although increasing concentrations of gadolinium appears to destabilize ProCA-31 secondary structure under low salt conditions, the presence of high salt helps stabilize the metal-dependent structural changes (Figure 4.11). Additionally, the CD spectral differences associated with a 1 to 1 and 1 to 2 binding ratio are inconsistent with the relaxivity values under low salt conditions and consistent with the little variance in relaxivity values for these ratios under high salt conditions. It is apparent that the structural destabilization under low salt conditions is not significant enough to alter the relaxivity values.

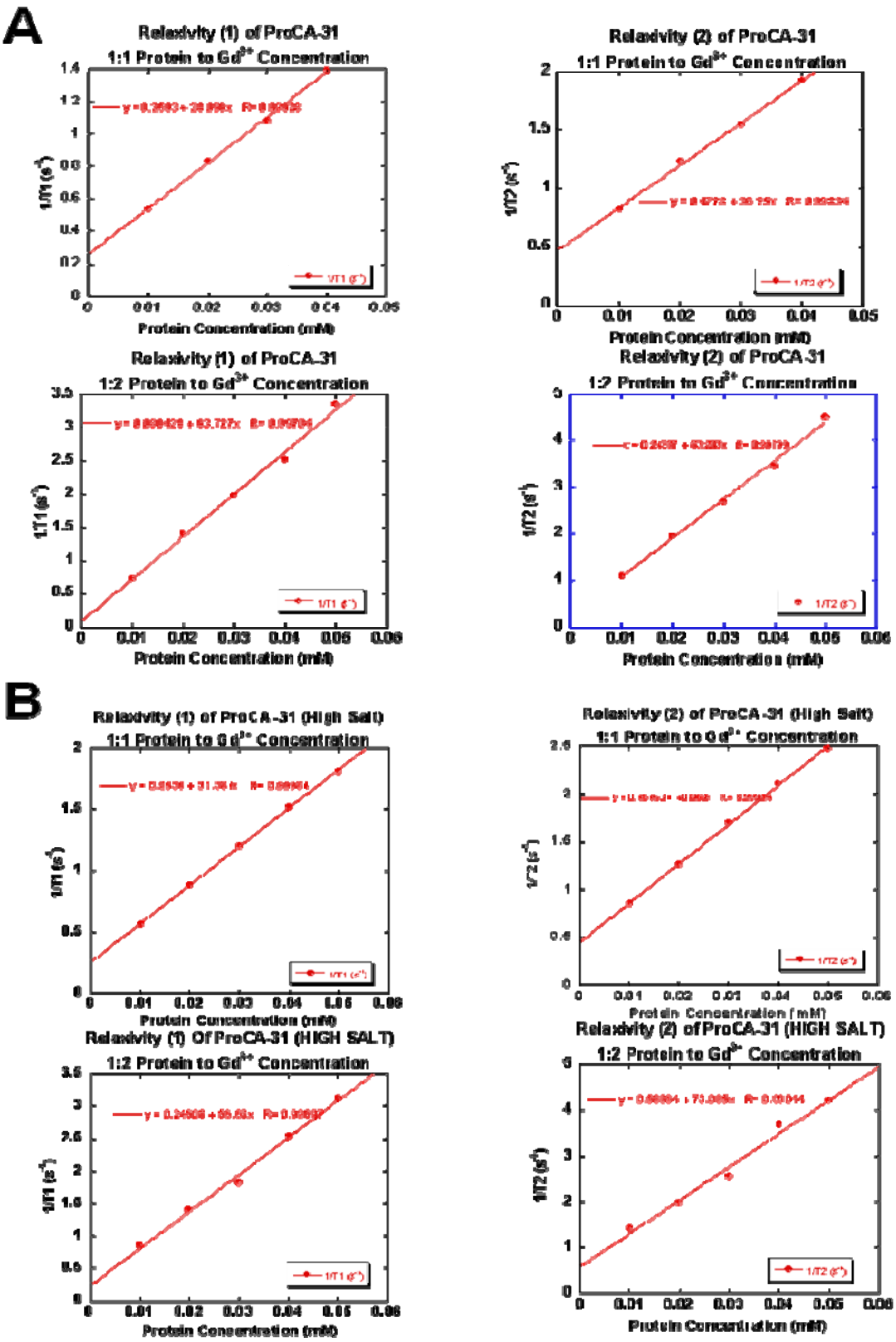

Figure 5.5. ProCA-31 R1 and R2 linear plots of $1/T_{1,2}$ vs. protein concentration. (A) Linear plots under low salt conditions. (B) Linear plots under high salt conditions.

It appears that ProCA-30 and ProCA-31 have nearly identical relaxivity values. If one recalls, these two agents represent the control and pseudo-control agents for Class ProCA-3. It is apparent that the F103W mutation made just outside of the EF loop (ProCA-31) of the skeletal structure of the protein does little to perturb its intrinsic relaxation times. These results are exciting, as they not only reveal relaxivity 1 and 2 values significantly higher than those of commercial Gd-DTPA of 3.8 mM^{-1} s^{-1} and 4.5 mM^{-1} s^{-1}, respectively, but also allow one to conclude that the introduction of a tryptophan residue at position 103 proves as an effective tool to potentially monitor the intrinsic fluorescence of Class ProCA-3 agents for future structural and metal-binding studies. A high salt environment only slightly lowers the relaxivity values for ProCA-31 as compared to low salt conditions.

The relaxivity of ProCA-32 yields interesting results. As one can observe, the T1 and T2 values shorten as the protein to metal ratio increases for both low and high salt conditions (Figure 5.6).

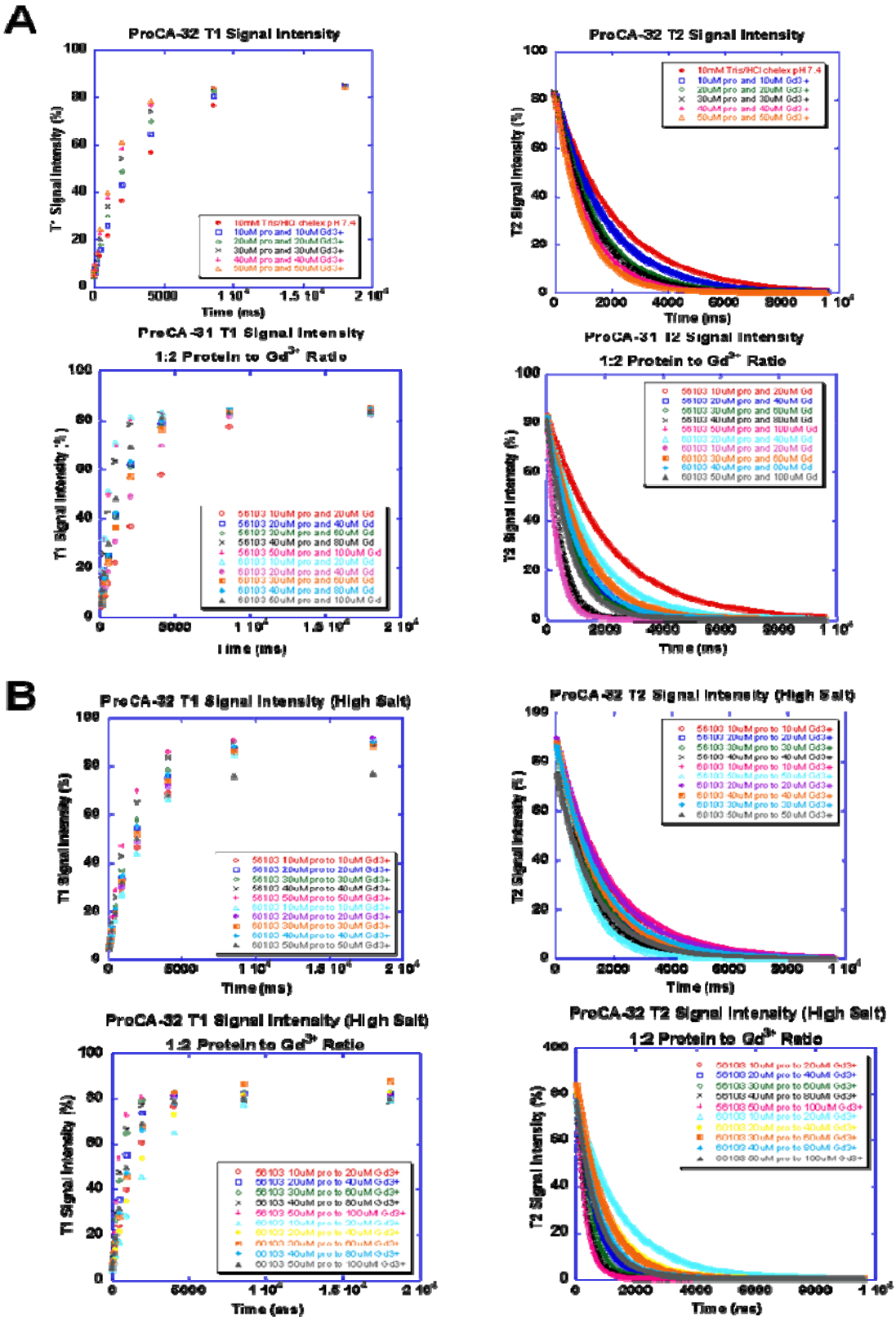

Figure 5.6. ProCA-32 T1 and T2 Signal Intensity Plots per traditional relaxivity methodology. (A) Signal intensity under low salt conditions. (B) Signal intensity under high salt conditions.

The average R1 and R2 values for ProCA-32 under low salt conditions for a 1:1 binding ratio are 7.64 ± 0.2 mM^{-1} s^{-1} and 10.04 ± 1 $mM^{-1}s^{-1}$, respectively while for a 1:2 binding ratio, the values are 20.40 ± 6 mM^{-1} s^{-1} and 26.64 ± 7 mM^{-1} s^{-1}, respectively. The average R1 and R2 values under high salt conditions for a 1:1 binding ratio are 9.46 ± 0.3 mM^{-1} s^{-1} and 12.17 ± 0.3 mM^{-1} s^{-1}, respectively while for a 1:2 binding ratio, the values are 21.07 ± 1 mM^{-1} s^{-1} and 27.52 ± 1 mM^{-1} s^{-1}, respectively (Figure 5.7).

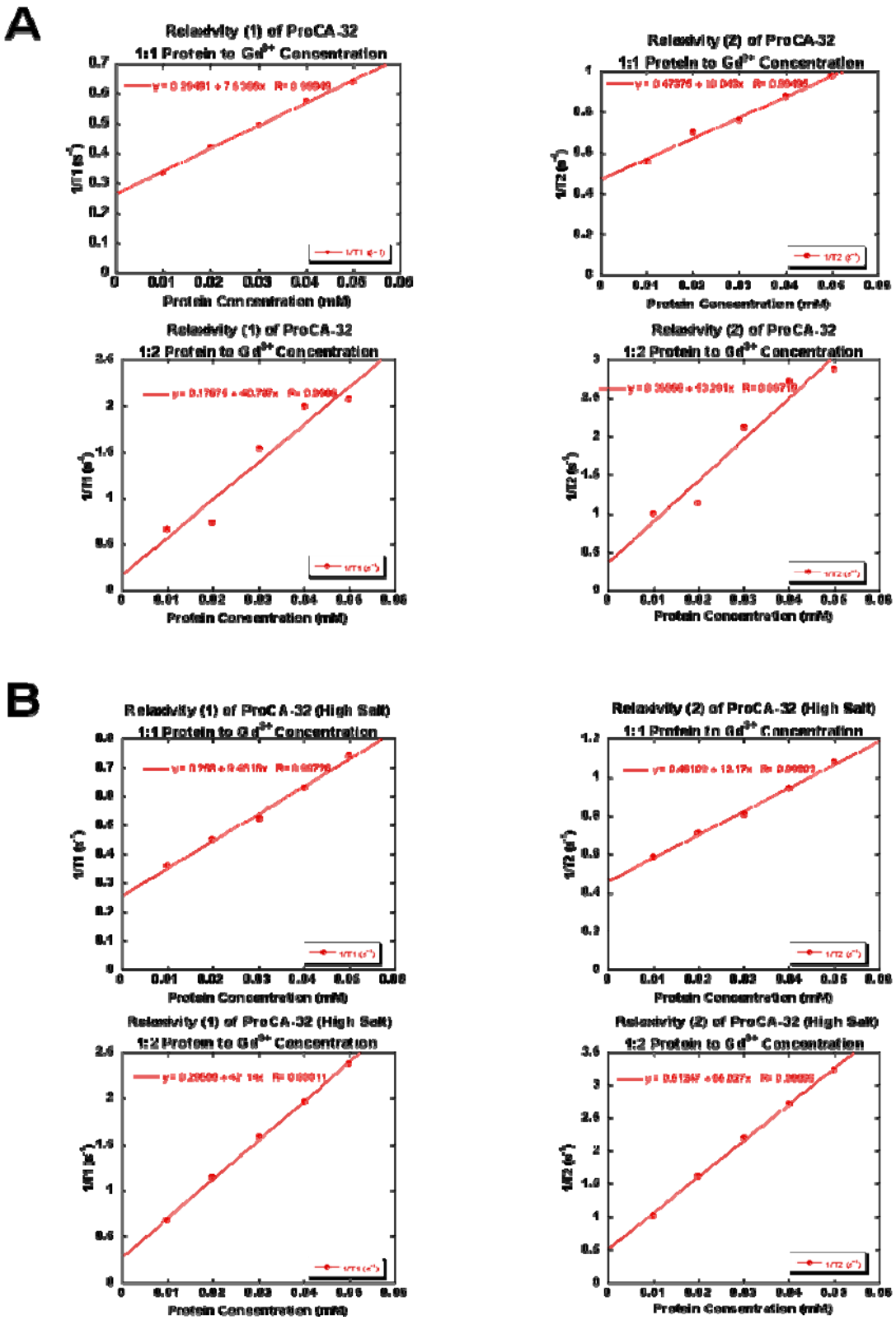

Figure 5.7. ProCA-32 R1 and R2 linear plots of $1/T_{1,2}$ vs. protein concentration. (A) Linear plots under low salt conditions. (B) Linear plots under high salt conditions.

The 1 to 1 relaxivity values under low salt conditions are slightly lower than those under high salt conditions. However, the 1 to 2 binding ratios under both salt conditions are within the range of error. This indicates that high salt has a more positive effect on increasing the relaxivity at the 1 to 1 ratio versus the 1 to 2 ratio. As one can infer, the 1:2 ratios are nearly 2.5 times higher that of the 1:1 under both low and high salt conditions. Correlating this with the CD data in chapter 4 (section 4.4.3), increasing concentrations of gadolinium appears to stabilize ProCA-32 secondary structure under both salt conditions. However, as with the 1 to 1 relaxivity samples, the presence of high salt helps better stabilize the metal-dependent structural changes (Figure 4.12). The lack of CD spectral differences associated with a 1 to 1 and 1 to 2 binding ratio under both salt conditions is inconsistent with the increase in relaxivity values for these ratios. It appears that the measured relaxation times of ProCA-31 are independent of metal-induced changes in secondary structure.

Previous binding studies of this class of agents have shown that ProCA-32 bears the highest binding affinity to gadolinium. Here, it appears that the introduction of an additional charged residue into the CD site of the contrast agent significantly improves the relaxivity of the contrast agent at a 1:2 ratio versus a 1:1 ratio. These results are exciting, revealing relaxivity 1 and 2 values significantly higher than those of commercial Gd-DTPA of 3.8 mM^{-1} s^{-1} and 4.5 mM^{-1} s^{-1}, respectively. The presence of high salt does little to significantly alter the relaxivity values. By design, the site-directed mutagenesis approach has improved the relaxivity of the agent following metal saturation. However, it's important to note here that the relaxivity of ProCA-30 and ProCA-31, void of CD or EF site mutations, maintain higher relaxivity values than that of ProCA-32. These results are not well understood. It's possible that the introduction of an additional charged residue enhances dimerization of the agent in solution, hampering the

relaxivity or rather increasing the relaxation times measured. This negative effect could possibly be related to significantly slowing the rotational correlation time.

Like ProCA-32, the relaxivity results for ProCA-33 yield unexpected values. Like the previously mentioned members of Class ProCA-3 agents, the T1 and T2 intensity values for ProCA-33 decrease as the protein to metal ratio decreases for both low and high salt conditions (Figure 5.8).

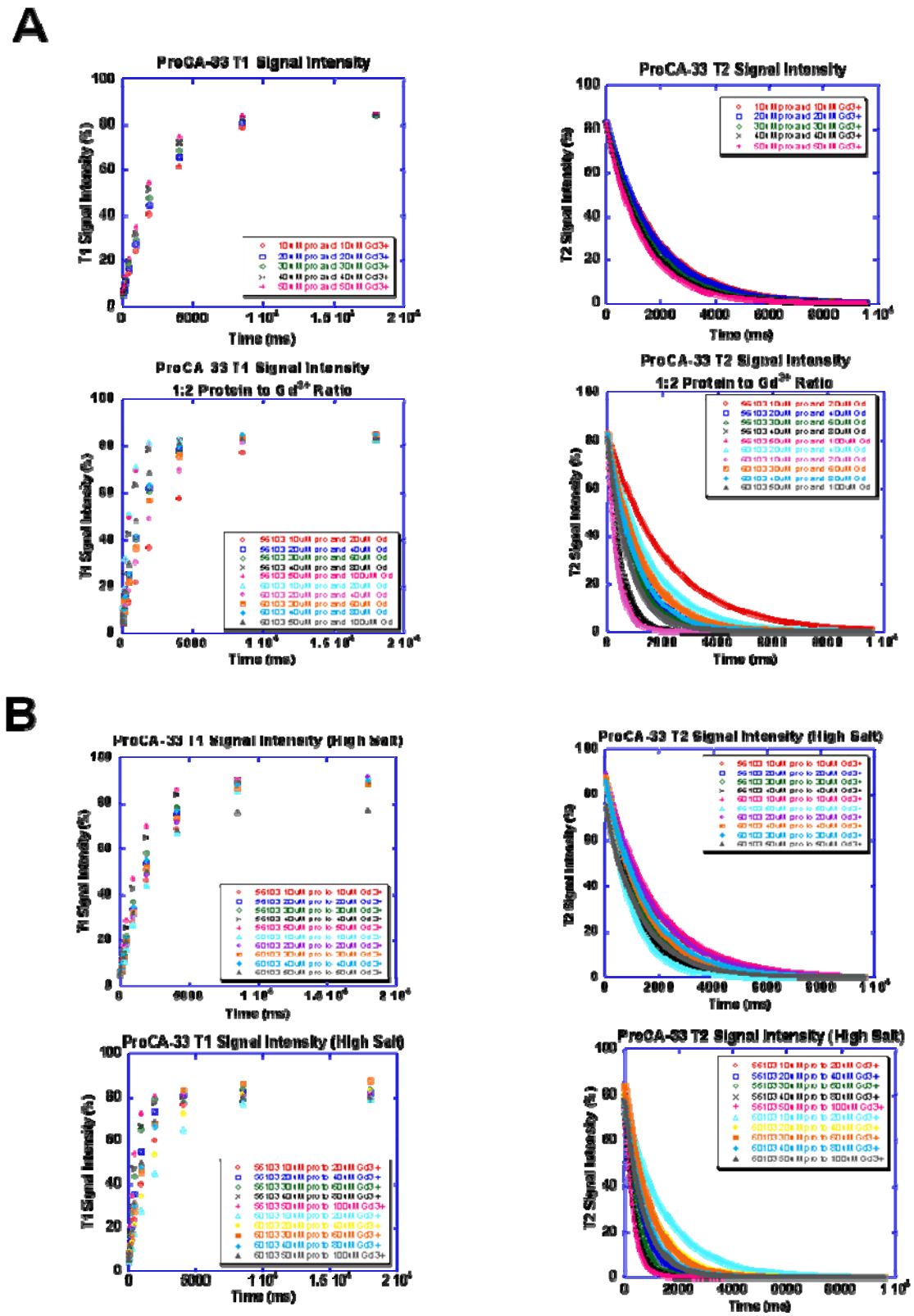

Figure 5.8. ProCA-33 T1 and T2 Signal Intensity Plots per traditional relaxivity methodology. (A) Signal intensity under low salt conditions. (B) Signal intensity under high salt conditions.

The average R1 and R2 values under low salt conditions for a 1:1 binding ratio are 5.065 ± 0.1 mM^{-1} s^{-1} and 5.49 ± 1 mM^{-1} s^{-1}, respectively while that for a 1:2 binding ratio are 8.08 ± 1 mM^{-1} s^{-1} and 10.43 ± 1 mM^{-1} s^{-1}, respectively. The average R1 and R2 values under high salt conditions for a 1:1 binding ratio are 5.05 ± 0.2 mM^{-1} s^{-1} and 5.55 ± 0.3 mM^{-1} s^{-1}, respectively while that for a 1:2 binding ratio are 7.82 ± 1 mM^{-1} s^{-1} and 8.62 ± 1 mM^{-1} s^{-1}, respectively (Figure 5.9).

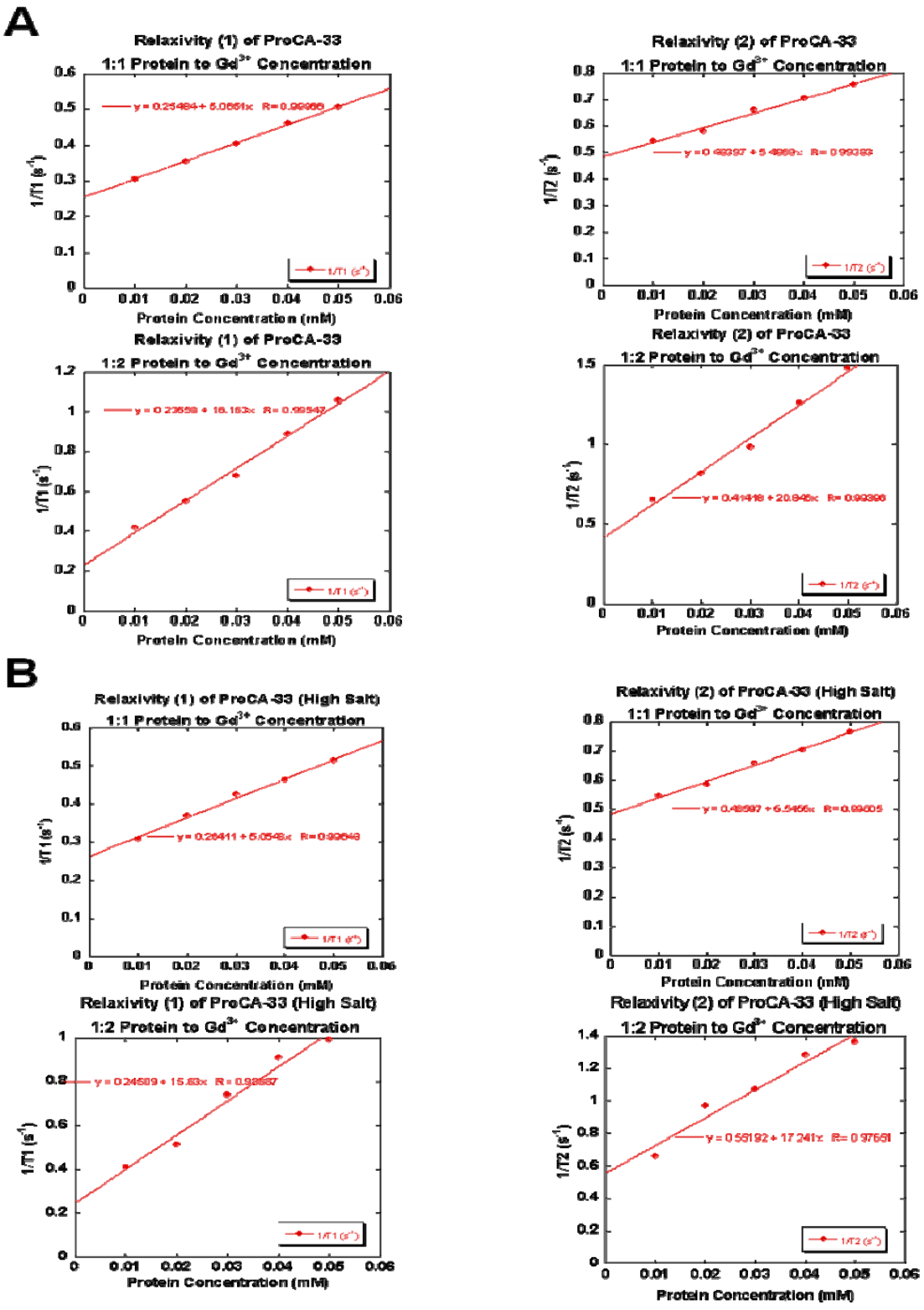

Figure 5.9. ProCA-33 R1 and R2 linear plots of $1/T_{1,2}$ vs. protein concentration. (A) Linear plots under low salt conditions. (B) Linear plots under high salt conditions.

The presence of high salt does little to significantly alter the relaxivity values. Furthermore, the 1:2 ratios are only slightly higher than that of the 1:1 under both low and high salt conditions. Correlating this with the CD data in chapter 4 (section 4.4.4), increasing concentrations of gadolinium appears to stabilize ProCA-32 secondary structure under low salt conditions (Figure 4.12). The presence of high salt appears to stabilize the metal-dependent structural changes (Figure 4.12). The lack of CD spectral differences associated with a 1 to 1 and 1 to 2 binding ratio under both salt conditions is consistent with the measured relaxivity values for these ratios.

The ProCA-33 results do not reveal relaxivity 1 and 2 values *significantly* higher than those of commercial Gd-DTPA of 3.8 mM^{-1} $s^{-1}$and 4.5 mM^{-1} s^{-1}, respectively. It seems the introduction of a slightly shorter residue in the CD site of the skeletal design of the agent (E60D) may perturb the intrinsic properties of the CD gadolinium binding site and hamper the optimal effects associated with the rate of water exchange in the metal binding site. Hence, there are minimal changes in relaxivity associated with the saturation of the protein agent with two gadolinium ions versus one metal ion. Additionally, the low relaxivity values may also be due to the same dimerization phenomenon given as an explanation for ProCA-32's lower relaxivity. The notably low relaxivity values for ProCA-33 compared to those of previously discussed members of Class ProCA-3 requires further investigation.

In summary, it appears that the measured relaxivity values are not necessarily affected by metal-induced structural changes. ProCA-32 is the only member of Class ProCA-3 whose increase in relaxivity from the 1 to 1 to the 1 to 2 ratio under both salt conditions doesn't correlate significant changes in the protein's secondary structure. The remaining members yield positive correlations with the CD data between their consistent relaxivity values under both salt conditions at 1 to 1 and 1 to 2 ratios.

5.4. Measuring Relaxivity by Fixing [Gd^{3+}] and Increasing Protein Concentration

The primary goal of this experiment is multifaceted. Using different fixed concentrations of gadolinium (10, 50, or 100 μM) with increasing protein concentration, we are able to determine the optimal range for approximating the binding affinity of gadolinium to the protein used, the binding stoichiometry (that is whether the protein binds one, two, etc gadolinium ions), and the average relaxivity. *It's important to note here that for proteins with multiple binding sites, an assumption has been made that all the binding sites have equal binding affinities (based on published results of parvalbumin for example) and the data can thus be fit by a 1 to 1 equation. This method is still in further development and therefore not mentioned in this protocol.* Still, using the optimal fixed concentration of gadolinium and increasing the protein concentration, we can effectively determine the binding mode of the protein and approximate the maximum relaxivity 1 and 2 (R1 and R2) of the contrast agent used.

5.4.1. Protocol Optimization Using ProCA-30

To determine whether the protein to metal binding is truly at a 1:2 ratio, $GdCl_3$ was fixed at varying concentrations and the concentration of protein was steadily increased. Figure 5.10 depicts the change in relaxation times of ProCA-30 as the ratio of protein to gadolinium increases for fixed 10μM, 50μM, and 100μM gadolinium.

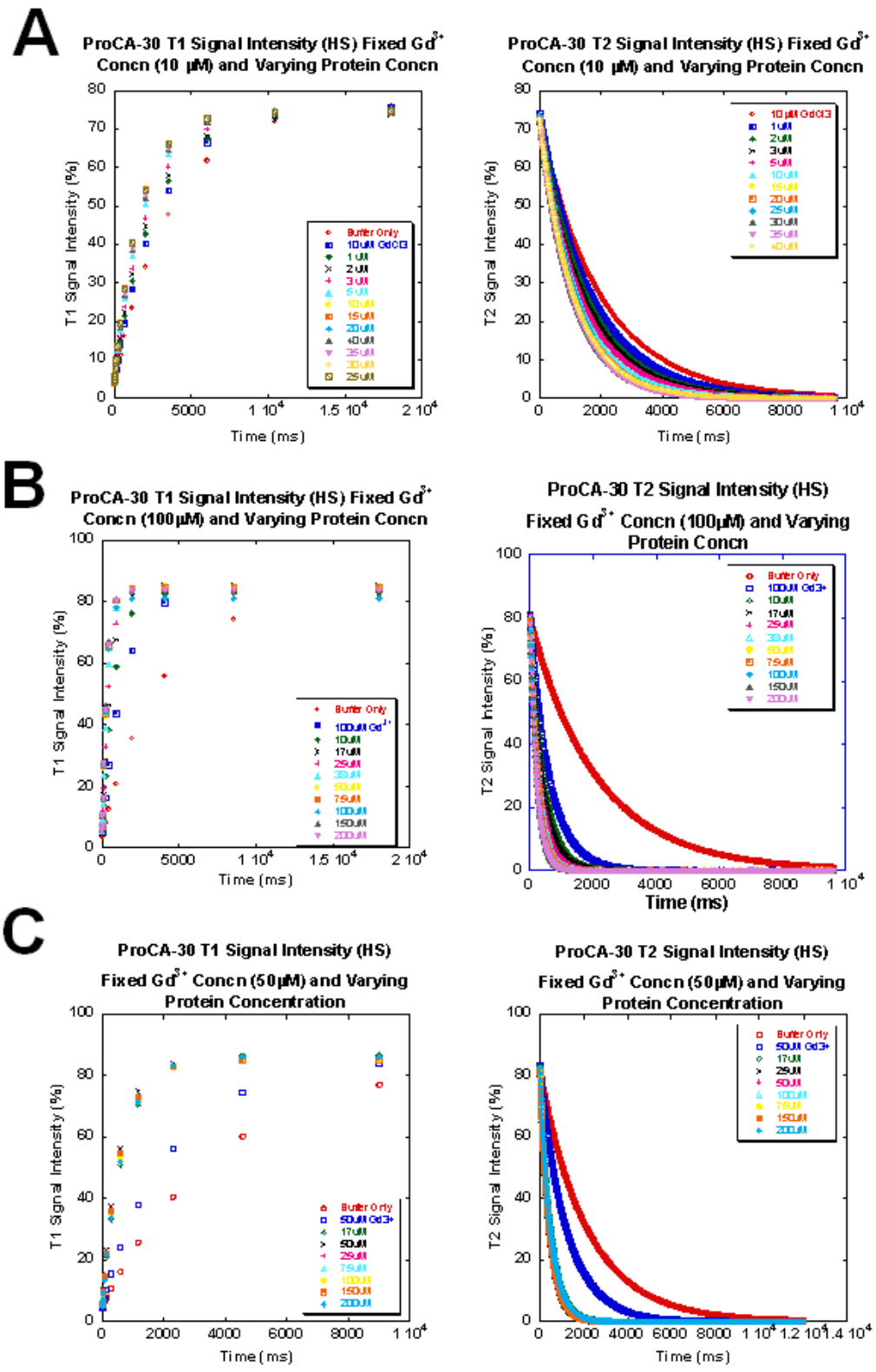

Figure 5.10. ProCA-30 T1 and T2 Signal Intensity Plots per fixed 10, 50, and 100µM Gd^{3+} concentration.

The protein concentration was then plotted as a function of the reciprocal T values to yield a hyperbolic curve. If the binding is 1:1, the curve will reach saturation at a protein concentration equal to that of the fixed Gd^{3+} concentration. If the binding is 1:2, the curve will reach saturation at a protein concentration equal to one-half of the fixed Gd^{3+} concentration (Figure 5.11).

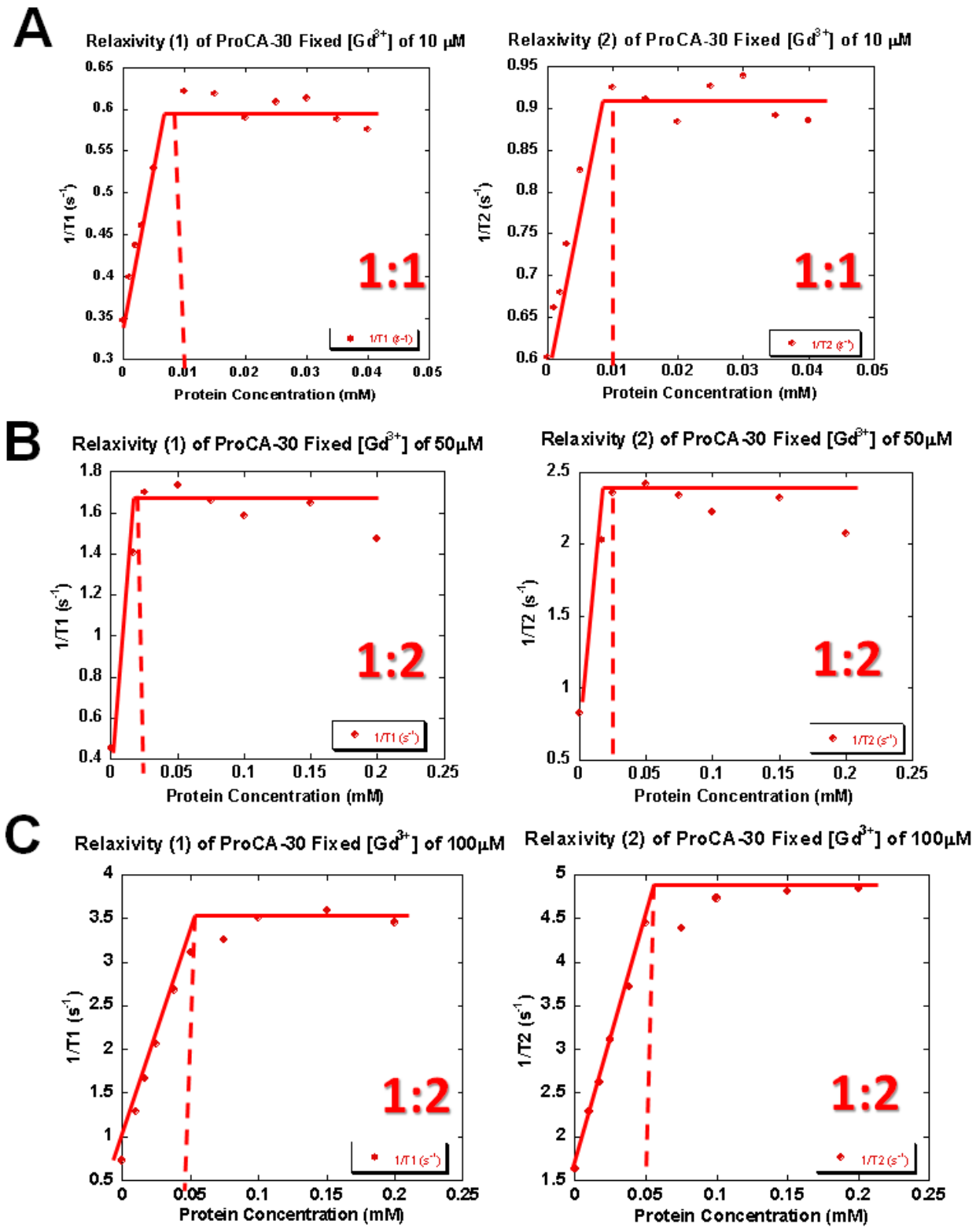

Figure 5.11. Relaxivity curves of ProCA-33 at different fixed concentrations of Gd^{3+}. (A) ProCA-30 at fixed 10µM [Gd^{3+}]. (B) ProCA-30 at fixed 50µM [Gd^{3+}]. (C) ProCA-30 at fixed 100µM [Gd^{3+}].

At a fixed 10μM concentration of Gd^{3+}, the curve reaches saturation at 10μM of protein concentration. It appears that the binding is 1:1 at this concentration. However, there are minimal changes in the relaxation times as the ratio of protein to gadolinium increases, indicating that the measured values have a fairly large range of error. Furthermore, it's likely that this low fixed concentration of gadolinium is not ideal for determining the binding mode or relaxivity, as background metal contamination due to calcium or magnesium may significantly interfere with gadolinium binding to the designed metal binding site in the contrast agent. For example, if calcium background "contamination" is equal to or higher than that of fixed 10μM gadolinium, then at a 1:1 protein to gadolinium concentration ratio, the ratio of protein to gadolinium may be equal to that of protein to calcium. This implies that the binding sites of the contrast agent may be saturated with calcium and gadolinium and thus gadolinium cannot completely displace calcium from the binding site at such a low fixed concentration. Thus, the relaxivity of the contrast agent cannot be accurately measured. At fixed 50 and 100μM concentrations of Gd^{3+}, the curves reach saturation at one-half of their respective fixed Gd^{3+} concentrations (Figure 5.11 B-C). The change in relaxation times are much more pronounced as the ratio of protein to gadolinium increases when compared to that of a fixed 10μM concentration of Gd^{3+}. From our experiments thus far, we have found that a fixed concentration of 100 μM gadolinium (and to a slightly lesser degree 50 μM) yields the most accurate range for measuring changes in relaxation times with increasing protein concentration at a fixed gadolinium value. Thus, this concentration range is optimal for determining the binding mode and average relaxivity of a contrast agent.

Both the fixed 50μM and 100μM concentrations of Gd^{3+} indicate that ProCA-30 binds Gd^{3+} in a 1:2 protein to gadolinium ratio and the possibility of nonspecific binding can be excluded from the potential alternative binding modes of the protein (Figure 5.11 B-C). The

average R1 and R2 for ProCA-30 were calculated to be 31 ± 2 mM^{-1} s^{-1} and 42 ± 2 mM^{-1} s^{-1}, respectively. These values are nearly identical to those calculated from the traditional method (Table 5.2).

5.4.2. ProCA-31

Using a fixed concentration of 100µM Gd^{3+}, the signal intensity trends of relaxation time follow a similar pattern to that of ProCA-30 (Figure 5.12). The relaxation times shorten as the ratio of protein to gadolinium increases until the protein becomes fully saturated with gadolinium.

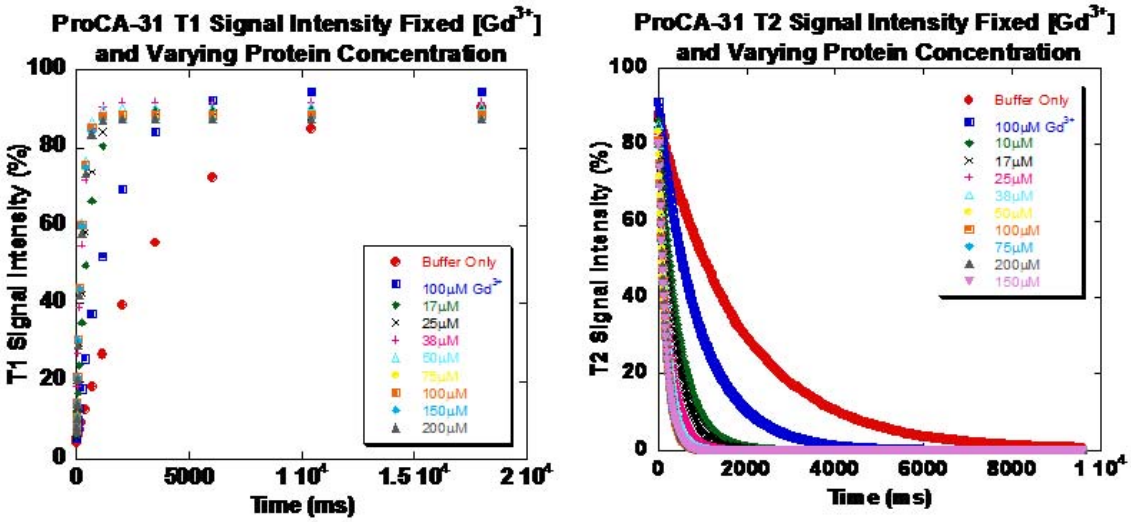

Figure 5.12. ProCA-31 T1 and T2 signal intensity plots at a fixed [Gd^{3+}] of 100µM.

The change in relaxation times reaches saturation at 50µM ProCA-31, indicating that the binding is 1:2. The average R1 and R2 values calculated from the saturated portion of the curve in are 42.87 ± 1 mM^{-1} s^{-1} and 55.75 ± 1 mM^{-1} s^{-1}, respectively (Figure 5.13). Comparing these values to that of the 1:2 relaxivity values approximated by the traditional method, ProCA-31 has a higher relaxivity (Table 5.2). Furthermore, it maintains relaxivity values nearly ten times that of ProCA-30. The reasons behind this significant difference in R1 and R2 values are not well

understood. One could postulate that the addition of a tryptophan residue just outside of the EF gadolinium binding site changes the inner sphere water coordination, slowing the rate of water molecule exchange with the bulk solvent. As a result, the relaxation time is shortened and the relaxivity increases. Still, this must be further investigated.

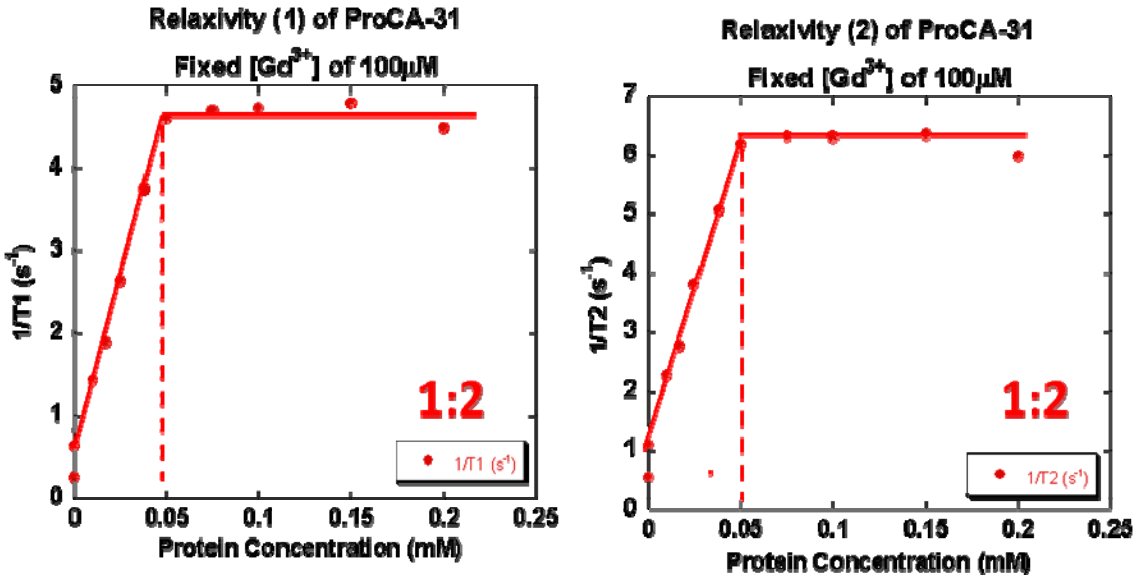

Figure 5.13. Relaxivity curves of ProCA-31 at a fixed 100µM concentration of Gd^{3+}.

5.4.3. ProCA-32

Like ProCA-30 and ProCA-31, the relaxation times shorten as the ratio of protein to gadolinium increases until the protein reaches a 1:2 concentration ratio with gadolinium. However, as the ratio of protein to gadolinium begins to increase above this ratio, the relaxation times begin to steadily lengthen (Figure 5.14, Figure 5.15). Thus, the overall relaxivity calculated from the slope of the ratios above 1:2 yield a relaxivity value significantly lower than anticipated. Using a fixed concentration of 100µM Gd^{3+}, the change in decreasing relaxation times peaks at 50µM ProCA-32, indicating that the binding is 1:2. The average R1 and R2 values calculated from the saturated portion of the curve in Figure 5.15 are 15.39 ± 0.4 mM^{-1} s^{-1} and

19.95 ± 1 mM^{-1} s^{-1}, respectively. Comparing these values to that of the 1:2 relaxivity values approximated by the traditional methods, ProCA-32 has a lower relaxivity (Table 5.2).

It is unclear why the curve rapidly drops at ratios higher than 1:2 (Figure 5.15). The reasons behind this observed phenomenon are not well understood. One possible explanation could be due to the heterogeneous nature of ProCA-32 gadolinium binding sites. The serine to aspartic acid mutation made at position 56 is identical to the serine to aspartic acid mutation made at position 55 of Michael Henzl's studies of rat α- and β-parvalbumins neglecting our phenylalanine to tryptophan mutation added at position 103 outside of the EF loop (Henzl's numbering of parvalbumin residues counts the first methionine cleaved as residue number one whereas our studies do not) [34]. Henzl's studies report macroscopic stepwise calcium binding constants for the S55D mutation in buffer 0.025M Hepes 0.15M NaCl pH 7.4 at 25˚C, where K_1 (M^{-1}) is 2.1 (0.2) x 10^8 and K2 (M^{-1}) is 5.0 (0.2) x 10^7 [34]. Assuming that the properties of gadolinium binding are comparable to that of calcium binding due to their positive charge and comparable ionic radii, one can assume that this mutation maintains ten-fold differentiated metal binding sites. We assume here that the CD loop is the higher affinity metal binding site while the EF loop is the weaker metal binding site, as the ProCA-32 mutation yields a higher overall dissociation constants compared to the pseudo wildtype ProCA-31 (Figure 4.21) [34]. This provides an explanation for the attenuated increase in relaxation times above 50μM ProCA-32. At concentrations of 50μM and below, the relaxivity signal is predominantly due to saturation of both the weak (lower affinity EF site) and strong (higher affinity CD site) metal binding sites, as the protein concentration is significantly lower than that of the fixed gadolinium concentration of 100. The slope of this portion of the curve yields the average relaxivity of ProCA-32 and excess free gadolinium. Above 50μM protein, the introduction of excess protein or unoccupied metal

binding sites "recruits" gadolinium ions to the stronger metal binding site, leaving the weaker metal binding sites unoccupied. Therefore, the increasing concentration of protein reduces the concentration of total saturated metal binding sites and relaxivity decreases. The slope of the curve above 50µM ProCA-32 corresponds to the relaxivity of the strong metal binding sites.

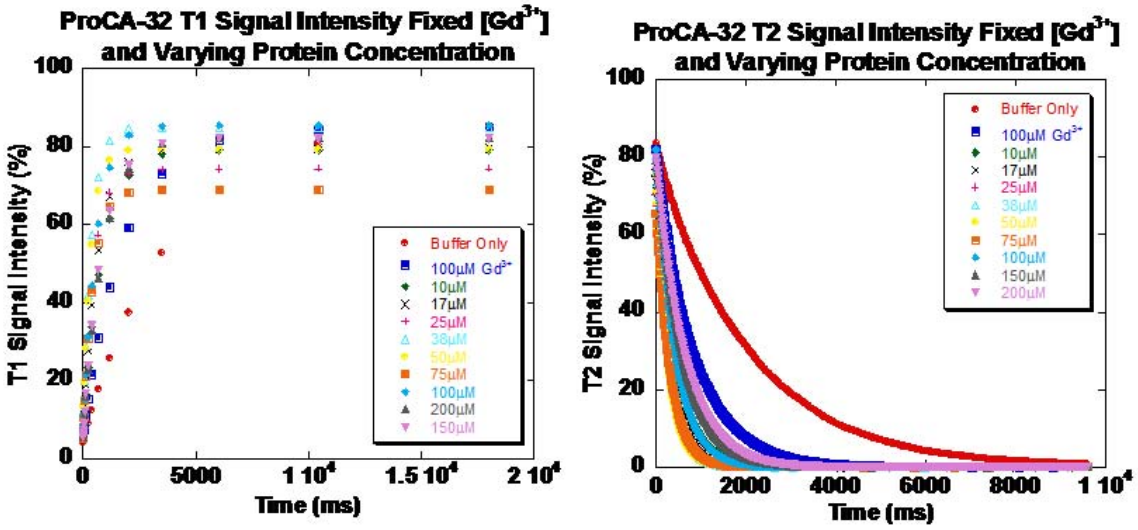

Figure 5.14. ProCA-32 T1 and T2 signal intensity plots at a fixed [Gd^{3+}] of 100µM.

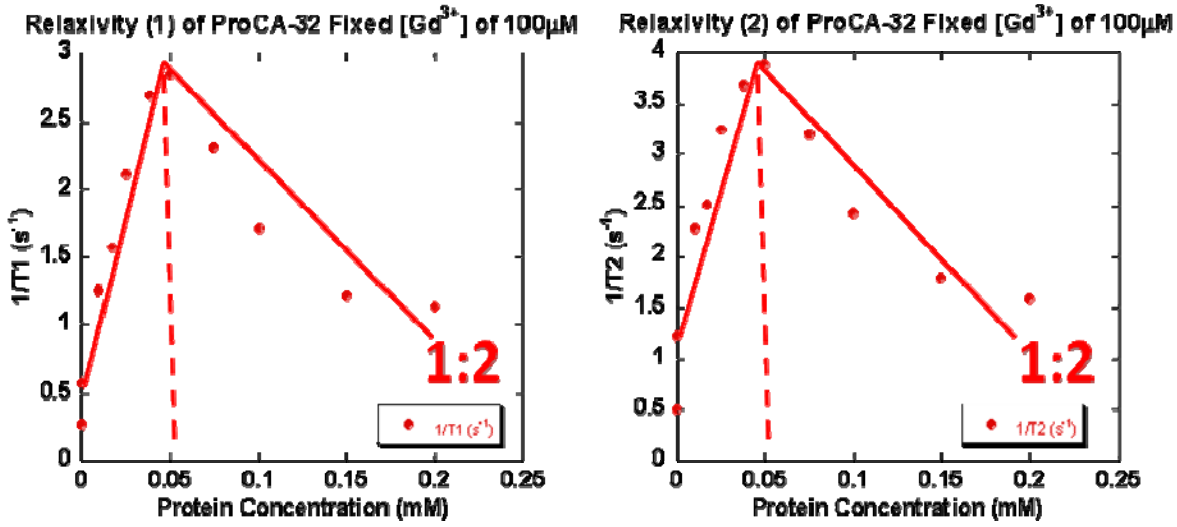

Figure 5.15. Relaxivity curves of ProCA-32 at a fixed 100µM concentration of Gd^{3+}.

5.4.4. ProCA-33

The relaxation times of ProCA-33 shorten as the ratio of protein to gadolinium increases until the protein reaches a 1:3 concentration ratio with gadolinium (Figure 5.16, Figure 5.17). The relaxation times rapidly drop at the 1:2 ratio. Above the 1:2 ratio, the relaxation times begin to plateau. Because of this unexpected lengthening of relaxation times, the overall relaxivity calculated from the slope of the ratios above 1:2 yield a relaxivity value significantly lower than anticipated. Furthermore, using a fixed concentration of 100μM Gd^{3+}, the change in decreasing relaxation times peaks at 38μM ProCA-33 indicating that the binding is 1:3. However, this phenomenon is not well understood. It's possible that at this concentration ratio, the dimerization of the protein begins to occur. To further address the binding mode of ProCA-33, a reverse titration of the fixed gadolinium experiment was performed. ProCA-33 concentration was fixed at 50μM and increasing amounts of gadolinium was titrated into the system up to a 1 to 4 ProCA-33: Gd^{3+} ratio (Figure 5.18). The sharp increase noted at the 100μM gadolinium indicates that the binding is 1:2. Thus, devoid potential dimerization effects, ProCA-33 binds two gadolinium ions. While the reverse titration method can provide more detailed information concerning the binding mode, it cannot accurately represent the average relaxivity of a contrast agent due to the variances in gadolinium concentration. Thus, the average R1 and R2 values calculated from the saturated portion of the curve in Figure 5.17 are 7.16 ± 0.7 mM^{-1} s^{-1} and 8.34 ± 1 mM^{-1} s^{-1}, respectively. Comparing these values to that of the 1:2 relaxivity values approximated by the traditional methods, the values for ProCA-33 are nearly identical (Table 5.2).

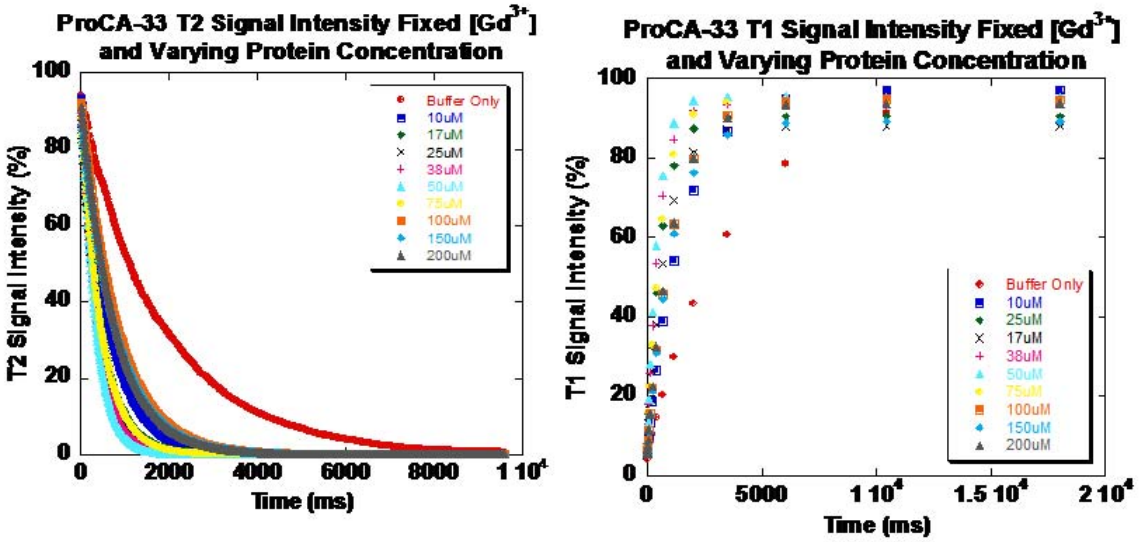

Figure 5.16. ProCA-33 T1 and T2 signal intensity plots at a fixed [Gd^{3+}] of 100µM.

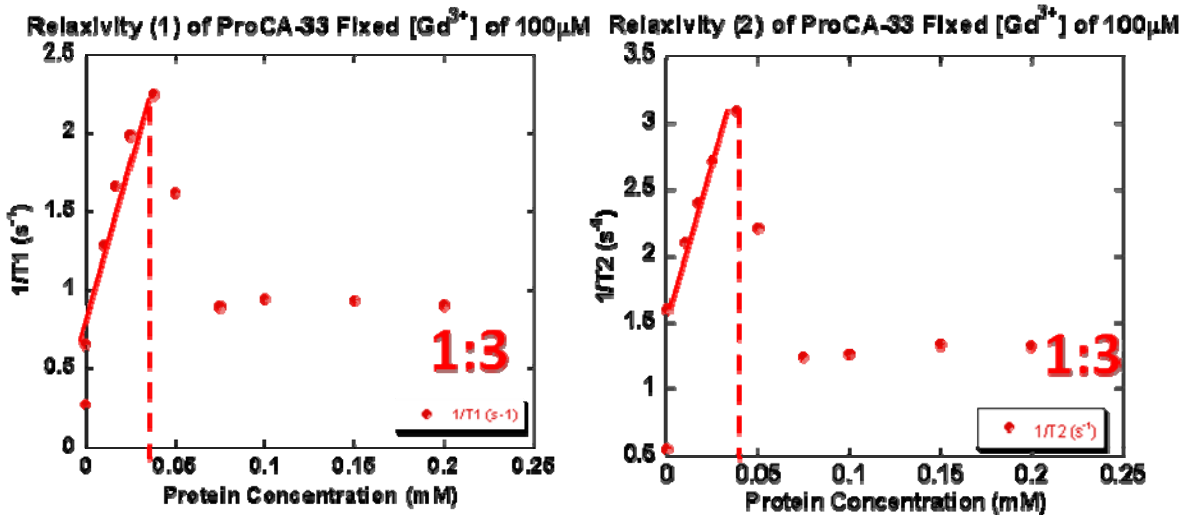

Figure 5.17. Relaxivity curves of ProCA-33 at a fixed 100µM concentration of Gd^{3+}.

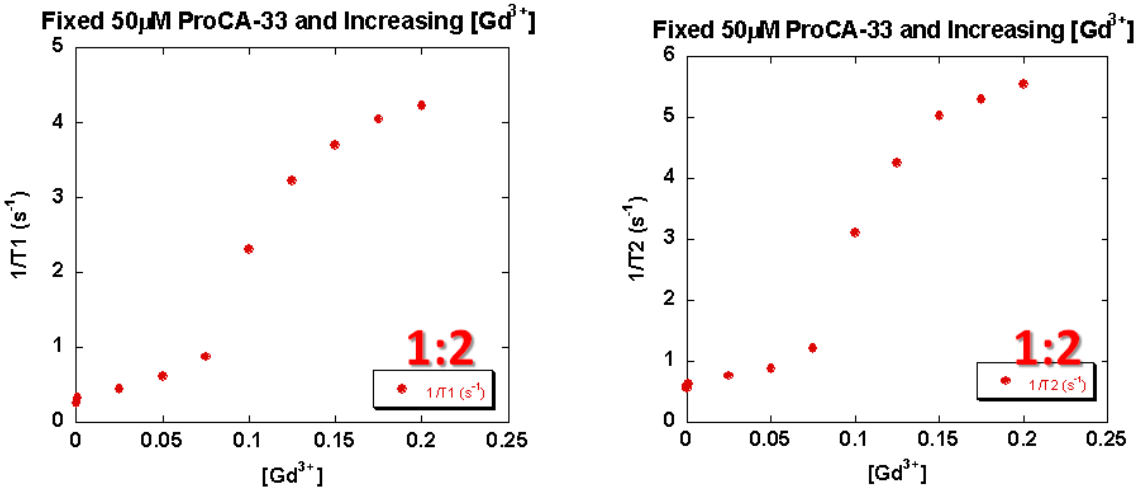

Figure 5.18. ProCA-33 reverse titration for binding mode determination.

It was suggested that the sudden increase in relaxation times noted for ProCA-32 and ProCA-33 (Figures 5.15 and 5.17) was due to the presence of excess EDTA introduced into the system during the FPLC separation purification process. Theoretically, excess EDTA at comparable concentrations of contrast agent would competitively compete with the protein for gadolinium. The reduced availability of free gadolinium would result in an increased concentration of free protein in the measured sample and thus a longer relaxation time (lower relaxivity). Because the significant change in relaxation times was not noted for high concentrations of ProCA-30 and ProCA-31, for this argument to be valid, the process for reducing the concentration of EDTA via dialysis prior to relaxivity experiments may not have been as efficient for ProCA-32 and ProCA-33. This is highly unlikely since identical expression and purification procedures were implemented for isolation of all members of Class ProCA-3 agents. Still, to investigate whether ProCA-32 and ProCA-33 had significant amounts of excess chelator present in their stock samples relative to ProCA-31, a fluorescence titration with rhodamine-5N was completed by senior research David Xue. The instrumental conditions for

this experiment were identical to those listed in chapter 2 (section 2.5). Concentrations of 50µM ProCA-31 (control), ProCA-32, and ProCA-33 were each combined with 1µM of dye in 10mM Tris/HCl 100mM NaCl chelex pH 7.44. Increasing concentrations of gadolinium were titrated into the system (Figure 5.19).

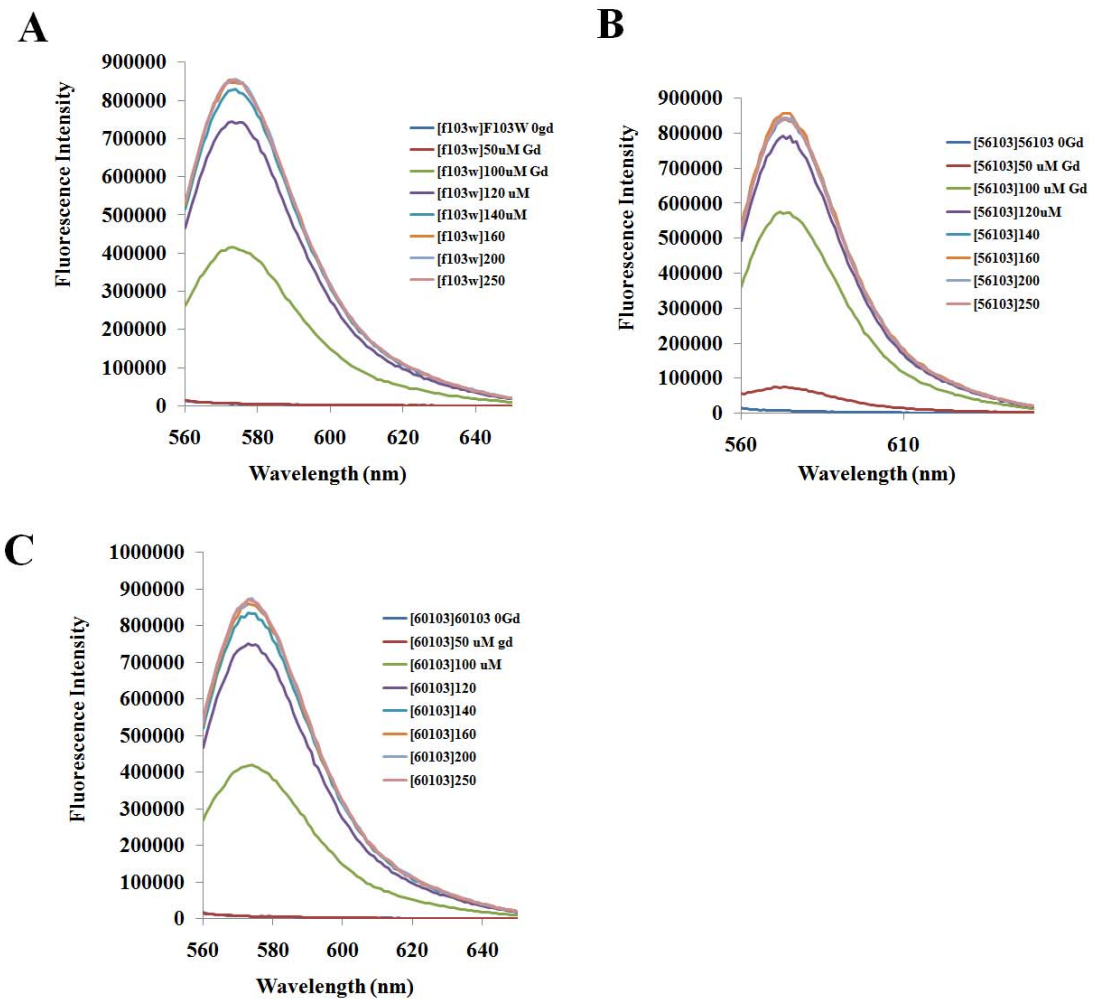

Figure 5.19. Determination of excess EDTA in contrast agent samples. (A) Fluorescence intensity spectrum of ProCA-31. (B) Fluorescence intensity spectrum of ProCA-32. (C) Fluorescence intensity spectrum of ProCA-33. Sample conditions: 1µM rhodamine-5N, 50µM protein in 10mM Tris 100mM NaCl chelex pH 7.44.

Assuming that the binding of the tested agents to gadolinium is 1 to 2, the fluorescence intensity above 100µM added gadolinium (1 to 2 ratio) should not increase if excess EDTA is present. Here, EDTA would compete with rhodamine-5N for binding gadolinium. However, this

effect is not observed. Above 50µM of added gadolinium, the fluorescence intensity sharply increases for all tested contrast agents, allowing excess free gadolinium to bind to rhodamine-5N (Figure 5.20). Due to the lack of points collected between 50µM and 100µM added gadolinium, one cannot determine the whether the sharp increase exclusively occurs above 50µM added gadolinium. This would provide further insight into the binding mode of the tested agents. Nevertheless, this data indicates that not only is there very little free EDTA present in the protein stock samples, but the concentration of this chelator does not vary from protein to protein. Therefore, this phenomenon cannot be used to explain the lowered relaxivity. Additionally, while this fluorescence titration method has the potential to offer insight into the lowered relaxivity of ProCA-32 and ProCA-33, it does not effectively address the significant increase in relaxation times at higher concentrations of protein. Thus, it is more likely that the effect seen for ProCA-32 and ProCA-33 lowered relaxivities is due to dimerization or the heterogeneous nature of the gadolinium metal binding sites for the reasons previously outlined in this chapter.

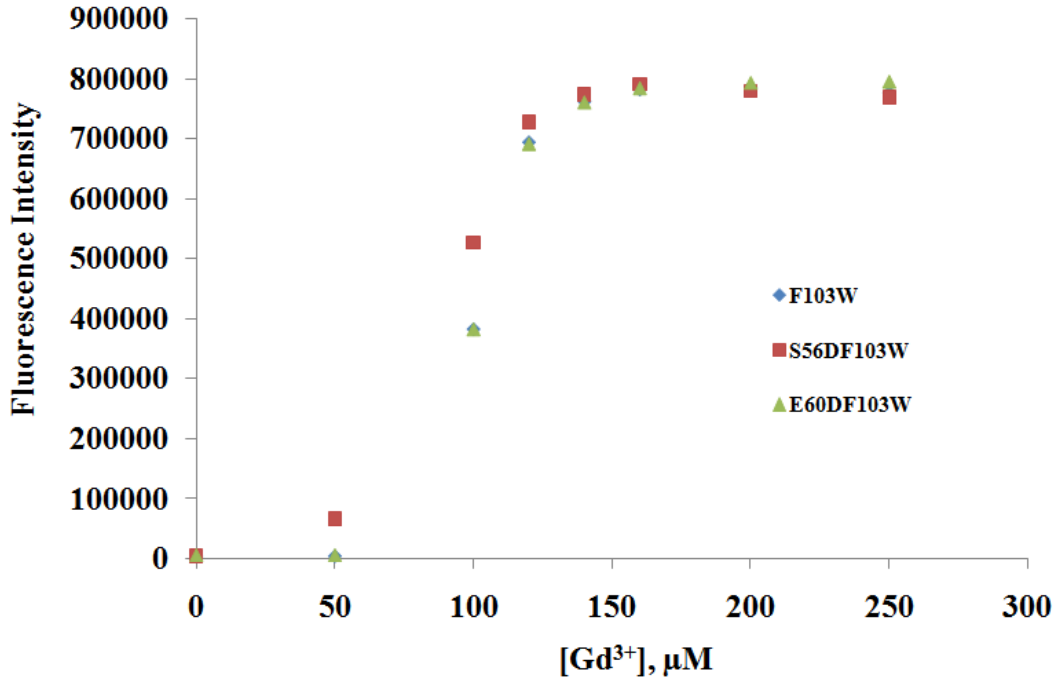

Figure 5.20. Effects of increasing concentrations of gadolinium on fluorescence intensity.

While dimerization effects may present a possible explanation for the significant increase in relaxation times for ProCA-33 in Figure 5.17, it is important to note the sharp increase in relaxation times above 38μM protein compared to the attenuated increase in that of ProCA-32 in Figure 5.15. If the effects seen were due to dimerization effects, the slope of increasing relaxation times for both ProCA-32 and ProCA-33 should be nearly identical. Though each variant maintains an aspartate mutation at different positions within the CD site, one would not expect that this positioning would significantly affect the relative dimerization potential of each agent. Thus, the heterogeneity of the metal binding sites presents a more plausible explanation for this phenomena observed in both ProCA-32 and ProCA-33. The glutamate to aspartic acid mutation made at position 60 is identical to the glutamate to aspartic acid mutation made at position 59 of Michael Henzl's studies of rat α- and β-parvalbumins (Henzl's numbering of parvalbumin residues counts the first methionine cleaved as residue number one whereas our studies do not) [34]. These studies report that the macroscopic association constants for calcium binding of the ProCA-33 mutation are as follows: K_1 (M^{-1}) is 1.2 (0.1) x 10^8 and K_2 (M^{-1}) is 7.8 (0.3) x 10^6 [34]. Here, we assume that the CD site is the weaker gadolinium affinity site compared to that of the EF site in the E60D mutant (ProCA-33) compared to the wildtype association constants of α-parvalbumin (ProCA-30) in Henzl's paper [34]. Assuming that the nature of calcium and gadolinium binding are similar for the reasons previously stated, it appears that ProCA-33 has a lower overall metal binding affinity (Figure 4.21). Still, the increased binding affinity differentiation between the CD and EF sites is enhanced in ProCA-33 compared to ProCA-32, as there is nearly a 100-fold differentiation between the association constants of ProCA-33 compared to the 10-fold difference in the ProCA-32 constants [34]. Therefore, a more

drastic increase in relaxation times is noted above 38μM protein (Figure 5.17). Theoretically, this increase should occur above 50μM protein. However, it's possible that there is an error in estimation of the protein concentration due to the inconsistencies in the reported molar extinction coefficient for this variant. At concentrations of approximately 38-50μM and below, the relaxivity signal is predominantly due to saturation of both the weak (lower affinity CD site) and strong (higher affinity EF site) metal binding sites, as the protein concentration is significantly lower than that of the fixed gadolinium concentration of 100. The slope of this portion of the curve yields the average relaxivity of ProCA-33 and excess free gadolinium. Above 38-50μM protein, the introduction of excess protein or unoccupied metal binding sites "recruits" gadolinium ions to the stronger metal binding site, leaving the weaker metal binding sites unoccupied. Therefore, the increasing concentration of protein reduces the concentration of total saturated metal binding sites and relaxivity decreases. The slope of the curve above 38-50μM ProCA-33 corresponds to the relaxivity of the strong metal binding sites.

5.5. Summary

Overall, both the traditional method of measurement and the fixed gadolinium experiments yield comparable relaxivity values, with the exception of ProCA-32. ProCA-32 and ProCA-33 maintain notably lower relaxivities compared to ProCA-30 and ProCA-31 members which do not bear a CD site mutation. This is primarily due to the significant increase in relaxation times following the 1:2 ratio for ProCA-32 and the 1:3 ratio for ProCA-33. As previously explained, this is likely due to the heterogeneous nature of the metal-binding sites.

It appears that all members of Class ProCA-3 bind gadolinium in a 1:2 ratio. ProCA-33 appears to bind gadolinium in a 1:3 ratio by the fixed gadolinium method. However, a reverse titration of the fixed gadolinium method allows one to conclude that the binding is 1:2. There are

a number of plausible explanations provided as an explanation for the lowered relaxivities of ProCA-32 and ProCA-33 compared to that of ProCA-30 and ProCA-31. Initially, dimerization effects were assumed to be the cause for the drastic increase in relaxation times above the 1 to 2 ratio in ProCA-32 (Figure 5.15) and 1 to 3 ratio in ProCA-33 (Figure 5.17) due to the introduction of additional charged residues in the CD site compared to that of ProCA-30 and ProCA-31. However, this assumption does not address the gradual increase in relaxation times for ProCA-32 versus the sharp increase for ProCA-33. A more plausible explanation for the sharp increase in relaxation times is due to the heterogeneous nature of the metal binding sites within class ProCA-3 agents. As noted by the fixed gadolinium curves in Figures 5.15 and 5.17, initially, gadolinium occupies the strong affinity site (low relaxivity) site and then occupies the weak affinity site (higher relaxivity). The 100-fold differentiation noted in ProCA-33 compared to the 10-fold differentiation in ProCA-32 explains why a more pronounced increase in relaxation times was noted for ProCA-33. At higher concentrations of protein, the fixed concentration of gadolinium preferentially binds the strong metal binding affinity sites, reducing the concentration of protein saturated and lowering the overall relaxivity measured. Thus, lower relaxivities using the fixed gadolinium-increasing protein concentration method are noted for ProCA-32 and ProCA-33. Our secondary structure results from circular dichroism in chapter 4 do not reveal any significant structural changes in the native structure of this class of contrast agents due to the CD site mutations made in ProCA-32 and ProCA-33. To provide a more concrete explanation to explain lower than expected relaxivity phenomenon noted by traditional method calculations, further investigation is required.

6. FINAL CONCLUSIONS AND FUTURE WORK

In summary, the current expression protocol used yields a high quantity of overexpressed parvalbumin and its variants according to SDS Page gel analysis. However, this conclusion is based on evidence of consistency in loading samples onto the gel and on the contingency that the dense band observed at 12 kDa is primarily due to the presence of the desired protein. Minor modifications can be made to the procedure by eliminating overnight growth for expression. Though differences in optical density indicate enhanced cellular growth, overnight incubation does not yield a significant difference in the amount of protein expressed compared to three to four hours after induction.

Through the development of optimal streptomycin sulfate precipitation conditions and salt gradient modification of the program used for FPLC Q-column separation, significant improvements were made (from 31.70 mg to 109.12 mg for ProCA-30; from 37.50 mg to 76.16 mg for ProCA-31; from 32.60 mg to 60.21 mg for ProCA-32) compared to the old protocol to yield a significantly higher quantity of ProCA-30, ProCA-31, and ProCA-32. The yield for ProCA-33 did not increase due to experimental error made during the washing of the Q-column prior to FPLC injection. Nevertheless, newly modified purification protocol not only allows for excellent abstraction of the protein from the cell pellet but is also yields a high concentration of protein absent from DNA or RNA as compared to previous purification results.

In the absence of EGTA sample treatment, all of the discussed members of Class ProCA-3 yield alpha-helical structures that are sustained in the presence and absence of salt in varying concentrations of magnesium, calcium, gadolinium, and terbium. A high salt environment does little to destabilize the secondary structure of the protein. Additionally, one can conclude that the introduction of mutations within the CD binding site does not significantly alter the secondary

structure of the native form of the protein. Furthermore, the results indicate that the secondary structure is maintained in the presence of gadolinium under high salt conditions. This is of grave importance, as it gives insight into the structural stability of the contrast agents. From the observed CD spectrum analyses, a random coil formation was noted for all variants in the presence of 5mM gadolinium and terbium in the presence of 5mM EGTA. The denaturation of the aforementioned proteins is primarily due to a significant decrease in pH due to EGTA binding gadolinium or terbium.

The relaxivity values obtained for ProCA-30, ProCA-31, ProCA-32, and to lower degree ProCA-33 seem to be very promising for the future of contrast agents because their relaxivity values are significantly higher than that of many commercial contrast agents (Tables 5.1 and 5.2). With the exception of ProCA-32 values, the relaxivity values calculated by the traditional method are nearly identical to those achieved using the fixed gadolinium increasing protein concentration experiments. Reasons behind this observed phenomenon is not well understood. Failure to achieve identical relaxivity values for ProCA-32 requires further investigation. From the fixed 100μM Gd^{3+}-varied protein concentration relaxivity experiments, strong experimental evidence supports ProCA-30, ProCA-31, and ProCA-32 binding gadolinium in a 1:2 protein to metal ratio. Studies of ProCA-33 using a reverse titration of the aforementioned binding mode experiment also allow one to assume that the contrast agent binds two gadolinium ions. The lower relaxivity values and attenuated or sharp increase in relaxation times for the fixed gadolinium-varied protein concentration experiments for ProCA-32 and ProCA-33 are likely due to the heterogeneous nature of the metal binding sites. Dimerization effects or the presence of residual EDTA present in the sample from our purification process are less likely to explain the effects observed. Correlating the relaxivity data with the circular dichroism data, it appears that

the measured relaxivity values are not necessarily affected by metal-induced structural changes. Once again, ProCA-32 is the only member of Class ProCA-3 whose increase in relaxivity from the 1 to 1 to the 1 to 2 ratio under both salt conditions doesn't correlate significant changes in the protein's secondary structure. The remaining members yield positive correlations with the CD data between their consistent relaxivity values under both salt conditions at 1 to 1 and 1 to 2 ratios.

Future fluorescence experiments will allow one to quantify the experimental metal dissociation constant of the members of Class ProCA-3. Future relaxivity experiments will be devoted to metal competition experiments to determine at what concentration gadolinium can be competed out of the contrast agent binding sites by physiologically relevant metal ions such as calcium, magnesium, zinc, etc. 1D and NMR diffusion experiments will further characterize the nature of differentiation between the metal binding sites in class ProCA-3 agents. The results from these experiments will allow for further screening for an optimal variant that will function as a contrast agent for MRI diagnostics.

Overall, the studies of this thesis have made a significant contribution to the development of Class ProCA-3 agents. Because animal experiments and clinical trials require large amounts of highly concentrated contrast agent of 5mM or higher be injected into an animal or patient for image-enhancement screening, the optimized purification protocol aids in achieving a pure, high quantity of contrast agent to be used. The structural stability studies provide insight into the metal stability of the contrast agents and more specifically into the stability of the agents when saturated with gadolinium. The higher relaxivity values measured for the contrast agents compared to commercial analogue Gd-DTPA implies that there is a higher dose efficiency associated with contrast agent performance, meaning less contrast agent will be required to

achieve heightened differential signal intensity in an MR image compared to that of the commercial agents. This is a highly desired result as a lower injection dosage reduces the potential for the toxic effects associated with the release of a high concentration of free gadolinium (nephrogenic systemic fibrosis). Combined with future gadolinium-binding studies, metal selectivity studies, serum stability observations, and *in vivo* observations of image-enhancement, Class ProCA-3 agents have the potential to be developed as general and targeted agents, making significant strides in the efficacy of MRI.

REFERENCES

1. *Medical Imaging*. Available from: en.wikipedia.org/wiki/Medical_imaging.
2. *How Innovations in Medical Imaging Have Reduced Radiation Dosage*. 1-28.
3. Yang, J.J., et al., *Rational design of protein-based MRI contrast agents.* J Am Chem Soc, 2008. 130(29): p. 9260-7.
4. Faulkner, W.M. (1996) *Basic Principles of MRI*.
5. Voyvodic, J. *Basic Principles of MRI*.
6. Mackiewich, B. *Basic Principles of MRI*. 1995 August 19, 1995 [cited 2010 April 28]; Available from: http://www.cs.sfu.ca/~stella/papers/blairthesis/main/node11.html.
7. Caravan, P., *Protein-targeted gadolinium-based magnetic resonance imaging (MRI) contrast agents: design and mechanism of action.* Acc Chem Res, 2009. 42(7): p. 851-62.
8. Krause, W., ed. *Contrast Agents I Magnetic Resonance Imaging*. 2002, Springer-Verlag Berllin: Heidelberg.
9. *Nuclear Magnetic Resonance Spectroscopy Theoretical Principles*. Biosciences.
10. Caravan, P., *Strategies for increasing the sensitivity of gadolinium based MRI contrast agents.* Chem Soc Rev, 2006. 35(6): p. 512-23.
11. van der Molen, A.J. and M.F. Bellin, *Extracellular gadolinium-based contrast media: differences in diagnostic efficacy.* Eur J Radiol, 2008. 66(2): p. 168-74.
12. Laurent, S., L.V. Elst, and R.N. Muller, *Comparative study of the physicochemical properties of six clinical low molecular weight gadolinium contrast agents.* Contrast Media Mol Imaging, 2006. 1(3): p. 128-37.
13. Esqueda, A.C., et al., *A new gadolinium-based MRI zinc sensor.* J Am Chem Soc, 2009. 131(32): p. 11387-91.

14. Bellin, M.F. and A.J. Van Der Molen, *Extracellular gadolinium-based contrast media: an overview.* Eur J Radiol, 2008. 66(2): p. 160-7.

15. *Contrast agents for MRI tomography*. Group of Coordination and Bioinorganic Chemistry [cited 2010 February 7]; Available from: http://www.natur.cuni.cz/anorchem/19/E/Vyzkum.htm.

16. *Kidney Dialysis & Renal Failure Patients at Highest Risk to MRI Contrast Dye with Gadolinium*. MRI Side Effects Lawsuit - Nephrogenic Systemic Fibrosis (NSF) [cited 2010 April 30]; Available from: http://www.mri-side-effects.com/.

17. (2007) *Gadolinium and nephrogenic systemic fibrosis* Kidney International 72, 229.

18. Evenepoel, P., et al., *Nephrogenic fibrosing dermopathy: a novel, disabling disorder in patients with renal failure.* Nephrol Dial Transplant, 2004. 19(2): p. 469-73.

19. Idee, J.M., et al., *Clinical and biological consequences of transmetallation induced by contrast agents for magnetic resonance imaging: a review.* Fundam Clin Pharmacol, 2006. 20(6): p. 563-76.

20. *Gadolinium Based Contrast Agents Used in MRIs Get New FDA Black Box Warning*. 2007 September 28, 2007 [cited 2009 September 16]; Available from: http://www.newsinferno.com/archives/1861.

21. Aime, S., et al., *Pushing the sensitivity envelope of lanthanide-based magnetic resonance imaging (MRI) contrast agents for molecular imaging applications.* Acc Chem Res, 2009. 42(7): p. 822-31.

22. Rawat, S., C. Raman Suri, and D.K. Sahoo, *Molecular mechanism of polyethylene glycol mediated stabilization of protein.* Biochem Biophys Res Commun, 2010. 392(4): p. 561-6.

23. Yang, J.J. *Our Research Focus*. Available from: http://chemistry.gsu.edu/faculty/Yang.

24. Fohr, U.G., et al., *Human alpha and beta parvalbumins. Structure and tissue-specific expression.* Eur J Biochem, 1993. 215(3): p. 719-27.

25. Pauls, T.L., et al., *Metal binding properties of recombinant rat parvalbumin wild-type and F102W mutant.* J Biol Chem, 1993. 268(28): p. 20897-903.

26. Henzl, M.T., J.D. Larson, and S. Agah, *Influence of monovalent cation identity on parvalbumin divalent ion-binding properties.* Biochemistry, 2004. 43(10): p. 2747-63.

27. Pauls, T.L., J.A. Cox, and M.W. Berchtold, *The Ca2+(-)binding proteins parvalbumin and oncomodulin and their genes: new structural and functional findings.* Biochim Biophys Acta, 1996. 1306(1): p. 39-54.

28. Yang, W., et al., *Rational design of a calcium-binding protein.* J Am Chem Soc, 2003. 125(20): p. 6165-71.

29. Voet, D.a.J.G., ed. *Nucleic Acid Structures and Manipulation*. 2nd ed. 1995, John Wiley & Sons Inc.: Canada.

30. Inc., B. *BVTech Plasmid*. Plasmid map of pet-22b(+) 2005 [cited 2010 April 29]; Available from: http://www.biovisualtech.com/bvplasmid/pET-22b%28+%29.htm.

31. Walker, J.H., ed. *SDS Polyacrylamide Gel Electrophoresis of Proteins*. 2nd ed. 2002, Humana Press Inc.: Totwa.

32. *Sonication*. Available from: en.wikipedia.org/wiki/Sonication.

33. *French Pressure Cell Press*. Available from: en.wikipedia.org/wiki/French_pressure_cell_press.

34. Henzl, M.T., S. Agah, and J.D. Larson, *Rat alpha- and beta-parvalbumins: comparison of their pentacarboxylate and site-interconversion variants.* Biochemistry, 2004. 43(29): p. 9307-19.

35. Heizmann, C.W., M.T. Hauptle, and H.M. Eppenberger, *The purification, characterization and localization of a parvalbumin-like protein from chicken-leg muscle.* Eur J Biochem, 1977. 80(2): p. 433-41.

36. Ltd., A.P. *Circular Dichroism (CD) Spectroscopy*. Available from: http://www.photophysics.com/circular dichroism.php.

37. Arockiados, T., Xavier, F., and M. Babu *Isolation and Characterization of Metal-Doped Protein as Semiconducting Polymer.* Materials Chemistry and Physics, 2008. 111(2-3): p. 517-523.

38. Inc., M.P. *Rhod Calcium Indicators*. 2005 [cited 2010 January 5]; Available from: http://probes.invitrogen.com/media/pis/mp01244.

39. Permyakov, S.E., et al., *Apo-parvalbumin as an intrinsically disordered protein.* Proteins, 2008. 72(3): p. 822-36.

40. *Dietary Supplemental Fact Sheet: Calcium*. [electronic] December 4, 2008 [cited 2008 December 10]; Available from: ods.od.nih.gov/factsheets/calcium.asp.

41. *Calcium*. [electronic] 2008 December 15, 2008 [cited 2008 December 10]; Available from: en.wikipedia.org/wiki/Calcium.

42. Means, A., *Determinants That Govern High-Affinity Calcium Binding.* Advances in Second Messenger and Phosphoprotein Research, 1995. 30.